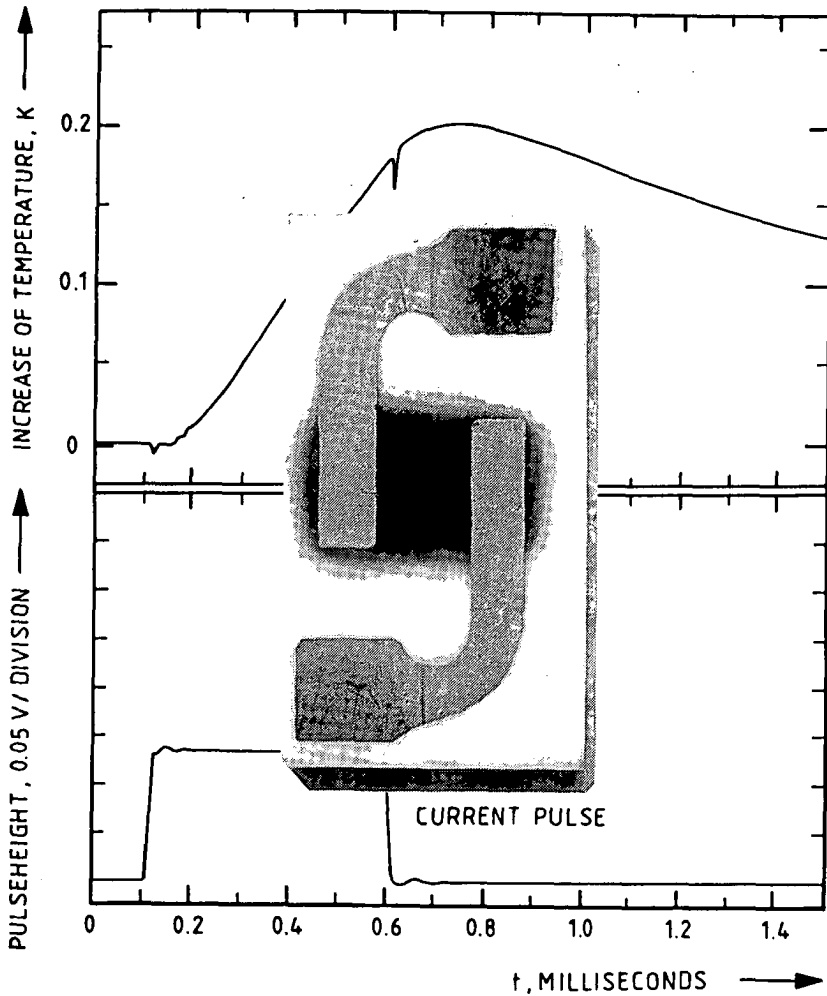# TRANSIENT HEAT TRANSFER TO SUPERCRITICAL

HELIUM AT LOW TEMPERATURES

W.B. BLOEM

TRANSIENT HEAT TRANSFER TO SUPERCRITICAL

HELIUM AT LOW TEMPERATURES

PROEFSCHRIFT

ter verkrijging van de graad van
doctor in de technische wetenschappen
aan de Technische Universiteit Delft,
op gezag van de Rector Magnificus
prof. dr. J.M. Dirken,
in het openbaar te verdedigen
ten overstaan van het College van Dekanen
op donderdag 20 november 1986
te 14.00 uur

door

Willem Berend Bloem

natuurkundig ingenieur
geboren te Beverwijk

Dit proefschrift is goedgekeurd door
de promotor Prof. dr. H. Postma.

Aan mijn Ouders

ℓ

CONTENTS

SUMMARY

Applied superconductivity is mainly used in constructing large elec-
trical magnets. These magnets can be used in fields like energy con-
version, in accelerators and detectors for high energy particle
physics, medical research and magnetic separation. Because supercon-
ductivity occurs only at very low temperatures, a few degrees above
absolute zero, it is required to cool superconducting devices. The
only fluid permitting these temperature levels is helium. For large
scale systems the low temperature environment can be realized by a
forced flow of supercritical helium through cooling channels along
the conductors.
The stable performance of a superconducting magnet can be disturbed
by small heat releases in the conductors caused by magnetic or mecha-
nical instabilities. These instabilities are transient effects
(milliseconds) and so the transient heat transfer to the cooling
fluid is of importance in ensuring a superconducting magnet. In this
thesis experimental results are reported on transient heat transfer
to a forced flow of supercritical helium flowing through a rectangu-
lar copper tube with a hydraulic diameter of 5 mm. The temperatures
were measured with specially developed multipurpose fast response
thermometers, which had a response time smaller than one millisecond.
The conditions of the helium flow were: range of the inlet bulk tem-
perature of the fluid 4.2 K - 6 K, pressures from 3 bar to 10 bar and
Reynolds numbers between 5000 and 200000. The tube was heated on four
sides with heat fluxes up to 9800 W/m^2.
A second test section had been equipped with small fast response
pressure transducers. From these pressure transducers the existence
of pressure waves, propagating with the velocity of sound in
supercritical helium, induced by heat pulses could be detected.

From the experiments it followed that during the first tens of milli-
seconds the heat transfer is governed by heat conduction in a small
layer of the coolant along the wall. The transient heat transfer

coefficient is, apart from time, a function of the helium properties
thermal conductivity λ, density ρ and specific heat c_p.
Although these helium properties depend strongly on pressure and tem-
perature, it was remarkable that the temperature increase during a
heat pulse was nearly the same at different helium pressures at
4.2 K. At higher bulk inlet temperatures differences occurred.
After analysing the data the heat transfer phenomena could be ex-
plained by regarding the product ε of the helium properties λ, ρ and
c_p as a function of temperature and pressure.
After 0.1 s the heat transfer becomes stationary and the steady state
heat transfer in supercritical helium could be described by the
Dittus-Boelter correlation with improved constant:
$$Nu = 0.0236 \ Re^{0.8} \ Pr^{0.4}.$$
The radial heat transport in the fluid is governed by turbulence,
radial heat conduction is of less importance because of the fact that
the thermal diffusivity of helium is very small at low temperatures.
Some of the measurements have been numerically simulated with the aid
of a computer simulation model, developed by Cornelissen [65]. The
numerical results agree well with the measurements.

From the results it can be concluded that at 4.2 K there is no advan-
tage to work at low pressure, the peak in the heat absorption does
not manifest in the heat transfer.
It is recommended to work at high pressures because 1) the heat ab-
sorption of helium is relatively large with increasing temperature,
2) there is a small probability of pressure oscillations and 3) when
the inlet bulk temperature is higher than 4.2 K the heat absorption
by helium will still increase when the temperature rises. The heat
transfer improves at Reynolds numbers higher than 10^5.
When the largest possible mass flow of supercritical helium flowing
through a cooling tube is realized, the only possibility remaining to
enlarge the (transient) heat transfer coefficient is enlargement of
the heat exchanging surface.

SAMENVATTING

Supergeleiding vindt voornamelijk haar toepassing in de constructie
van grote elektromagneten. Deze magneten worden gebruikt in gebieden
als energieconversie, in versnellers en detectoren ten bate van de
hoge energiefysica, medische apparatuur en magnetische separatie.
Omdat supergeleiding zich alleen openbaart bij erg lage temperaturen,
een paar graden boven het absolute nulpunt, is het een vereiste om de
supergeleidende apparaten te koelen. Het enige koelfluïdum dat bij
deze temperaturen voorhanden is, is helium. Bij grote supergeleidende
systemen kunnen de lage temperaturen worden bewerkstelligd door het
systeem te koelen met een geforceerde stroming van superkritisch
helium door koelbuizen langs of in de geleiders.
Het stabiele gedrag van een supergeleidende magneet kan worden ver-
stoord door het vrijkomen van kleine hoeveelheden warmte, veroorzaakt
door magnetische of mechanische instabiliteiten. Deze instabiliteiten
zijn snel verlopende processen (milliseconden) en dus is de warmte-
overdracht gedurende korte tijden van belang voor het beveiligen van
supergeleidende systemen.
In dit proefschrift worden experimentele resultaten gepresenteerd
aangaande warmteoverdracht gedurende korte tijden naar een geforceer-
de stroming van superkritisch helium in een rechthoekige koperen buis
met een hydraulische diameter van 5 mm. De temperaturen werden geme-
ten met nieuw ontwikkelde snelle respons thermometers, welke ook in
andere experimentele cryogene testopstellingen kunnen worden ge-
bruikt. De responstijd van de thermometers was kleiner dan 1 milli-
seconde.
De condities van de heliumstroming waren: bereik inlaattemperatuur
4,2 K - 6 K, drukbereik 3 - 10 bar en Reynoldsgetallen tussen 5000 en
200000. De buis werd aan vier zijden verwarmd met warmtestromen tot
9800 W/m^2.
Een tweede testsectie werd voorzien van kleine snelle respons druk-
sensoren. Met behulp van deze drukopnemers was het mogelijk het be-

staan van drukgolven, die zich voortplanten met de geluidssnelheid in su-
perkritisch helium en werden geïnduceerd door warmtepulsen, aan te tonen.

Uit de meetresultaten volgt dat gedurende het eerste tiental milli-
seconden de warmteoverdracht wordt bepaald door warmtegeleiding in
een dunne laag helium langs de binnenzijde van de buis. De warmte-
overdrachtscoëffciënt gedurende deze korte tijden is een functie van
de tijd en van de heliumeigenschappen; de warmtegeleidingscoëfficiënt
λ, dichtheid ρ en soortelijke warmte c_p.
Alhoewel deze heliumeigenschappen sterk druk- en temperatuurafhanke-
lijk zijn, was het opmerkelijk dat een temperatuurstijging gedurende
een warmtepuls vrijwel gelijk was voor verschillende drukken bij
4.2 K. Bij hogere inlaattemperaturen van het helium kwamen wel ver-
schillen naar voren. Na analyse van de meetgegevens konden de warmte-
overdrachtsverschijnselen worden verklaard aan de hand van de groot-
heid ε, het produkt van de heliumeigenschappen λ, ρ en c_p, als
functie van temperatuur en druk. Na 0,1 s wordt de warmteoverdracht
in superkritisch helium stationair en deze kan worden beschreven door
de Dittus-Boelter correlatie met een beter bepaalde constante:
$Nu = 0,0236 \ Re^{0,8} \ Pr^{0,4}$. Het radiale warmtetransport in het fluidum
wordt beheerst door turbulentie; radiale warmtegeleiding is niet van
belang daar de warmtevereffeningscoëfficiënt van helium zeer klein is
bij lage temperaturen. Enkele metingen zijn numeriek nagerekend met
behulp van een computersimulatiemodel ontwikkeld door Cornelissen
[65]. De numerieke resultaten zijn in goede overeenstemming met de
metingen.

Naar aanleiding van de resultaten kan worden geconcludeerd dat het
niet voordelig is om te werken met helium onder lage druk bij 4.2 K.
Het mogelijk voordeel van de piek in de warmteabsorptie uit zich niet
in lage temperatuurstijgingen. Daarentegen wordt het aanbevolen om te
werken met helium onder hoge druk omdat 1) de warmteabsorptie rela-
tief groter wordt bij stijging van de temperatuur, 2) er een kleine
kans is op drukoscillaties en 3) als de inlaattemperatuur van het
helium hoger is dan 4,2 K, de warmteabsorptie door het helium nog zal

toenemen als de temperatuur stijgt. De warmteoverdracht wordt beter
bij Reynoldsgetallen boven de 100000.
Als de grootst mogelijke massastroom van superkritisch helium stro-
mend door een koelbuis is gerealiseerd, dan resteert enkel nog de
mogelijkheid van oppervlaktevergroting om de warmteoverdrachtscoëffi-
ciënt, zowel voor korte tijden als stationair, te verhogen.

LIST OF SYMBOLS AND ABBREVIATIONS

A	cross section	m^2
A	surface	m^2
a	thermal diffusivity $(\lambda/(\rho c_p))$	m^2/s
a_T	thermal diffusivity	m^2/s
a_M	magnetic diffusivity (ρ_e/μ_o)	m^2/s
B	magnetic field	T
B_c	critical magnetic field	T
B_{c_o}	critical magnetic field at absolute zero (T = 0)	T
c_p	isobaric specific heat	$J/(kg\ K)$
D	diameter	m
D_h	hydraulic diameter	m
D_w	wetted diameter	m
d	thickness of thermometer (substrate)	m
E	absorbed heat	J
f	fraction of superconducting alloy	
f	friction factor	
$f(T)$	thermal conductivity function of superfluid helium	$W^3/(m^5\ K)$
G	flow rate	$kg/(m^2\ s)$
g	acceleration due to gravity	m/s^2
H	enthalpy	J/kg
h	heat transfer coefficient	$W/(m^2\ K)$
h_{tr}	transient heat transfer coefficient	$W/(m^2\ K)$
I	electrical current	A
I_c	critical electrical current	A
J	current density	A/m^2
J_c	critical current density	A/m^2
J_{c_o}	critical current density at absolute zero (T = 0)	A/m^2
L	length	m
ℓ	Prandtl mixing length	m
m	mass of copper test tube	kg
$\dot{m}$	mass flow	kg/s
MFBF	minimum film boiling flux	W/m^2

n	constant defined by eq. (7.20)	
Nu	Nusselt number (hD/λ)	
Nu_{tt}	Nusselt number at time t_t	
Nu_{tr}	transient Nusselt number (eq. (7.18)(7.19))	
OFHC	oxygen free high conducting	
p	pressure	bar
Pe	Peclet number (vD_h/a)	
PNBF	peak nucleate boiling flux	W/m²
Pr	Prandtl number ($c_p\eta/\lambda$)	
Q	heat flow	W
q	heat flow	W
q_{cr}	critical heat flux	W/m²
R	electrical resistance	Ω
Re	Reynolds number ($\rho vD/\eta$, $4\dot{m}/(\pi\eta D)$)	
R_K	Kapitza thermal boundary resistance	Km²/W
RRR	residual resistance ratio ($\rho_{e,300K}/\rho_{e,4.2K}$)	
S	sensitivity of thin carbon film thermometer	Ω/K
T	temperature	K
T_b	bulk temperature	K
T_c	critical temperature	K
T_{tc}	transposed critical temperature	K
T_w	wall temperature	K
T_λ	lambda temperature	K
t	time	s
t_p	pulse time, duration of heat pulse	s
t_t	take-over-time (eq. (7.13)	s
u^*	friction velocity ($\sqrt{\tau_w/\rho}$)	m/s
u^+	ratio of velocity v and friction velocity u^*	
v	velocity	m/s
$\bar{v}$	mean velocity	m/s
x	quality	
x	distance	m
y	distance perpendicular on the wall of the cooling tube	m
y^+	$y\sqrt{\rho\,\tau_w}/\eta$	

α	Stekly parameter (eq. (2.2))	
α	Fourier number (at/d^2)	
α_p	Fourier number pulse time $(a\,t_p/d^2)$	
β	stability parameter (eq. (2.7))	
δ_{eff}	thickness of the effective layer	m
δ_T	penetration depth of temperature	m
ϵ	product of λ, ρ and c_p; heat absorption coefficient	$J^2/(m^4\ K^2\ s)$
ϵ_H	eddy diffusivity of heat	m^2/s
ϵ_M	eddy diffusivity of momentum	m^2/s
η	dynamic viscosity	$kg/(m\ s)$
λ	thermal conductivity	$W/(m\ K)$
λ_m	London penetration depth of magnetic field	m
μ_o	vacuum permeability	$m\ kg/C^2$
ν	kinematic viscosity	m^2/s
ρ	specific mass	kg/m^3
ρ_e	specific electrical resistivity	Ωm
τ_d	delay time of thermometer	s
τ_h	characteristic time for surface cooling	s
τ_M	characteristic time for magnetic diffusion	s
τ_r	response time of thermometer $(\tau_r = d^2/a)$	s
τ_T	characteristic time for thermal diffusion	s
τ_w	wall shear stress	N/m^2
ϕ	magnetic flux	Wb
ϕ	heat flow	W
$\phi_{released}$	released heat flow	W
ϕ_{He}	heat flow absorbed by helium	W
ψ	flow function of state of flow (eq. (3.8))	

CHAPTER 1

INTRODUCTION

When certain metals are cooled to very low temperatures they become
perfect conductors of electricity. This phenomenon of superconducti-
vity was discovered by Kamerlingh Onnes in 1911 [1]. Unlike the gra-
dual changes in electrical resistance shown by all metals at more
familiar temperatures, superconductivity appears quite abruptly at a
critical temperature T_c which is characteristic of the metal in ques-
tion. At this temperature the electrical resistance drops almost dis-
continuously to zero. It was seen from the results of very sensitive
experiments that below T_c the electrical resistivity of a supercon-
ductor is absolutely zero [2], [3].
Kamerlingh Onnes realized that the new property would open a new
field for numerous applications. While attempting to construct a
superconducting electromagnet, he discovered that a current-carrying
wire of superconducting lead returns to the normal state if a
critical current is exceeded [4]. A later discovery [5] showed that
a superconductor will become normal in the presence of a magnetic
field above a critical value but returns to the superconducting state
when the field is removed. So, apart from the critical temperature T_c
the superconducting state is defined by a critical field B_c and a
critical current density J_c. For the metals which Kamerlingh Onnes
investigated, i.e. mercury, lead and tin, the critical field B_c is
small, ≈ 0.05 T. However, during the last thirty years a new class of
superconducting metals was discovered. The newly discovered mate-
rials, like the alloy NbTi and the intermetallic compound Nb_3Sn,
remain superconducting in strong magnetic fields. They can also carry
extremely high-current densities. These new materials made it possi-
ble to develop reliable high field superconductors, whose use as
current conductors at low temperatures has led to new technological
systems of increased performance and efficiency [6]. Examples of
working systems include superconducting magnets for beam control and

particle detection in high energy physics, for plasma containment in
controlled thermonuclear reaction studies, and test facilities for
high field superconductors, such as SULTAN [78, 59, 48]. Serious con-
sideration is being given to superconducting motors, generators,
transmission lines, magnetic filtration techniques and magnetic levi-
tation systems for high-speed ground transport. New developments are
going on in the medical nuclear-magnetic resonance imaging tech-
niques, where superconducting magnets are used. Other applications
will certainly be developed with more reliable magnet technology.

Because superconductivity occurs only below the critical temperature,
e.g. T_c = 9.5 K for NbTi and T_c = 18.5 K for Nb_3Sn, it is required to
cool the superconducting devices to low temperatures. The suitable
cooling fluid in this temperature region is helium. In practice, the
usual operating temperature for superconducting systems is 4.2 K, the
boiling temperature of liquid helium under atmospheric pressure. The
helium technology must keep pace with the development of the super-
conducting systems. For relatively small laboratory systems it is
common simply to immerse the conductor in a container supplied with
liquid helium vented at atmospheric pressure and thus maintained at
4.2 K (pool boiling). However, as the system size, cost and complex-
ity increase, it is important to take a closer look at the means for
maintaining the low temperature environment.
When pool boiling is used for large magnets, the windings of the coil
have to be spacered so that a great part of the coil will be in con-
tact with the liquid helium. A disadvantage of this method is that
cooling is less effective at the spacers. In addition the construc-
tion is mechanically less rigid. For effective cooling the windings
are usually not impregnated with insulation material. When the zero
resistance of the conductor vanishes and the magnet quenches, high
electrical fields can exist between the windings of the coil. In case
of poor electrical insulation there is a probability of electrical
breakdown. During a quench the risk of breakdown increases because a
great part of the helium evaporates.
A second method is cooling by a forced flow of supercritical or boil-
ing helium through flow channels. The state of supercritical helium
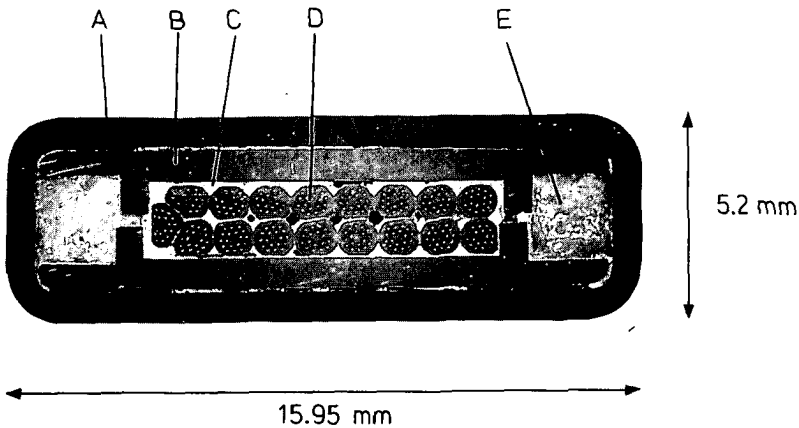
Figure 1.1   Cross section of ECN 10000 A 8T conductor [80].
            A. stainless steel housing
            B. copper stabilizer
            C. lead-tin solder
            D. superconducting wire with 18 Nb_3Sn filaments
            E. cooling channel

is defined by helium pressures larger than the critical helium pres-
sure of 2.27 bar. There is no difference between liquid and vapour,
and no coexistence of liquid and vapour phase. The cooling channels
are usually part of the conductor, the so-called composite conductor
(Fig. 1.1). Apart from the channel the composite conductor exists of
a superconducting cable and sometimes support materials like stain-
less steel are included. The cable is a strand of copper wires in
which a large quantity of superconducting filaments is embedded.
These filaments are made from the superconducting materials. Before
the coil is wound from the composite conductor, electrical insulation
material is wrapped around the conductor. Finally the coil is impreg-
nated with resin to get a stiff construction. Compared with pool
boiling magnets this construction technique of forced flow cooled
magnets has a few advantages. Firstly the heat transfer conditions
along the conductors are uniform (no spacers, no vapour locking),
secondly only a vacuum vessel is required for thermal insulation and
thirdly the cooling channel can resist high helium pressures during a
quench. A disadvantage is that in principle the cooling channels are
as long as the conductor length, thus a large pressure drop can occur
over the channel.

The stable performance of a magnet is a function of the conductor
dimensions. For optimal stability the diameters of the filaments are
limited and the copper-superconductor ratio plays a role (intrinsic
stability [7]). The onset for a quench is a small energy release in
the conductor caused by magnetic and/or mechanical instabilities [8].
The cooling of the magnet should be designed in such a way that the
stationary heat inleak from the environment will be absorbed and that
it is sufficient to absorb the heat pulses of the instabilities. The
magnetic and mechanical instabilities are transient effects, so tran-
sient heat transfer to the cooling fluid plays an important role in
ensuring a superconducting system.

The origin of the magnetic and mechanical instabilities are described
in chapter 2. In this chapter also an estimation is made of the time
scale on which the disturbances and their heat releases take place.
The cooling modes for superconducting devices are dealt with in chap-
ter 3. A literature survey is given on recent results of heat trans-
fer to liquid helium. Although it is possible to predict the heat
transfer to liquid He I on basis of some empirical correlations, it
still remains a problem that the small latent heat of vaporization of
helium and the drastic expansion to the vapour phase make such cool-
ing systems highly unstable with respect to hot spots.

Steady state heat transfer to supercritical helium can be predicted
by correlations based on the Dittus-Boelter correlation. Only near
the critical point errors are introduced in these predictions. Apart
of the large heat transfer coefficients cooling with superfluid
helium has the advantage of the increase of the critical current den-
sity by virtue of the reduced temperature. Only the cooling circuit
has to be very tight; when (super)leaks occur the system can be
heavily damaged.

For measuring transient heat transfer it was required in the course
of this project to develop fast response thermometers. The construc-
tion and characteristics of the sensors are described in chapter 4.
In chapter 5 the arrangement of the experimental equipment passes in
review.

A part of the blow down loop for the supercritical helium flow avail-
able at Netherlands Energy Research Foundation ECN, had to be modi-
fied. The development of a fast response heater was a special prob-

lem. Because a lot of experimental data became available it was re-
quired to computerize the data handling.

The experimental results of chapter 6 are discussed in chapter 7 and
a correlation has been derived for predicting transient heat trans-
fer. Also the comparison between numerical data, based on a numerical
computer simulation model developed by other authors, and the present
experimental results will be discussed.

7. De toegestane dissipatie door kernfysische reacties in een tref-
   plaat gevuld met vloeibaar ^{3}He, welke op basis van natuurlijke
   circulatie wordt gekoeld, neemt aanzienlijk toe indien men een
   expansievaatje bovenin het koelcircuit opneemt.
   (Meyer, H.C., Postma, H., Bloem, W.B., Nucl. Instr. and Meth.
   Phys. Res. A 234 (1985) 421)

8. Voor een juiste verificatie van een numeriek rekenmodel zal de
   doorgerekende geometrie goed moeten aansluiten op de afmetingen
   van de testsectie waaraan de experimentele resultaten zijn ver-
   kregen. (Dit proefschrift)

9. Bij warmteoverdrachtsverschijnselen naar superkritisch helium
   speelt de Kapitza-weerstand geen rol van betekenis.
   (Dit proefschrift)

10. Daar in "donkere" perioden de ene teleurstelling wel eens snel
    volgt op de andere, is het goed te realiseren dat "na regen komt
    zonneschijn" alleen overdag geldt.

11. De extra meerprijs van exclusieve sportauto's door toepassing van
    duurzame metaallegeringen voor het plaatwerk zijn een fractie van
    de restauratiekosten van jaren later, indien normaal plaatijzer
    wordt gebruikt.

12. De fysicus is een energiezuinig mens.
    (Born, W., Stuit, M., Halverhout, H.A.M., Het volkomen kookboek,
    Zomer en Keuning, Ede (1984) 14)

13. Het komt het onderzoek bij research-instellingen niet ten goede als
    managementfuncties qua salariëring "beter af" zijn dan wetenschap-
    pelijke functies, daar na verloop van tijd medewerkers voortijdig
    van de laatste naar de eerste functie zullen proberen over te
    stappen.

14. Menigeen spreekt de afkorting kcal. op de verpakking van levens-
    middelen uit als calorie, zich niet realiserende dat de kleine
    toegevoegde k een geweldige dikmaker is.

STELLINGEN

behorende bij het proefschrift van Wim Bloem

1. Uit het oogpunt van thermische stabiliteit verdient het de voorkeur
   om bij de koeling van supergeleidende systemen met superkritisch
   helium te werken met een hoge heliumdruk. (Dit proefschrift)

2. De transiënte warmteoverdracht in holle supergeleidende kabels met
   interne koeling met superkritisch helium kan met een factor vier
   worden vergroot ten opzichte van bestaande systemen (SULTAN) door
   zowel de massastroom als door het warmteuitwisselend oppervlak met
   groeven te vergroten. (Dit proefschrift)

3. In economisch opzicht zal het voordeel van het koelen van super-
   geleidende magneetsystemen met superfluid helium wel eens groten-
   deels teniet kunnen worden gedaan door de strenge eisen die gelden
   voor de lekdichtheid van het koelcircuit.
   (Wipf, S.L., Proc. Stability of Superconductors, International
   Institute of Refrigeration, Paris (1981) 119)

4. Het vertrouwen van de mens in de techniek heeft deze eeuw twee keer
   een deuk opgelopen door het ontstaan van fatale lekkages, eerst in
   1912 toen de onzinkbare lijnboot Titanic op haar eerste reis verging
   en voor de tweede maal in 1986 bij de ramp met het ruimteveer
   Challenger.

5. Het verdient de voorkeur om bij de constructie van geforceerd
   gekoelde geleiders voor supergeleidende magneten zoveel mogelijk
   gebruik te maken van geprefabriceerde koelbuizen.
   (Plaum, J.M., Roeterdink, J.A., Priv. Comm. ECN (1986);
   Roeterdink, J.A., Elen, J.D., Franken, W.M.P., Proc. 9th Int.
   Conf. Mag. Tech., Zürich (1985) 402)

6. Bij samengestelde supergeleiders doet een roestvaststalen omhul-
   sel de stabiliteit toenemen, daar instabiliteiten veroorzaakt door
   het vrij komen van spanningen in het omliggende epoxymateriaal in
   thermische zin vrijwel niet door het staal heen komen.
   (Iwasa, Y., Apgar, B.A., Cryogenics 28 (1978) 267)

CHAPTER 2

INSTABILITIES

2.1. Superconducting materials and the origin of magnetic
instabilities

The superconducting state is characterized by condensation of the
conduction electrons of a metal into a state of lower energy. The
theory of Bardeen, Cooper and Schrieffer (BCS theory) [9] have shown
that this condensation can be explained in terms of an attractive
force between pairs of electrons (Cooper pairs), which is transmitted
via lattice vibrations (phonons) in the crystal. The strength of the
interaction peaks sharply when the electrons are in states of opposi-
te spin with equal and opposite momentum. It has the effect of in-
creasing their kinetic energy above that expected in the normal Fermi
distribution but of reducing their potential energy by a greater
amount, so that their total energy is reduced.
The firstly discovered superconductors, like e.g. tin, lead and mer-
cury, are known as "type I" superconductors. When these materials are
cooled below their critical temperature T_c and placed in a magnetic
field $B < B_c$ they will expell the magnetic flux from the interior of
the specimen (Meissner effect). This effect occurs when the specimen
enters the superconducting state and it is a reversible process inde-
pendent of the sequence of events reaching the superconducting state.
Type I superconductors are unsuitable to use for magnets, their cri-
tical field B_c is too small.
Fortunately, there exists another class of "high field" or type II
superconductors which react somewhat differently to magnetic fields.
This class includes all high field materials. Up to a certain lower
critical field B_{c1}, type II superconductors behave just like type I,
excluding the field completely. Above this field, however, they are
able to admit magnetic flux while remaining in the superconducting

state. Ginzburg, Landau, Abrikosov and Gorkov [18] formulated the
theory of type II superconductivity. They showed that the criterion
for type II behaviour is determined by the ratio $\kappa = \lambda/\xi$, the
Ginzburg-Landau parameter. Here, λ is the penetration depth of a mag-
netic field into a superconductor on microscopic scale and the coher-
ence length ξ is the range of interaction for the Cooper pairs. If κ
exceeds $1/\sqrt{2}$ the material is type II; the magnetic flux may enter the
superconductor at fields above B_{c1}. That means that the magnetic
field penetrates further than a coherence length in the superconduc-
tor.

The magnetic field penetration is in the form of discrete flux lines
or fluxoids, each carrying one quantum unit of magnetic flux
$\phi_o = h/2e$, where h is Planck's constant and e is the electronic
charge. The core of a fluxoid is in the normal state and it is en-
closed by a circular vortex of supercurrent. Fluxoids behave just
like Faraday's lines of force, exhibiting line tension and a force of
mutual repulsion perpendicular to the lines. As the field is in-
creased more fluxoids enter the specimen and the fluxoids are pushed
closer together. In a homogeneous crystal they will arrange them-
selves into a regular triangular lattice, which is the configuration
of lowest energy. When the field is further increased until the upper
critical field B_{c2} the normal cores overlap completely and the speci-
men has become entirely normal.

When an electrical current is flowing in a "clean" type II supercon-
ductor a Lorentz force will act on the fluxoids and they will start
to move in the conductor, producing a voltage drop across the speci-
men and causing it to develop a resistance. The critical current cor-
responds to the point at which the fluxoids start to move. Only when
the fluxoids are pinned down in the crystal lattice of the conductor,
the current will flow through the conductor without causing dissipa-
tion. Flux pinning is thought to be caused by forces between the
fluxoids and certain inhomogeneities in the crystal lattice. The core
of a fluxoid is in the normal state thus if the core of a fluxoid
resides on a small inclusion of normal metal, its energy will be

lowered because there is no longer any need to drive a previously
superconducting region normal. Examples of pinning centres are dislo-
cations, precipitates and lattice boundaries. Because the fluxoids
are arranged in a lattice only a few fluxoids have to be pinned
in order to position a lot of fluxoids in the crystal. However, the
distribution of the pinning centres in the crystal lattice does not
always fit with the triangular fluxoid lattice. When the electrical
current increases, the Lorentz forces on the fluxoids increase and
become larger than the repulsive fluxoid forces so that a fluxoid can
jump into a pinning centre (flux jump). It is also possible that a
whole fluxoid lattice will move (flux creep) because of the bad
"fitting" of the pinning centres and the fluxoid lattice. Flux jumps
and flux creep are dissipative processes. These magnetic instabili-
ties will produce heat and cause a temperature increase. On the other
hand the critical current (or pinning strength) falls with increasing
temperature and this will generally produce flux motion. When the
heat is not sufficiently absorbed or cooled away this is the start of
a chain reaction. Greater parts of the conductor become normal and
more heat is generated. The conductor quenches.

2.2. Mechanical instabilities

A superconducting system consists of various components like 1) the
conductors, 2) a substructure (construction supports, e.g. stainless
steel and impregnation resins) and 3) the cooling fluid (helium). If
the system is cooled down to low temperatures stresses will be in-
duced by different shrinkage of the components. In an electrically
loaded system the Lorentz forces on the conductors are considerably
large, especially in magnets. This induces also stresses in the
system. The stresses can cause conductor motion or epoxy breaking and
both attend heat releases. Besides the conductor motion and the epoxy
cracks resistive joints in the conductor are external sources for
heat releases.
It is stated by Iwasa [8] that conductor motion is the most important

source of external heat releases.

Calculations [11] have shown that a conductor motion over a distance
of $\approx$ 1 μm is sufficient to generate an energy density of $\approx$ 1 mJ/cm^3
in a conductor. To be harmful this small amount of energy must be
generated and delivered quickly to the conductor.

The effect of the mechanical instabilities is of significance in
superconducting systems because the heat capacities of the materials
are extremely small at 4.2 K, for example the specific heat of copper
at 4.2 K is 0.1 J/(kg K) and of stainless steel 2 J/(kg K), at room
temperature 383 J/(kg K) and 478/(kg K) respectively.

Measurements with acoustic emission techniques of Tsukomoto and Iwasa
[13] showed that the heat releases caused by conductor motion were
within one millisecond.

Bobrov et al. [10] concluded from a theoretical investigation on
epoxy-impregnated superconducting magnets that the most damaging pro-
cess is the cooldown during which large tensile stresses develop in
the resin because of the differential thermal contractions of the
epoxy and metal components. The tensile stresses are sufficient to
cause microcracks in the epoxy matrix, which occur at the epoxy-
conductor interface. These microcracks become sites for the initia-
tion of further cracks when the composite is subjected to Lorentz
force-induced stresses. The stresses lead to epoxy fracture, and
hence to dissipation of heat and finally to magnet quenches. The con-
clusion of Bobrov et al. was confirmed by experiments [12].

2.3. Stability criteria

When a flux jump occurs in a superconductor there is a movement of
magnetic flux through the specimen, but because of the dissipative
character of the jump also heat will be released. The flux as well as
the heat will diffuse through the conductor and it depends on the
diffusivities which quantity moves faster. The magnetic flux can in-
troduce another flux jump and the accompanying heat pulse gives a
temperature rise ΔT_1 in the superconductor. An increase in tempera-
ture leads to reduction in the critical current density J_c (T). Also
the magnetic penetration depth λ_m is a function of temperature, e.g.
the London penetration depth $\lambda_m = \lambda_{mo}[1 - (T/T_c)^4]^{-0.5}$; the magnetic
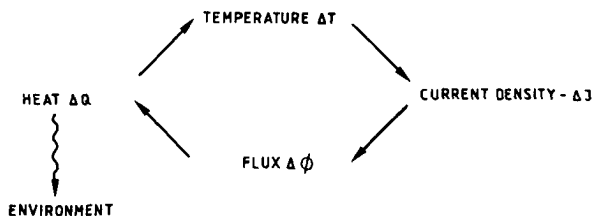
Figure 2.1   Chain of events in a superconductor in case of the
occurrence of an instability.

field penetrates further into the bulk superconductor. This latter
flux movement leads to a temperature rise ΔT_2 (see Fig. 2.1).
If $\Delta T_2 < \Delta T_1$ then the temperature rise reaches asymptomatically a
final value after many cycles and the situation becomes stable. If
$\Delta T_2 > \Delta T_1$ then the temperature rise will increase and a thermal run-
away or catastrophic flux jumps will occur. The quantitative evalua-
tion of this heating process is complicated as some heat escapes from
the superconductor to the environment by thermal diffusion.
As was said, the heating depends on the speed of the thermal diffu-
sion (a_T) by which heat is removed and the magnetic diffusion (a_M) by
which flux $\Delta\phi$ is admitted. The thermal diffusivity a_T is given by
$\lambda/(\rho c_p)$ (λ is the thermal conductivity, ρ the specific mass (den-
sity), c_p isobaric specific heat) and the magnetic diffusivity a_M by
ρ_e/μ_o (ρ_e electrical resistivity, μ_o vacuum permeability).
Compilation of some values of λ, ρ, c_p and ρ_e at 4.2 K shows that
there are differences between "pure" metal conductors (e.g. typical
high conductivity copper) and alloys (e.g. cupro-nickel or supercon-
ducting materials in the normal state). We can make the following
simple generalizations:

    i)   in pure metals, heat moves much faster than magnetic flux,

    ii)   in alloys, magnetic flux moves much faster than heat,

    iii) a_T for a superconducting material is roughly the same as a_M
        for a pure metal.

This effect is demonstrated in Table 2.1 for copper and NbTi.

With this knowledge it is possible to construct a superconductor
which can absorb small heat releases. We can distinguish the next
methods of stabilization.

	Copper				$Nb_{41}Ti_{59}$
RRR	100		300		
B (T)	0	6	0	6	0
λ (W/(m K))	90	37	300	112	0.325
c_p (J/(kg K))	0.1	0.1	0.1	0.1	0.5
ρ (kg/m³)	8900	8900	8900	8900	6200
ρ_e (Ω m)	$1.57\ 10^{-10}$	$4.47\ 10^{-10}$	$5.18\ 10^{-11}$	$3.2\ 10^{-10}$	$55\ 10^{-8}$
a_T (m²/s)	0.1	0.04	0.33	0.126	$1.05\ 10^{-4}$
a_M (m²/s)	$1.25\ 10^{-4}$	$3.56\ 10^{-4}$	$4.12\ 10^{-5}$	$2.55\ 10^{-4}$	0.44

Table 2.1. Thermal and magnetic diffusivity of copper and NbTi.

RRR = Residual Resistance Ratio = $\rho_{e,300K}/\rho_{e,4.2K}$

$\mu_o = 1.2566\ 10^{-6}$ m kg/C²
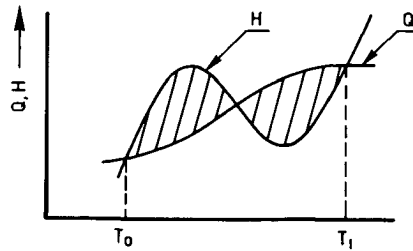
$\rho_{Nb} = 8570$ kg/m³, $\rho_{Ti} = 4540$ kg/m³

Figure 2.2 Equal area criterion for boiling helium heat transfer.

2.3.1. Cryostatic stabilization

The superconducting material is embedded as a single wire in copper
of high electrical conductivity. When the superconductor becomes nor-
mal the electrical current will flow through the copper because of
its lower electrical resistivity compared to the normal state of the
superconductor. On the other hand the heat transport to the cooling
fluid is good because of the large thermal conductivity of copper.
When the heat transport velocity is larger than the heat production
the conductor is stable.
If the superconductor temperature rises to a temperature T_c (by any
reason) at a governing magnetic field the electrical current I_c is
flowing through the copper with resistivity $\rho_{e,Cu}$ and cross section
A_{Cu}. Is f the fraction superconductor and 1-f the copper fraction in
the conductor with total cross section A, then the critical current
I_c is defined by $I_c = f \, A \, J_c$. The generated heat per unit length is

$$\rho_{e,Cu} \, I_c^{\ 2} \, / \, A_{Cu} = \rho_{e,Cu} \, \frac{f^2}{1-f} \, A \, J_c^{\ 2} \ . \tag{2.1}$$

On the other hand the heat is transferred to the cooling fluid at a
temperature T_o. The transferred heat per unit length is given by
$h \, D_w \, (T_c - T_o)$; h the heat transfer coefficient and D_w the wetted
perimeter. The normal region formed in the conductor will recover
when $\alpha < 1$, where the Stekly parameter α is defined as:

$$\alpha = \frac{\rho_{e,Cu} f^2 \, J_c^{\ 2}}{(1-f) \, h(T_c - T_o)} \, \frac{A}{D_w} \ . \tag{2.2}$$

This Stekly criterion is a steady state solution and no axial heat
conduction effects are included. It was the first reliable cure for
coil degradation and has formed the basis of all large superconduct-
ing magnets since it was invented by Kantrowitz, Stekly and Zar
[14,15] in 1965.
Maddock, James and Norris [16] derived a theory in which the axial

heat conduction between hot and cold zones in the conductor are taken into account. When the heat is generated by an amount $Q(T)$ (per unit volume) and the heat transfer to the coolant is given by a function $H(T)$ (per unit area), Fig. 2.2, then the one-dimensional equation of heat conduction along the conductor is

$$\frac{d}{dz} \left(A \lambda(T) \frac{dT}{dz} \right) = D_w H(T) - A Q(T) \quad . \tag{2.3}$$

Substituting $S = \lambda(T) \frac{dT}{dz}$ so that $\frac{dS}{dz} = \frac{dS}{dT} \frac{dT}{dz} = \frac{dS}{dT} \frac{S}{\lambda(T)}$ and integrating (2.3)

$$\int_{S_0}^{S_1} S\,dS = \frac{1}{2} S^2 \Big/ \begin{matrix} S_1 \\ S_0 \end{matrix} = \int_{T_0}^{T_1} \lambda(T) \left\{ \frac{D_w}{A} H(T) - Q(T) \right\} dT \quad . \tag{2.4}$$

It is assumed that for the ends of the conductor the heat transfer to the coolant and the generation are equal $\big(H(T) = Q(T) \big)$. This can be for one end the superconducting state at coolant temperature T_0 and for the other end a temperature T_1 at which heat transfer and generation are in balance. At the ends the derivative $\frac{dT}{dz} = 0$, thus $S_1 = S_0 = 0$ and if $\lambda(T)$ does not depend on temperature, eq. (2.4) reduces to

$$\int_{T_0}^{T_1} \left\{ \frac{D_w}{A} H(T) - Q(T) \right\} dT = 0 \quad . \tag{2.5}$$

This criterion is the equal area criterion. The hatched areas in Fig. 2.2 between the generation and cooling curves should be enclosed although locally the generation can be larger than the cooling. The Stekly criterion is more restrictive because it requires that anywhere cooling is larger than generation.

2.3.2. Intrinsic stabilization

The modern superconducting wires were developed during the last 20 years when it was discovered that a fine subdivision of the supercon-ducting material in filaments in the copper matrix reduces the ten-tendency of flux jumps.

2.3.2.1. Adiabatic stability.

Firstly, fine subdivision in filaments reduces the distance which flux is able to move through the superconducting alloy and thus the energy which can be released by a given magnetic disturbance. When an external magnetic field is shielded by a current density J_c and a temperature disturbance ΔT_1 occurs after a little heat release, the field will penetrate the conductor. Because in the superconducting alloy $a_M > a_T$ the heat cannot escape easily (adiabatic condition) and there will be a further increase of temperature; ΔT_2. If $\Delta T_2 < \Delta T_1$, the system is stable against small perturbations. Wilson et al. [17] and later Brechna [18] presented an adiabatic theory in which they derived a maximum filament thickness (diameter) d_{fa} of a superconduc-tor for which it stays stable for small disturbances;

$$d_{fa} < \frac{1}{J_c} \sqrt{\frac{3\rho \, c_p \, T_0}{\mu_o}} \quad . \tag{2.6}$$

The specific heat c_p and the thermal conductivity λ refers to the superconducting alloy and T_0 is defined by $T_0 = J_c/(-\partial J_c/\partial T)$. For NbTi and Nb_3Sn T_0 can be approximated as $T_c - T_s$ due to the linear dependence of J_c on temperature. T_s is the temperature of the conduc-tor before the onset of the instability. Rewriting eq. (2.6) using $T_0 = T_c - T_s$ gives

$$\frac{\mu_o \; J_c^{\;2} \; d_{fa}^{\;2}}{\rho \; c_p (T_c - T_s)} \; = \; \beta \; < \; 3 \tag{2.7}$$

where β is defined as the stability parameter.

For completeness it should be mentioned that the equation above, in addition to indicating the use of finer superconducting filaments, also suggests two other ways of preventing flux jumps:

i)   increasing ρc_p, by incorporating in the conductor a high thermal capacity material such as lead;

ii) decreasing J_c. This is, of course, unattractive from a magnet design point of view, but it provides the explanation for improved stability of superconducting coils when immersed in a higher magnetic field.

2.3.2.2. Dynamic stability.

A second benefit of fine subdivision in filaments is the improvement in cooling. Superconducting alloys have a very low thermal conductivity and fast flux jumping in bulk material can be regarded as an adiabatic process. If the superconductor is finely divided and embedded in a good conducting normal metal, the heat generated by flux motion will be conducted away. In addition, however, the magnetic damping of the normal conductor caused by eddy currents slows down flux motion to allow more time for heat conduction. In other words, the situation is changed from the superconducting bulk material, where the magnetic diffusivity a_M >> thermal diffusivity a_T, to a matrix material where a_T >> a_M. This is called dynamic stability. Various authors [7, 17, 18] derived correlations for a maximum filament thickness. The thicknesses are all a function of the superconductor fraction f, the electrical resistivity ρ_e of the matrix material (copper) and the thermal conductivity λ of the filament. Only the maximum limit for d_{fd} differs by the authors (different numerical constants). The value of d_{fd} is given by Wilson et al. [17]:

$$d_{fd} < \frac{1}{J_c} \sqrt{\frac{32 \; \lambda(1-f)}{f} \; \frac{T_c - T_s}{\rho_e}} \quad . \tag{2.8}$$

The dynamic stability had to be satisfied for stability against flux jumps, but it does not fully guarantee stability (e.g. influences of microcracks).

The dynamic criterion is a weaker condition than the adiabatic condition. For example the ratio of the two critical diameters is given by

$$\frac{d_{fa}}{d_{fd}} = \sqrt{\frac{3}{8} \; \frac{a_{M_m}}{a_{T_s}} \; \frac{f}{1-f}} \quad . \tag{2.9}$$

Here, a_{M_m} is the magnetic diffusivity of the matrix (e.g. copper) in which the superconducting filaments have been embedded and a_{T_s} the the thermal diffusivity of the filaments. From Table 2.1 it can be seen that the diffusivities are of the same order, thus the ratio is determined by the superconductor fraction.

2.4. Time scale

To give an indication on which time scale the instabilities occur a slab of superconducting material of thickness d is considered. In case of thermal diffusion the ends of the slab are kept at zero temperature ($T = 0$ at $x = 0$ and $x = d$) and the initial temperature is $T = f(x)$, with $0 < x < d$.
The differential equation to be solved is

$$\frac{\partial T}{\partial t} = a_T \frac{\partial^2 T}{\partial x^2} \quad . \tag{2.10}$$

The equation has solutions of the form (Carslaw and Jaeger [19])

$$T = \sum_{1}^{\infty} A_n \sin \frac{n \pi x}{d} \ e^{-a_T n^2 \pi^2 t/d^2} \quad . \tag{2.11}$$

The dominant term $(n = 1)$ will decay with a characteristic time

$$\tau_T = \frac{d^2}{\pi^2 a_T} \quad . \tag{2.12}$$

In a similar way we can define a characteristic time for the magnetic diffusion

$$\tau_M = \frac{d^2}{\pi^2 a_M} \quad . \tag{2.13}$$

In this slab geometry it is possible to define a characteristic time for the cooling at the surface. When the heat transfer coefficient between the slab and the cooling fluid has the value h, then the temperature of the slab varies per unit time by an amount $\frac{dT}{dt}$ according to (slab symmetry at $x = \frac{1}{2} d$, both sides cooled)

$$\rho \ c_p \ \frac{d}{2} \ \frac{dT}{dt} = h \ \Delta T \quad . \tag{2.14}$$

We can define a characteristic time τ_h for surface cooling, which is given by

$$\tau_h = \frac{\rho \ c_p \ d}{2h} \quad . \tag{2.15}$$

The ratio of τ_h and τ_T

$$\tau_h/\tau_T = \frac{\pi^2}{2} \quad \frac{\lambda}{h\ d} \tag{2.16}$$

gives an impression for the importance of good cooling at the surface of the conductors.

For example for copper (RRR = 300) with λ = 300 W/(m K), slab thickness of 1 mm and h = 1000 W/(m^2 K) (steady state), the ratio τ_h/τ_T = 1480. Surface cooling is thus like magnetic diffusion (see Table 2.1) a slower process than heat conduction. It depends on the value of h, and because the instabilities are transient effects it is desirable to know h in the transient region, especially because $h_{transient}$ is larger than the steady state value of the heat transfer coefficient. A better knowledge of the transient heat transfer can contribute to better conductor designs in protection against instabilities.

For copper at 4.2 K τ_T is $3.4*10^{-7}$ s (d = 1 mm) and as we will see h_{tr} = 0.5 $\sqrt{\pi\lambda\rho c_p/t}$ = 0.5 $\sqrt{\pi\lambda\rho c_p/\tau_T}$ $\approx$ $1.5*10^5$ W/(m^2 K) (λ, ρ and c_p of the cooling fluid at 4.2 K) gives a ratio τ_h/τ_T of about 9.7. This is an enhancement of a factor 150 in comparison with the steady state value of 1480. The heat transfer approaches the rate of the heat conductivity mechanism. When not well purified copper is used λ can decrease with a factor 3 (Table 2.1) and working at high magnetic fields (e.g. B = 6 T) λ decreases also with a factor 3. So, it is possible that in real superconducting systems the ratio τ_h/τ_T reaches the value 1, then heat transfer and heat conduction are mechanisms of the same order. On the other hand, the RRR value is a function of the temper of the copper. Thus annealing and bending processes have their influences on the final state of copper. According to the experiments of Fickett [20] the RRR value decreases when the copper becomes harder. When a hard copper sample is reannealed the RRR reaches a peak at an anneal temperature of about 400°C.
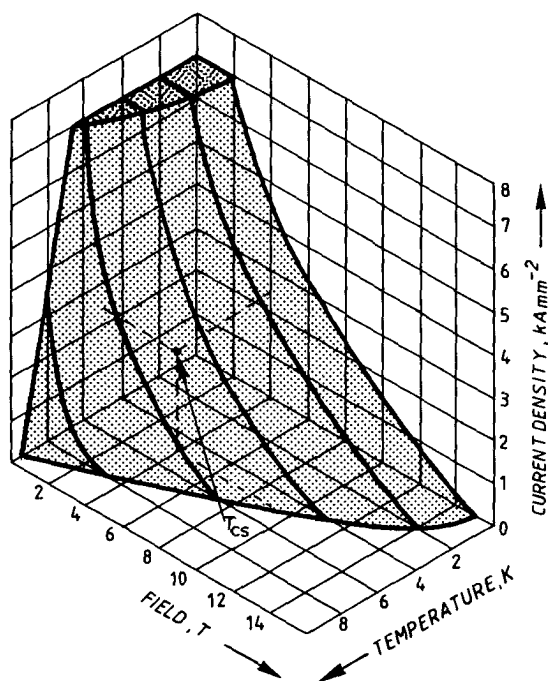
Figure 3.1   Superconducting region of NbTi.

CHAPTER 3

COOLING MODES FOR SUPERCONDUCTING SYSTEMS

3.1. Helium as cooling fluid

Apart from the technical realization, the choice of a cooling system
is determined by two main parameters: the level of temperature re-
quired and the heat exchange capacity.

The temperature level must be one or two degrees below the current
sharing temperature T_{cs} of the superconductor used. This temperature
is a function of the operating point defined by the magnetic field
and current density. T_{cs} is the temperature at the critical current
surface of a superconductor (Fig. 3.1). It approaches the critical
temperature T_c when B goes to zero and J goes to zero.

For commercially available NbTi alloys the current sharing temperature
values corresponding to a current density of 0.5 kA/mm^2 are approxi-
mately 6 K at 5 T, 4.5 K at 8 T and 2 K at 12 T. For a given field,
the operating temperature directly determines the current density
permissible in the superconductor.

The heat transfer has to be designed in such a manner that it will
operate under different conditions, which can be classified as fol-
lows:

- steady state regime, to remove the heat input from the cryostat and
  links (mounting, electrical), the local heat release of a (stable)
  defect in the conductor or a nonsuperconducting joint;

- transient regime to absorb the perturbation affecting the system
  which are due to current or field fluctuations, mechanical instabi-
  lities or to the penetration of nuclear radiation.

Because the superconducting systems operate at very low temperatures
it is obvious that the only fluid permitting these temperature levels
is helium. It might be well to realize that there are striking dif-
ferences between the behaviour of conventional fluids, such as water
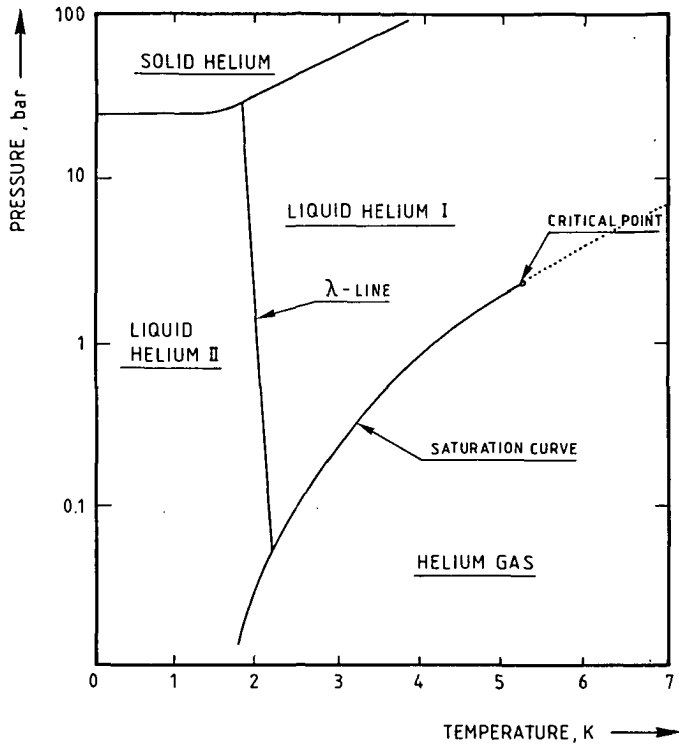and air, and helium. For helium, small pressure and temperature

Figure 3.2   Phase diagram of ^{4}He (critical pressure p_c = 2.2746 bar, critical temperature T_c = 5.2014 K). Dotted line marks the transposed critical curve.

ranges enclose the various fluid phases, Fig. 3.2. The critical point
is given by p_c = 2.27 bar, T_c = 5,2 K and ρ_c = 69.64 kg/m³. The
transposed critical line represents the maxima in the specific heat
and can be seen as an extension of the evaporation line. Helium will
only solidify under high pressure at low temperatures. Below the
λ-line liquid helium condensates into a quantum state and becomes
superfluid. Superfluid helium has zero viscosity and it is quite im-
possible that there will exist temperature gradients in the fluid.
The helium properties, specific heat, thermal conductivity, density
and viscosity in the supercritical phase are shown in the
Figs 3.3 - 3.6.
As can be seen from these figures, the properties alter markedly near
the transposed critical line, especially nearby the critical point.
There are three forms of cooling modes for superconducting system
with helium at low temperatures:
- boiling normal liquid helium (He I), pool or forced flow;
- supercritical helium   (He I);
- superfluid helium   (He II), pool or forced flow.

3.2. Cooling by boiling He I

3.2.1. Pool boiling

Heat transfer from solid surfaces to liquid helium I can be charac-
terized by three different states, as function of the heat flux per
unit surface area.

i.   At low heat fluxes, heat transfer takes place by conduction and
      convection.
ii.   With increasing heat flux bubbles appear on the surface which
      leads to an enhancement of the heat transfer followed by a
      steady increase in temperature difference ΔT between surface and
      bath temperature with increasing heat flux. The formation of
      bubbles takes place in cavities on the surface. Nucleate boiling
      depends on
      - surface roughness,
      - surface material,
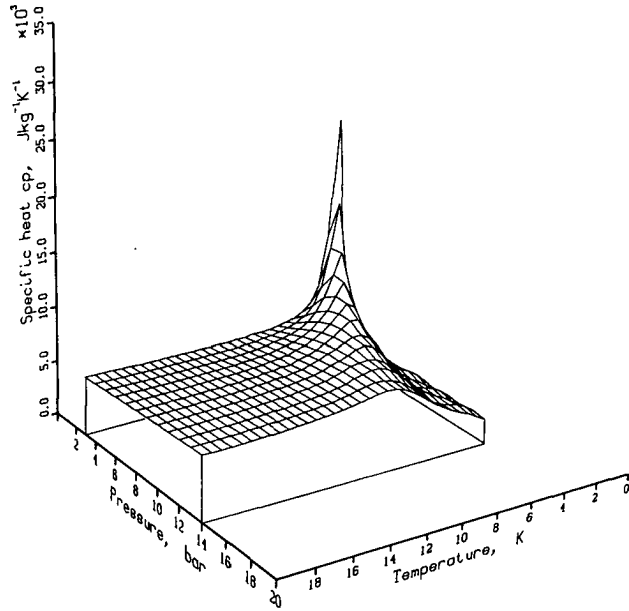   - surface condition (clean, oxidized, coated, etc.).

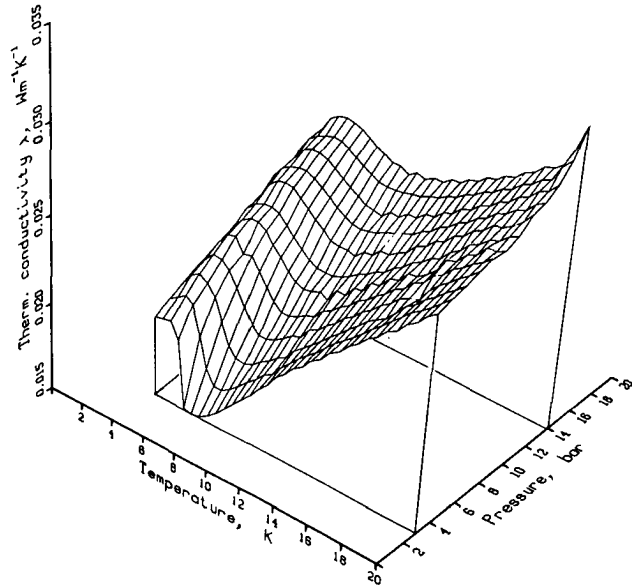Figure 3.3   Specific heat of ^{4}He as a function of temperature and pressure.

Figure 3.4   Thermal conductivity of ^{4}He as a function of temperature and pressure.
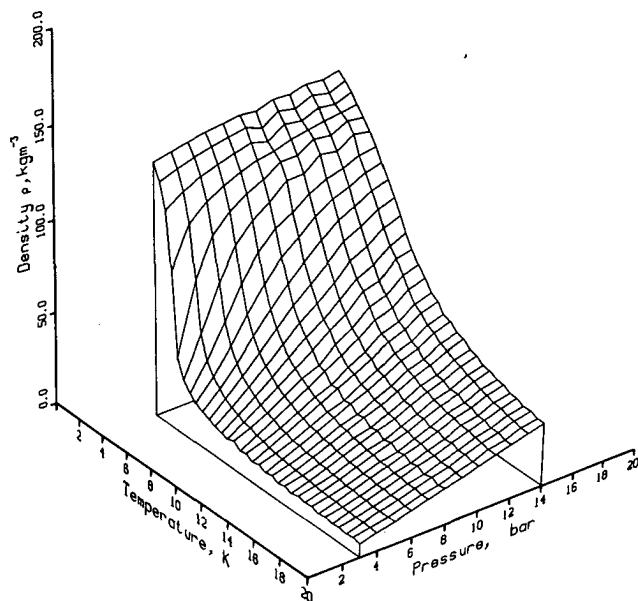
Figure 3.5   Density of ^{4}He as a function of temperature and
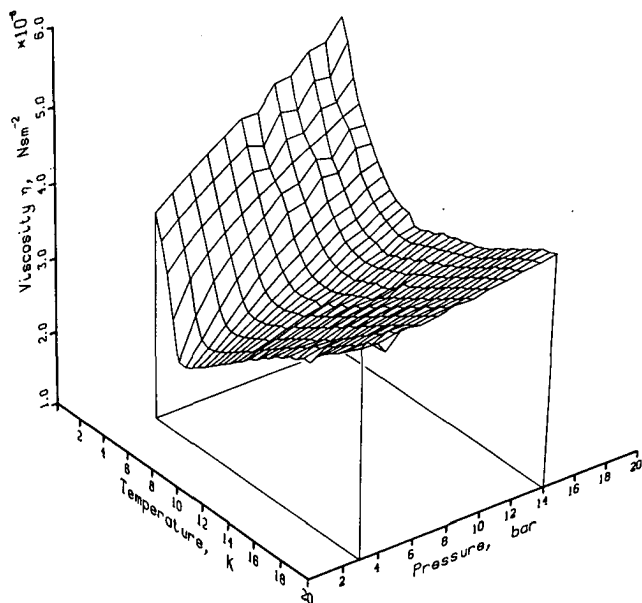pressure.

Figure 3.6   Viscosity of ^{4}He as a function of temperature and
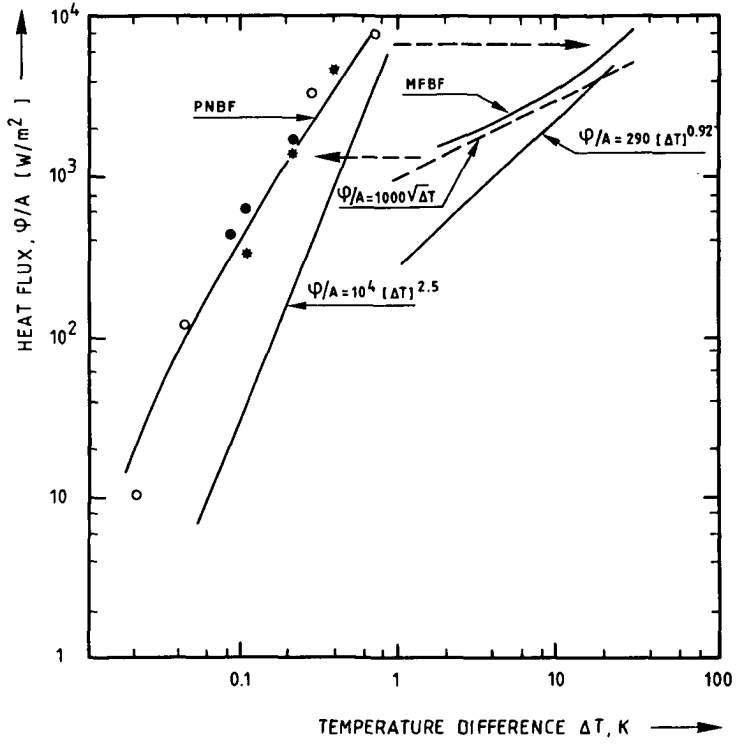pressure.

Figure 3.7   Steady state heat transfer characteristic of helium I at
4.2 K and 1 bar.

In first approximation the heat flow per unit area (φ/A) as
function of the temperature increase (ΔT) in the nucleate boil-
ing range may be fitted to the relation $\phi/A = c \cdot \Delta T^m$, where m in
most experiments lies between 2 and 3 and c scatters over a wide
range. Schmidt [21] proposed $c = 10^4$ and m = 2.5 for a conserva-
tive approach in stability calculations (ϕ/A in W/m^2). Most re-
sults reported in literature are on the left of this line. Fig.
3.7 shows the steady state heat transfer curve at 4.2 K, which
is composed of experimental results [22, 23] concerning polished
surfaces and the curve proposed by Schmidt.

iii. Beyond a certain critical heat flux, the peak nucleate boiling
flux (PNBF), a temperature jump of the order of 10 K occurs due
to the formation of an insulating gas film on the surface. As
the heat flux decreases, the temperature jumps back to the
nucleate boiling curve which occurs at a heat flux below the PNBF,
typically between 1 and 2 kW/m^2, the minimum film boiling flux
(MFBF). For surfaces facing upward the PNBF is of the order of 9
kW/m^2 and seems not to depend very much on the surface condi-
tion. The experiments of Lyon [22] showed that the angle of in-
clination of the surface is a parameter of the PNBF, Fig. 3.8.
The heat transfer coefficient in the film boiling regime is more
than an order of magnitude below that of the nucleate boiling
regime. Cumming and Smith [24] proposed to fit the experimental
data for film boiling on horizontal surfaces with the relation:

$$\phi/A = 290 \ \Delta T^{0.92} \qquad (W/m^2) \quad . \tag{3.1}$$

Ogata and Nakayama [25] did experiments on heat transfer to
boiling helium from machined and chemically treated copper sur-
faces. They concluded that in the film boiling regime the heat
transfer is improved by methods which
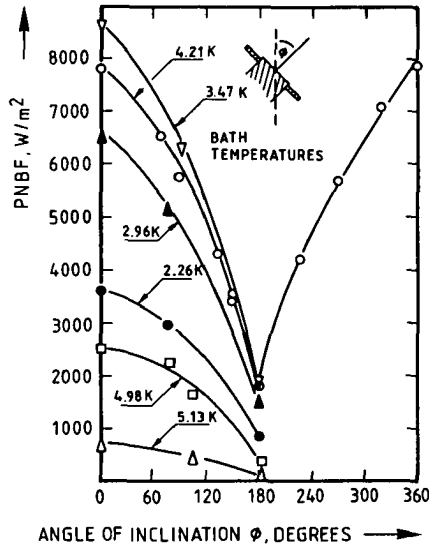
Figure 3.8   Nucleate boiling maximum for a platinum surface in
              liquid helium versus surface inclination (from Lyon [22]).

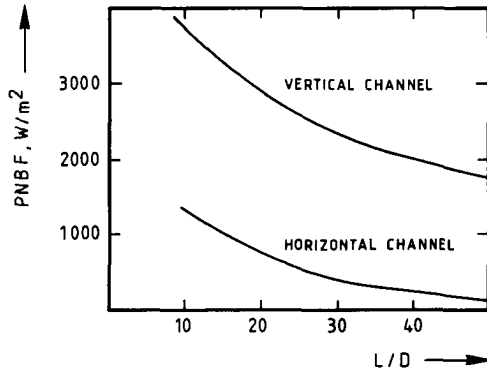Figure 3.9   Peak nucleate boiling flux in uniformly heated channels
              filled with boiling helium I at 1 bar (vertical channel
              from Lehongre et al. [26], horizontal channel from
              Bailey et al. [27]).

1. increase the real surface area by means of grooves and fins;
2. employ surface structures that facilitate removal of vapour
   bubbles. Recommended minimum width of the grooves is about
   0.3 mm to avoid blanketing the grooves by vapour;
3. oxidation of the surface helps to improve the transition from
   film boiling to nucleate boiling regime (the MFBF becomes
   higher).

When cooling channels are used the boiling process becomes quite
complex. In vertical cooling channels the liquid circulates due to
the thermosiphon action induced by the ascending bubbles. With in-
creasing heat flux film boiling starts at the top of the channel and
propagates to the bottom. The PNBF at the bottom of the channel can
reach more than twice the value at the top. Lehongre et al. [26] de-
rived an empirical formula which predicts the PNBF as function of the
distance of the top of the channel, namely

$$PNBF = \frac{10^4}{1.7 + 0.125 \ (L/D)^{0.88}} \qquad (W/m^2) \quad . \qquad (3.2)$$

Here, D is the hydraulic diameter (4 * cross section / wetted peri-
meter) and L the distance from the top of the tube. For horizontal
channels the PNBF is much lower as can be seen in Fig. 3.9. Beyond an
L/D ratio of 70 the PNBF is nearly constant for horizontal channels
($\approx$ 100 W/m^2) [27].

3.2.2. Forced flow cooling of two phase He I

In addition to cooling by a forced flow of liquid helium flowing
through tubes it is possible to stir the helium in which a supercon-
ducting system has been immersed. Tsuruga and Endoh [28] studied ex-
perimentally the heat transfer from a vertical copper surface sub-
merged in circulating helium. The helium was circulated in the dewar
by using a propeller.

The heat transfer increased with the increase of the liquid helium
velocity in the convective heat transfer region. The data in the con-
vective region were correlated with an empirical equation as Nusselt
number (Nu = hD/λ) versus Reynolds number (Re = $\rho vD/\eta$) and Prandtl
number (Pr = $c_p\eta/\lambda$), given by

$$Nu = 0.15 \; Re^{2/3} \; Pr^{1/3} \; . \qquad\qquad (3.3)$$

The PNBF decreased and the MFBF increased with increasing flow velo-
city. A PNBF is known to increase with flow velocity. This discre-
pancy is thought to be due to the geometry of the experimental appa-
ratus. Bubbles, which are generated at the heat transfer surface move
upwards slowly, because of its small diameter. The number of bubbles
may increase with flow velocity, then apparently the density for
liquid helium decreases. This might cause the low PNBF.

As was mentioned before, an induced flow of helium occurs by thermo-
siphon action in heated vertical channels with stagnant liquid
helium. Although there is no pump, this phenomenon is a kind of for-
ced flow cooling. Results were reported by Johannes and Mollard [29]
and they derived two equations which decribe the heat transfer within
20% of the measured data. The equations are functions of the heated
length L and the hydraulic diameter D;

$$\text{for } L/D \le 50 \qquad Nu = 5.5 \; Re^{0.8} \; x^{0.8} \; (y/D)^{-0.8} \qquad (3.4)$$

$$\text{for } \; 0 < x < 1$$

$$\text{for } L/D > 50 \qquad Nu = 0.24 \; Re^{0.8} \; x^{0.8} \qquad\qquad (3.5)$$

$$\text{for } \; 0 < x < 1 \; .$$

Here, y is the distance from the entrance of the channel and x the quality of the flow. The quality is a function of the enthalpies of vapour and liquid phase and is defined by

$$x(y) = \frac{H(y) - H_{sat.liquid}}{H_{sat.vapour} - H_{sat.liquid}} \qquad . \qquad (3.6)$$

H(y) is the enthalpy at distance y, and the intervals of the quality are

    x = 1   saturated vapour
    x > 1   superheated vapour
    x = 0   saturated liquid
    x < 0   subcooled liquid

    0<x<1   two phase region; the quality has the conventional
                 meaning of the ratio of vapour-mass and mixture mass
                 (or mass flow respectively)

$$x = \frac{\dot{m}_v}{\dot{m}_v + \dot{m}_l} \qquad . \qquad (3.7)$$

Johannes [30] realized that the development of helium I forced convection cooling systems could be an important key to solving some of the problems that superconducting magnet designers were facing in those days. Some of the advantages compared with the conventional pool boiling systems were simple cryostat design, modest refrigeration requirements (refrigerator directly coupled to the magnet coils), cooldown operations simplified and electrical insulation problems eliminated (due to a more rigid construction).
During the last 15 years some data on heat transfer to liquid helium flowing through tubes were published. Shah [31] compared data for various cryogenic fluids like argon, nitrogen, neon and helium, and

presented a correlation which predicts the heat transfer during boil-
ling of these liquids flowing in tubes. The correlation is a function
of the orientation of the tubes and can be mathematically expressed
by

$$h_{tp} = \psi \, h_1 \tag{3.8}$$

with h_{tp} the desired two phase heat transfer coefficient and h_1 the
superficial heat transfer coefficient of the liquid phase. To calcu-
late h_1, the following correlation known as the Dittus-Boelter equa-
tion [79]

$$h_1 = 0.023 \left(\, Re_1(1-x) \right)^{0.8} Pr_1^{0.4} \, \frac{\lambda_1}{D} \tag{3.9}$$

has to be used.
The quantity ψ is a function of the state of the flow, which is
characterized by the parameter N. The dimensionless parameter N is
defined by the Froude number of the liquid phase Fr_1 and a parameter
Co which is determined by the ratio of vapour and liquid in the flow,

$$Fr_1 = \frac{G^2}{\rho_1^2 \, g \, D} \tag{3.10}$$

$$Co = (\frac{1}{x-1})^{0.8} \, \frac{\rho_v}{\rho_1} \tag{3.11}$$

with g the acceleration due to gravity and ρ_1, ρ_v the density of
liquid and vapour respectively and G the mass velocity ($G = \dot{m}/A$, $\dot{m}$
is mass flow, A is cross section).
In case of vertical tubes at all values of Fr_1 and in case of hori-
zontal tubes with $Fr_1 \geq 0.04$

$$N = Co \tag{3.12}$$

For horizontal tubes with $Fr_l < 0.04$

$$N = 0.38 \ Fr_l^{-0.3} \ Co \quad . \tag{3.13}$$

Considering first the special case with all the fluid is in the liquid phase. Then ψ is given by

$$\psi_o = 230 \ \sqrt{Bo} \quad . \tag{3.14}$$

In this empirical relation of Shah Bo is the boiling number defined by the quotient of the released heat per unit area, ϕ/A, and the total latent heat of vaporization of the fluid

$$Bo = \frac{\phi/A}{G \ q_{lv}} \tag{3.15}$$

with q_{lv} being the latent heat of vaporization.

For $N>1$, $\quad \psi_{nb} = \psi_o \qquad$ (nucleate boiling) $\qquad$ (3.16)

$$\psi_{cb} = 1.8 \ N^{-0.8} \quad \text{(pure convective boiling)} \tag{3.17}$$

ψ is the larger value of ψ_{nb} and ψ_{cb}. Thus, if $\psi_{nb} > \psi_{cb}$, $\psi = \psi_{nb}$; if $\psi_{cb} > \psi_{nb}$, $\psi = \psi_{cb}$.

For $0.1<N\leq1$, ψ is the larger of ψ_{cb} and ψ_{bs}, where ψ_{cb} is given by eq. 3.17 and

$$\psi_{bs} = F\psi_o \exp(2.74 \ N^{-0.1}) \ \text{(bubble suppresion regime)} \quad (3.18)$$

For $N \leq 0.1 \quad \psi = \psi_{bs} = F\psi_o \exp(2.47 \ N^{-0.15})$. $\hspace{2cm}$ (3.19)

The empirical constant F is defined as

$$F = 0.064 \quad \text{when} \quad Bo \geq 11 \cdot 10^{-4} \hspace{2cm} (3.20)$$
$$F = 0.067 \hspace{1.5cm} Bo < 11 \cdot 10^{-4} \ .$$

It is stated by Shah that this correlation gives much better agree-
ment with data on forced flow boiling He I than other correlations.
Nine out of the eleven data sources available to Shah agree with the
correlation.
Subbotin et al. [32] derived from their experimental results an empi-
rical correlation which predicts the PNBF in cooling channels as
function of the quality x of the flow. The PNBF at which heat trans-
fer deterioration occurs is a complex function of the main operating
parameters like pressure, mass velocity G and flow quality x. Figure
3.10 shows the typically critical heat flux dependences on quality
when pressure and mass velocity are constant. If the mass velocity is
not high, three distinct parts of the curve can be seen (Fig. 3.10A).
The low quality range is characterized by high peak nucleate boiling
fluxes ($\phi_{PNBF} > 1500 \ W/m^2$). The magnitude of ϕ_{PNBF} decreases practi-
cally linearly when x increases. At intermediate values of x the PNBF
drops abruptly in a quite narrow quality range.
Here a critical quality x_c can be defined when this happens. For high
values of $x > x_c$ the PNBF is very low ($\phi_{PNBF} < 500 \ W/m^2$).
When pressure and mass velocity are increased the discontinuity dis-
appears slowly up to its complete disappearance (Fig. 3.10B). It was
found by Subbotin that x_c depends mainly on the mass velocity and
does not alter significantly with pressure.

Although the empirical correlations can predict the heat transfer
behaviour it still remains a problem that the small latent heat of
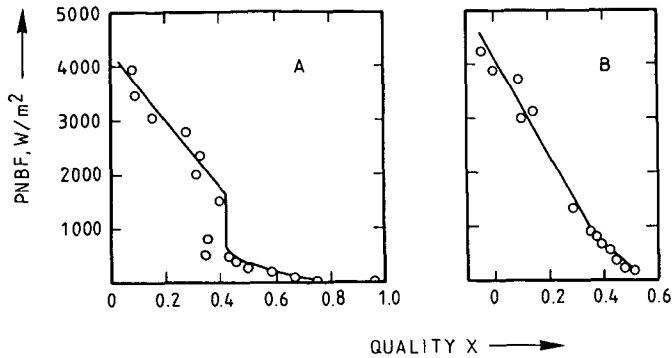vaporization (for He under 1 bar 20.5 J/g, for H_2O under 1 bar

Figure 3.10 Peak nucleate boiling flux versus quality x in a flow of
            boiling helium I.
            A. pressure 1.18 bar, mass flow rate G = 86 kg/(sm^2)
            B. pressure 1.76 bar, mass flow rate G = 211 kg/(sm^2)
            From Subbotin et al. [32].

2.26 kJ/g) and the drastic expansion to the vapour phase makes such
flow systems highly unstable with respect to local hot spots.
For large coils with long cooling channels the evaporated helium will
accumulate in the upper parts of the windings and become parts of
poorer cooling. At these places the pressure difference along the
conductor drops and the liquid will flow in an irregular manner. Thus
the remaining section of the coil will be pulse-cooled. The same ef-
fect occurs when a garden hose is badly connected to a tap, so this
phenomenon of bad cooling is called the "garden hose effect".
For superconducting coils, used in rotating systems like generators,
problems occur when liquid helium flows to the outer wall of the con-
ductor under influence of the centrifugal force. The gaseous helium
accumulates on the inner wall. Here the inner wall of the forced flow
cooled conductor becomes part of poorer cooling.
Although the forced flow cooled systems have advantages above pool
boiling, the afore-said examples show that there still exist problems
on cooling by forced flow helium I.

3.3. Supercritical helium

The unique property of helium of having a low critical pressure
2.27 bar) and the reluctance of helium to solidify under pressures up
to 100 bar at 4.2 K (Fig. 3.2), makes it possible to operate a cool-
ing circulation system under high pressures. Since there is no dis-
continuous change in physical properties above the critical point, or
in effect no definite distinction between the liquid and gaseous
phases, the heat transfer phenomena can be referred to one phase. At
a temperature of 4.2 K the pressure has to be larger than 2.27 bar
for operating the system in the supercritical phase. If the system is
operated at low pressures (< 5 bar) and the temperature rises, the
helium properties will alter drastically near the transposed critical
line.
Operating in that region can introduce flow instabilities and it
seems therefore favourable to operate the system at higher pressures
(> 6 bar) because the variations of the properties become less signi-
ficant.

The first experiments to get data for forced convection heat transfer
to supercritical helium were carried out by Johannes [30]. He pro-
vided data for operating conditions of 3 to 6 bar and bulk temperatu-
res from 4.2 to approximately 6 K. His results show heat transfer
coefficients that are slightly higher than obtained by the usual
Dittus-Boelter correlation [79]:

$$Nu = 0.023 \ Re^{0.8} \ Pr^{0.4} \quad . \tag{3.21}$$

The heat transfer coefficient ($h = Nu \ \lambda/D$) in the case of eq. (3.21)
is a constant independent of the heat flux for a given thermodynamic
state, and we have a linear heat transfer process. The experimental
results of Johannes appear to be of this kind. In order to be able to
apply a constant value of h, the thermodynamic state of the helium
must be away from the region of sharp property variation, i.e. tempe-
rature should be well above or below the transposed critical, or the
heat flux must be small.
The results of Johannes pertain to the situation where both bulk
fluid (T_b) and wall temperature (T_w) remained below the transposed
critical (T_{tc}), i.e. $T_b < T_w < T_{tc}$.

Giarratano, Arp and Smith [33] did experiments, which covered a wide range of thermodynamic states and all situations were encountered, i.e. $T_b < T_w < T_{tc}$; $T_b < T_{tc} < T_w$ and $T_{tc} < T_b < T_w$. Their results are best represented by a modification of the Dittus-Boelter correlation, namely

$$Nu = 0.0259 \ Re^{0.8} \ Pr^{0.4} \ (T_w/T_b)^{-0.716} \ . \qquad (3.22)$$

This correlation fits the data with a standard deviation of 8.5%. For a given thermodynamic state eq. (3.22) describes a slightly nonlinear
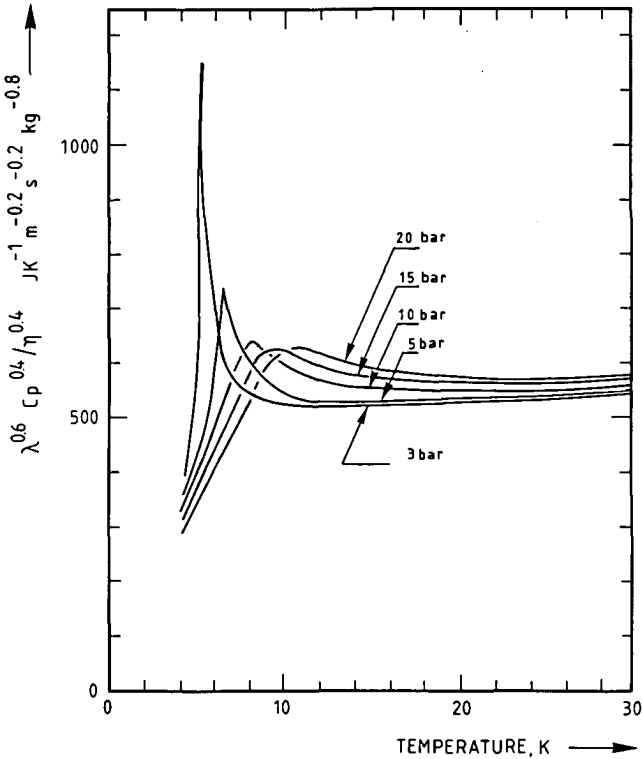
Figure 3.11 Variation of the properties parameter $\lambda^{0.6} \ (c_p/\eta)^{0.4}$ with temperature for constant pressure. From Giarratano et al. [33].
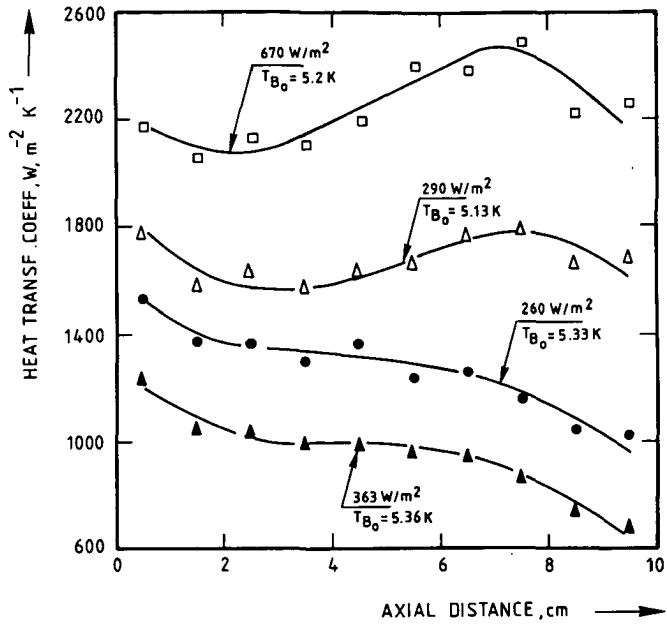
Figure 3.12 Heat transfer coefficients for supercritical helium [35] in a vertical tube 2.13 mm diameter, downward flow. Pressure was 2.5 atm., flow rate G = 68-76 kg/(m²s), bulk inlet temperature T_{b_i} = 5.04 K, T_{b_o} is bulk outlet temperature.
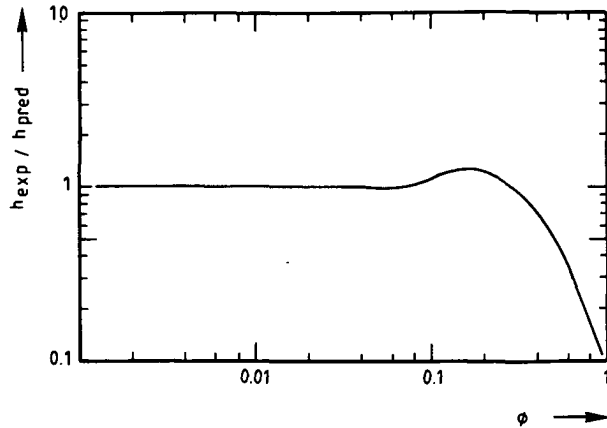

Figure 3.13 The ratio of the experimental and predicted heat transfer coefficients (eq. (3.22)) as a function of the parameter ϕ.

heat transfer process, but it is noted that for low heat flux and
temperature rise eq. (3.22) reduces to eq. (3.21) with a somewhat
larger factor. Equation (3.21) might be considered the limiting form
of the heat transfer coefficient for nearly homogeneous conditions.
In this limit eq. (3.22) predicts a heat transfer coefficient propor-
tional to the quantity $\lambda^{0.6} (c_p/n)^{0.4}$ for given hydraulic diameter
and mass flow. This quantity is dominated by the behaviour of c_p, and
reaches a maximum at the transposed critical temperature when plotted
against temperature at constant pressure (Fig. 3.11). Thus, when a
channel with constant mass flow and inlet conditions below T_{tc} is
used, the heat transfer coefficient at any point along the channel
should rise with heat input as the fluid temperature approaches T_{tc}.
For high heat flux, however, the wall temperature may be expected at
some point to exceed T_{tc} and the properties can vary across the chan-
nel.
In experiments reported by Ogata and Sato [34] bulk-wall fluid den-
sity ratios of about 5 were achieved at 3 bar pressure and in this
case heat transfer coefficients were obtained, which were less than
those given by eq. (3.22) at the highest heat fluxes.
Giarratano and Jones [35] investigated the situation of crossing the
transposed critical temperature at low pressures in more detail.
Their experiments were carried out at a pressure of 2.5 bar with in
all cases $T_b < T_{tc}$ and both $T_w < T_{tc}$ and $T_w > T_{tc}$. Figure 3.12 shows
a typical example of heat transfer coefficient profiles for a given
flow rate $G = \dot{m}/A$ and inlet temperature. The data are for a 2.13 mm
inside diameter tube of stainless steel. They found that the correla-
tion of eq. (3.22) could be applied for values of a dimensionless
correlating parameter ϕ up to 0.3 (Fig. 3.13). ϕ is defined as

$$\phi = \frac{4\ z\ q}{(H_{tc} - H_o)\ G\ D} \quad . \tag{3.23}$$

z is the position along the tube, q is the heat flux, H_{tc} the
enthalpy on the transposed critical line and H_o the inlet temperatu-

re. The parameter ϕ can be interpreted as the quotient of the heat flux that has been added to the fluid up to a given point z along the tube and the heat that would be required to bring it at the temperature T_{tc}. For $\phi \gtrsim 0.3$ a deviation occurs for the measured data and those predicted by eq. (3.22). The estimated systematic error in their measured heat transfer coefficients varies from 55% for the worst condition (high flow rate and low heat flux, 224 kg/(m²s) and 0.29 kW/m²) to 8% for the most favourable condition (low flow rate and high heat flux, 72 kg/(m²s) and 4 kW/m²).

An alternative approach to the deterioration in heat transfer to turbulent flow of helium relative to the standard constant property conditions, is given by Yaskin et al. [36]. They arrived at their correlation by considering the analogy between the heat transfer process to a gas with high thermal expansion and that which takes place in the presence of gas injection through a porous wall. They obtained the expression

$$Nu/Nu_o = \left(1 - 0.2 \, (Nu/Nu_o) \, \beta \, \Delta T \right)^2 \tag{3.24}$$

with $\beta = -\dfrac{1}{\rho} (\dfrac{\partial \rho}{\partial T})_p$ and $Nu_o = 0.023 \, Re^{0.8} \, Pr^{0.4}$.

This correlation fits the available data better than the correlation of Giarratano (3.22).

The former results on heat transfer data were obtained with test sections with inner diameters of 3 mm (Johannes), 2 mm (Giarratano, Arp, Smith), and 1 mm (Ogata and Sato). Brassington and Cairns [37] investigated heat transfer to supercritical helium flowing both up and down in a wider vertical tube (diameter 18 mm). In their experiments buoyancy effects played a role. These effects were not noticed by the other investigators because of the use of small diameters. Buoyancy-induced temperature peaks occurred in their upflow tempera-

ture profiles and according to their results the occurrence of a
peaked temperature profile can be well predicted by

$$Gr/Re^{2.7} > 2.4 \quad 10^{-5} \tag{3.25}$$

with Gr being the Grashoff number: $Gr = \rho_b(\rho_b - \rho_w)g \, D^3/\eta_b^2$ (ρ_b and ρ_w
are the fluid densities of the bulk and at the wall respectively).
The results of Brassington and Cairns can be represented by

$$Nu = c \, Re^{0.8} \, Pr^{0.4} \tag{3.26}$$

where $c = 0.0218$ for downflow and $c = 0.0201$ for upflow. The correla-
tion describes the results with a standard deviation of 12 %.
Bogachev et al. [38] presented new experimental data to supercritical
helium in vertical tubes. Their measurements covered the pressure
range of 2.3 - 4 bar and bulk temperature of 4.4 - 12 K. They stated
that the Brassington-Cairns correlation (3.26) does not take into
account the effects of buoyancy and property variation in the varying
property region. Although in case of quasi constant helium properties
(high pressure, relatively high temperature) eq. (3.26) predicts the
heat transfer results of Bogachev et al. rather well. It must be said
that the Brassington-Cairns correlation covers a pressure range of
2.2 - 14 bar and the data of Bogachev et al. are near in the pressure
(2.5 bar) of Giarratano and Jones [35]. On the other hand Bogachev et
al. got their data on a stainless steel test tube with an inner dia-
meter of 2.18 mm.

From these results it can be concluded that heat transfer predictions
in the range near the critical point are doubtful, but when a super-
conducting system is operated at low temperatures and high pressures
(range of nearly constant helium properties, see e.g. Fig. 3.3 - 3.6)
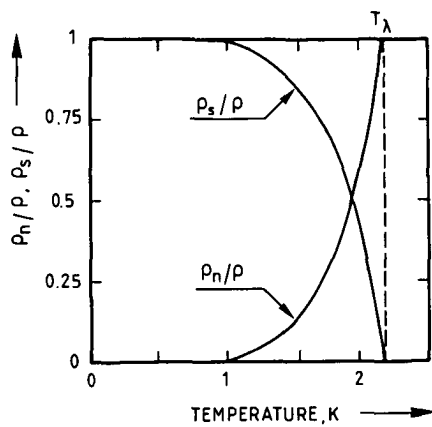reliable conclusions can be obtained from the heat transfer rela-
tions.

Figure 3.14   The superfluid and normal fractions of helium II as a
function of temperature under saturated vapour pressure.

3.4. Superfluid helium

3.4.1. Two fluid model

Is helium I an ordinary liquid in the sense that laws governing, for
example, the flow of the liquid and the conduction of heat in the
liquid are the same as those for ordinary classical liquids, helium
II is quite different in its behaviour and exhibits the phenomenon
that is called superfluidity. The two liquid phases helium I and
helium II are separated by the "λ line". The lower end of the λ line
is at 2.17 K, p = 0.05 bar and the upper end is at T = 1.76, p = 30.2
bar. At atmospheric pressure the λ transition occurs at T = 2.16 K
(Fig. 3.2). The transition of helium I into helium II when liquid
helium is cooled down below the λ line undergoes a kind of quantum
condensation.
Superfluid helium is characterized by a very low viscosity, a high
heat capacity and a high thermal conductivity. In its hydrodynamics,
and in the way it conducts heat, helium II exhibits a strange and
often apparently very complicated behaviour. This behaviour can be
described relatively simple in terms of a model which is called the
two-fluid model. According to this model helium II can be regarded as
an interpenetrating non-separable mixture of two fluids: a superfluid
component, density ρ_s; and a normal component, density ρ_n. The total
density is $\rho = \rho_n + \rho_s$. The normal part of the fluid behaves like an
ordinary liquid, with viscosity n_n, and it carries all the entropy
and thermal energy of the liquid (microscopically, the normal fluid
is formed from the thermal excitations of the superfluid component in
the liquid). The superfluid component behaves in the simplest situa-
tions like an ideal inviscid liquid and it carries no entropy or
thermal energy. The densities ρ_n and ρ_s depend on temperature as
shown in Fig. 3.14.
The transition to the superfluid phase is accompanied by a large peak
in the heat capacity. There is, however, no latent heat, the transi-
tion being continuous in the sense that the extent to which the
liquid is superfluid goes to zero continuously as the transition is
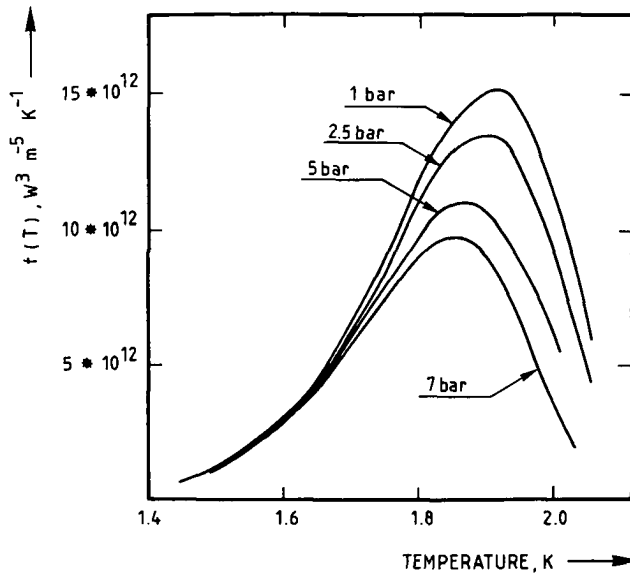approached from below (e.g. as measured by the superfluid density).

Figure 3.15 Temperature dependence of the conductivity function f(T) of superfluid helium for constant pressure.
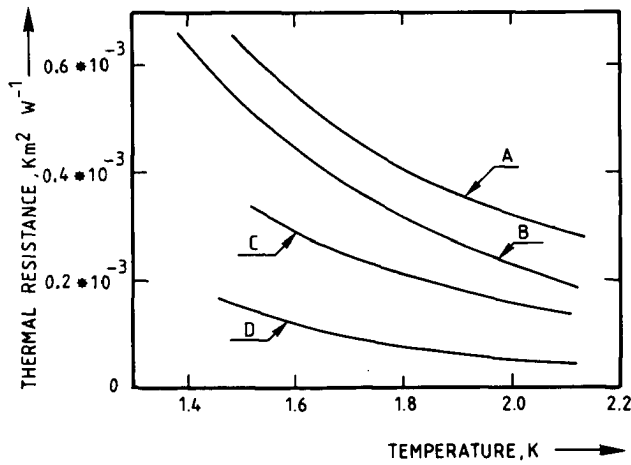

Figure 3.16 The thermal boundary resistance (Kapitza resistance) between liquid helium II and polished copper (A); quartz, surface ground (B); copper, surface etched (C) and lead, surface etched (D).

This means that superheating and subcooling cannot occur at the λ
transition; in contrast to the situation obtaining at the liquid-
vapour transition, metastable states of one phase cannot exist under
conditions where the other phase is stable.

The advantage of cooling a superconducting system by superfluid
helium is, apart from the large heat transfer coefficients, is the
increase of the critical current density (see Fig. 3.1) by virtue of
the reduced temperature. Only the cooling channels or bath have to be
very tight. Superleaks can even arise in a system which has been
tested for vacuum tightness carefully (a superleak is tight for He I
and open for He II; examples are extremely small hair cracks, porous
solder- or weld joints or even porous material components). With
superleaks the system can be heavily damaged, especially when a
superleak occurs between cooling bath/channel and the vacuum vessel
for thermal insulation.

3.4.2. Cooling by superfluid helium

3.4.2.1. Heat transport in superfluid helium

Heat transport through superfluid helium can be described in terms of
the two-fluid model. Heat conduction can be envisaged as a counter
flow convection process in which the energy is carried in one direc-
tion by the normal component while the superfluid component (zero
entropy) returns in the opposite direction. At the hot surface,
superfluid atoms receive energy which bring them into the normal
state. The counter flow of the two fluids, with no net mass flow, pro-
vides a very effective way of transporting heat and gives helium II a
very high effective thermal conductivity.

In the absence of superfluid turbulence the only dissipative process
that limits the conductivity to a finite value is viscous dissipation
in the flowing normal fluid. At very small heat fluxes the flow of
normal fluid remains laminar, but at larger heat fluxes the super-
fluid flow becomes turbulent (because of the very low viscosity of
the superfluid component) and leads to an effective mutual friction

between the two fluids. At large heat fluxes in wide channels this mutual friction is the dominant source of dissipation, and the relation between temperature gradient and mean heat flux ϕ/A becomes [39]:

$$(\phi/A)^3 = -f(T) \ \nabla(T) \ . \tag{3.27}$$

Recent results of $f(T)$ are shown in Fig. 3.15 [39]. From these values of $f(T)$ it can be seen that the heat transport in liquid helium II is extremely good. The thermal conductivity is proportional with $\sqrt[3]{f(T)/(\nabla T)^2}$ and e.g. at 1.8 $\lambda_{He \ II}$ is in the order of $1 * 10^5$ W/(mK) (the typical dT/dx = 0.1 K/m at this temperature (ϕ/A = 10,25 kW/m^2, from [39])).

3.4.2.2. Heat transfer between a solid body and superfluid helium

When heat flows from a solid material into superfluid helium there is a discontinuity in the temperature across the boundary separating the two media. The corresponding thermal resistance, the Kapitza resistance, is usually an important component in the chain of thermal resistances that are involved when superfluid helium is used as cooling agent.

The Kapitza resistance for solid-helium II interfaces is not well understood. According to the theory of Khalatnikov (Wilks [40]) the heat flow across the boundary must occur as a result of the transmission of phonons (sound waves) from one medium to the other. The speed of ordinary sound in superfluid helium is much less than the speed of sound in a typical solid, and the Kapitza resistance arises from the resulting mismatch. From the theory of Khalatnikov it follows that the Kapitza resistance is proportional with $1/T^3$ and thus the heat transfer coefficient h_K goes with T^3. If the temperature drops at the interface with an amount ΔT, the heat flux ϕ/A is given by

$$\phi/A = h_K \, \Delta T \quad . \tag{3.28}$$

It turns out from experiments that the magnitude of the resistance is very sensitive to the surface finish of the particular material used. In Fig. 3.16 some results are shown (from Wilks [40]). This figure shows that for copper h_K is in the order of 2500 $W/(m^2K)$ at 1.8 K. When a superconducting device is cooled to lower temperatures, the Kapitza resistance becomes larger and the heat transport mechanism in the superfluid becomes worse ($f(T)$ decreases).

3.4.3. Forced flow

As shown before, in liquid He I under saturated vapour pressure the PNBF marks the transition between nucleate boiling and film boiling. In liquid He II a critical heat flux has been observed at which the temperature of the solid, which was in contact with He II and heated, rises discontinuously above the lambda temperature T_λ. Srinivasan and Hofmann [39] recently showed that at a pressure of 1 bar the critical heat flux q_{cr} in He II can be predicted by

$$q_{cr}^3 \, L = \int_{T_b}^{T_\lambda} f(T) \, dT \tag{3.29}$$

with L being the length of the He II column between the heated section and the cold end. T_b is the cold end bulk temperature of He II or just the helium temperature before the heat is supplied. The cold end can be realized by a heat exchanger which is submerged in a large pumped He II bath.
Srinivasan and Hofmann did also experiments on forced flow cooling of He II. The forced flow was induced by a fountain pump (fountain effect see e.g. Zemansky [41]). They studied He II pressure ranges up to 7 bar, for cooling with a forced flow of He II there was no advantage in working at pressures larger than 1 bar. On the other hand the

cooling capacity of He II increases under forced flow conditions. It was possible to increase the heat flux above q_{cr} of eq. (3.29) without a temperature jump above T_λ of the cooled test section (correlation (3.29) counts for stagnant conditions). That means that the bulk temperature of He II remains below T_λ and no large volume of He II changes in He I with the corresponding decrease in heat transfer.

CHAPTER 4

A CRYOGENIC FAST RESPONSE THERMOMETER[*)]

4.1. Introduction

Steady state heat transfer phenomena can be investigated by measuring
temperature changes with relatively slow thermometers based on germa-
nium and carbon resistors under varying heat fluxes. For transient
effects the use of fast sensors such as thermocouples is required;
however, thermocouples have a low sensitivity.
The available data in literature on transient heat transfer are
mostly the results of experiments in which the intrinsic electrical
resistance of the sensor is used as heater and as thermometer.
The first results on transient heat transfer at low temperatures were
obtained by Jackson [43]. By measuring the temperature on basis of
the resistance change of a manganin wire in liquid helium during the
first milliseconds of heating the wire by an electrical current, he
was able to measure transient heat transfer coefficients. He only
concluded that these coefficients were very high. Schmidt [44] mea-
sured the transient heat transfer of a monofilamentary NbTi/Cu com-
pound conductor to liquid helium. The conductor was used as a heater
by applying a current larger than the critical current I_c and, via
the temperature dependence of I_c as thermometer with a response time
below 10 µs. From the measurements of Schmidt it followed that the
transient heat transfer in liquid helium could be described by a
heat-flux-independent transfer coefficient h = 50 kW/(m^{2}K) below a
"take-off" time t_0. At t_0 the heat transfer coefficient decreases
rapidly due to the onset of film boiling. t_0 is found to be propor-
tional with ϕ^{-2}, where ϕ is the heat flux.

---

*) A version of this chapter has been published in Cryogenics [42]
   The thermometers described in this chapter are now commercially
   available (Positronika, Appendix C).

Steward [45] investigated transient heat transfer to liquid helium by using a carbon film simultaneously as heater and thermometer. The carbon film was deposited onto a quartz substrate. He concluded that the initial heat transfer coefficients, being limited primarily by the Kapitza resistance, are 10 - 100 times greater than steady state values. The time to reach steady state varies from 10^{-5} to 1 s. Transient heat transfer to a forced flow of helium (pressure range 1 - 10 bar) was measured by Giarratano and Steward [46]. The test section existed of a small rectangular flow channel (wetted cross section 1.5 × 5 mm, length 10 mm); the temperature was measured and heat was supplied by a carbon film on one side of the channel (dimensions film 5 × 10 mm). They measured transient heat transfer coefficients in the range of 500 - 10 kW/(m²K).

A basic drawback of the above mentioned measuring techniques is that it cannot be generally applied in other experimental setups. Seki and Sanokawa [47] constructed a fast response germanium thin film thermometer by evaporation techniques. Here, the sensor was also indissolubly linked with a stainless steel heater.
For the transient heat transfer measurements it is desirable to develop fast response thermometers with high sensitivities, which can be applied to the experiments in a flexible way. Then the thermometers can be mounted on the test sections after the calibrations and the diverse test sections can be developed and constructed separately from the thermometers. The high sensitivity was desirable for measuring temperatures of one tenth of Kelvin. A temperature rise of 1 or 2 K is quite large at low temperatures, because the difference between the desired maintainance temperature of a superconduction device and its critical temperature is small (e.g. SULTAN 8 T inner coil [48]: inlet temperature of the coolant, supercritical helium, is 4.4 K, critical temperature at a magnetic field of 8.2 T is 5.5 K).

4.2. Design and construction of the thermometer

To minimize the heat transfer resistances between sensor and measu-
ring object the thermometer has to be soldered or glued rigidly onto
the different experimental test sections. For a fast response of the
thermometer it is required that the heat capacity of the sensor is
low (small size) and the contact surface is as large as possible. The
temperature adjustment of the thermometer has to be fast, so the
thermal conductivity of the sensor has to be large in addition to the
small heat capacity. Thus the thermal diffusivity of the sensor,
$a = \lambda/(\rho \, c_p)$ has to be optimized by proper selection of the construc-
tion materials.
When a large heat exchanging surface is combined with a small thick-
ness, a fast performance of the sensor might be expected. This size
definition, a flat sensor, and the possibilities of depositioning
thin films of materials by evaporating techniques were the premises
of the thermometer construction.
The test sections will exist of tubes made of copper and stainless
steel materials. The thermometer will transduce the temperature
changes into electrical signals. So, the thermal sensitive layer has
to be electrically insulated from the metal test sections by an insu-
lating substrate. Thus the thermometer will consist of a slab of
substrate material with electrical insulating properties on which at
one side the thermal sensitive layer will be situated and the other
side of the slab will be glued or soldered onto the tubes.

4.2.1. Response time definition

In first approximation the thermal behaviour of the thermometer is
comparable with the behaviour of an infinite slab of thickness d. One
side of the slab (x = 0) is thermally insulated; on this side the
thermally sensitive layer is situated. The temperature variations are
imposed on the other side (x = d), which will be mounted on the test
sections. When the infinite slab with temperature T_0 undergoes at
time t = 0 on x = d a temperature jump up to T_1, the temperature
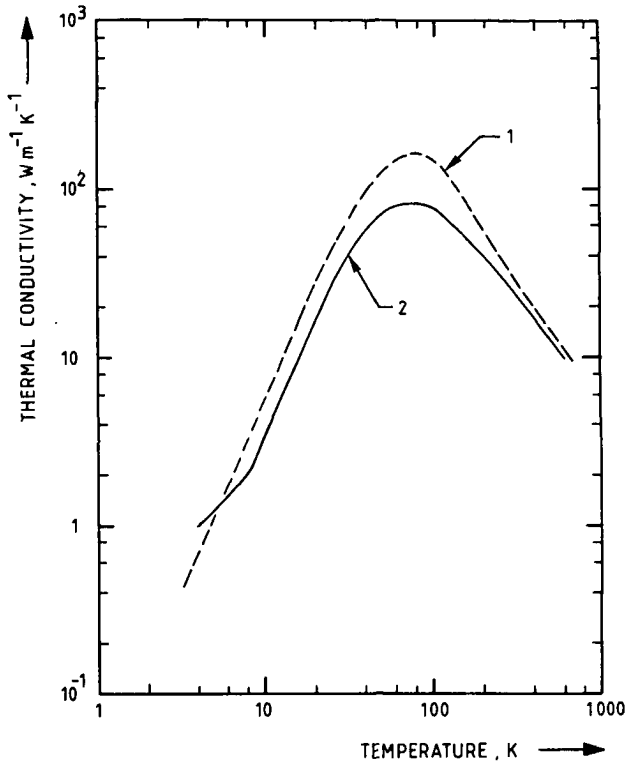distribution T(x,t) will be given by [19];

Figure 4.1   Thermal conductivity of sintered alumina as a function of temperature (1. Touloukian et al. [63]; 2. Nemoto et al. [69]).

$$T(x,t) = T_1 - \frac{4}{\pi}(T_1-T_0) \sum_{n=0}^{\infty} \frac{(-1)^n}{2n+1} \left\{ \exp(-a(2n+1)^2\pi^2 t/(4d^2)) \right. *$$

$$\left. * \cos\left[(2n+1) \pi x/(2d)\right] \right\} . \qquad (4.1)$$

After a long time, that is it $at/d^2 > 0.5$, the temperature T on the insulated side of the slab ($x = 0$) is given by:

$$T(0,t) \approx T_1 - \frac{4}{\pi} (T_1-T_0) \exp(-\frac{\pi^2}{4} \frac{at}{d^2}) . \qquad (4.2)$$

When at/d^2 equals 1 the temperature increase $T(0,t) - T_0$ on the insulated side of the slab is 89% of the original temperature difference $T_1 - T_0$. This occurs at the characteristic time τ_r,

$$\tau_r = d^2/a \qquad (4.3)$$

which is defined as the response time of the thermometer. This criterion is more rigid than the usual $1 - e^{-1}$ (63%) definition.
From the response time definition it can be seen that the thickness of the substrate is important in addition to the thermal diffusivity. A large diffusivity implies a large thermal conductivity λ and a small volume heat capacity ρc_p for the substrate in case of a fast response.

4.2.2. Material selection

The large negative temperature coefficient of semi-conductors at low temperatures makes these materials suitable for use as thermometer in the helium region. Carbon and germanium resistors are often used as thermometers. Carbon has the advantage above germanium because of the smaller influence of magnetic fields on the electrical resistivity [49].
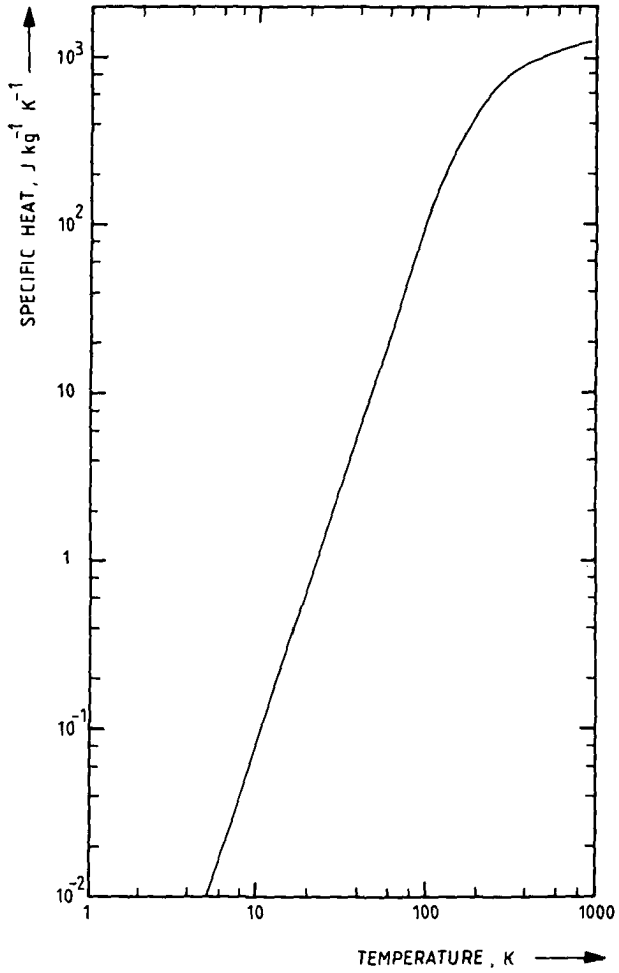
Figure 4.2   Specific heat of alumina (Touloukian and Buyco [70]).

When carbon films are applied a large temperature sensitivity is com-
bined with the characteristics for a fast response (relatively large
surface in ratio with the thickness). Carbon films are often made by
painting or spraying with a suspension of colloidal carbon in water.
A severe disadvantage of these methods is the vulnerability of the
film, while the absorption of gases causes resistivity changes [50].
Making films by vacuum deposition is a promising option to satisfy
requirements like film thickness, small size and stability.
In addition, when spraying and/or painting techniques are used the
sensors are indissolubly linked with the test sections. The whole
test section has to be cooled down for calibration experiments. When
the thermometers are fabricated as separate sensors, only the sensors
have to be calibrated.
To be applicable the carbon films have to be deposited on a substrate
with good thermal conducting and electrically insulating properties.
On the other hand it is desirable that the substrate can easily be
fixed on all kind of experimental devices. Soldering generally gives
a perfect thermal contact between sensor and sample. Thus the best
performance can be expected from metallic substrates. For example:
copper at 4.2 K: $a = 0.33$ m^2/s (Table 2.1), thus a thickness $d = 1$ mm
gives a response time in the order of 3 µs.
The first carbon thin film thermometers, which we produced, were
based on thin copper substrates covered with an insulation layer to
avoid electrical contact between the substrate and the carbon film.
Several insulators have been applied like vacuum evaporated alumina,
silicon monoxide and glass. However, the results were often not very
satisfactory. Sometimes there was an electrical short circuit between
substrate and carbon film or there was a large leak-resistance be-
tween them. After investigating the thermal properties λ and c_p and
the density of several insulating materials, finally alumina was
chosen as substrate material. Sintered alumina slabs with a thickness
of 0.2 inch $\approx$ 0.5 mm were commercially available. The manufacturer[*]
specifies a density of 3860 - 3900 kg/m^3 (alumina content 99.6%). The
λ and c_p of alumina are shown in Fig. 4.1 and 4.2 respectively. At
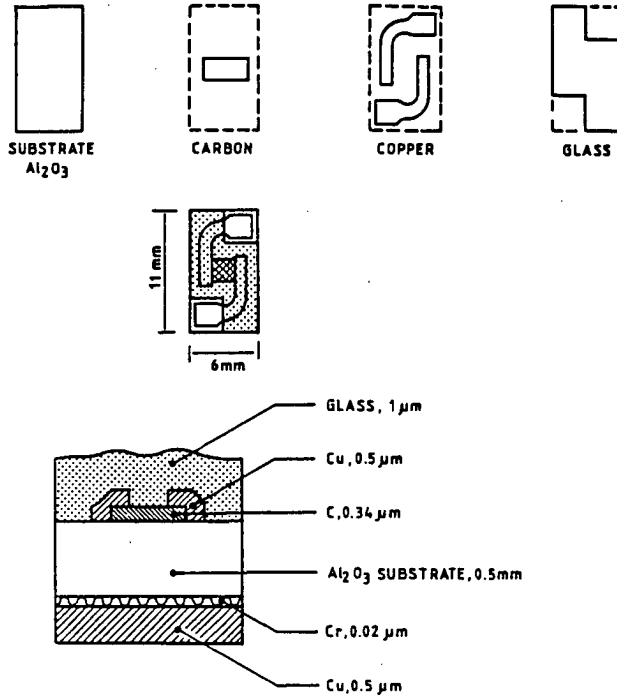
[*] M.R.C., see Appendix C

Figure 4.3   Structure of the carbon thin film thermometer.

Impurity	Concentration
Th	1.3 ppb
Cr	390 ppb
Ir	0.07 ppb
Cs	1.5 ppb
Sc	2.3 ppb
Co	15.5 ppb
Sb	1.7 ppb
Fe	9.7 ppm

Table 4.1. Impurities of carbon used
           for the thin film thermometers.

4.2 K λ is in the order of 1 W/(mK), $c_p \approx 10^{-2}$ J/(kgK), $\rho \approx 4000$ kg/m^3 and d $\approx 5 \cdot 10^{-4}$ m and thus $\tau_r \approx 10$ μs. Even when λ is a factor 10 worse, the response time is still of the order of 0.11 ms and sufficiently short for may purposes. Because some of the data of alumina were not very reliable and also some of the other materials (like carbon) influence the behaviour, it is necessary to determine the response time by experiments. Furthermore, electrical leads and solder may influence the response time.

4.2.3. Construction

The electrical resistivity σ of carbon is about 1.4 10^{-5} Ωm at room temperature. Experience showed that the resistance of commercially available resistors increases by a factor 10 - 100 when they are cooled down. Quite arbitrarily a thickness of 0.34 μm (3400 Å) was chosen for our carbon film. This thickness would give a square resistance of 40 Ω at room temperature.

On one side of the alumina substrates the carbon film (0.34 μm) and copper contacts (0.5 μm, terminals for the electrical leads) were deposited and covered by a glass film of 1 μm. The glass layer protects the carbon film and prevents the absorption of gases. On the backside of the alumina slabs a 0.5 μm copper film was deposited. This allows soldering of the thermometers onto metallic components of the test sections. Figure 4.3 shows schematically the final structure of these thermometers. The carbon used was of very high purity, in Table 4.1 the impurities are given (measured with neutron-activation analysis).

All the deposited films were prepared at room temperature by electron beam evaporating in a conventional bell jar at a pressure of about 10^{-3} Pa. Each step of the deposition process was made through photo-etched copper masks of 0.15 mm thickness.

The resistance of the carbon films at room temperature varied between 1250 Ω and 2500 Ω, even within one batch. These resistance variations have also been noticed by Adkins et al. [51]. They explained the variations by impurity contents and varying grain size in the films. At 4.2 K most of the sensors showed a resistance of more than 20 MΩ.

This latter value makes this type of thermometer unsuitable for cryo-
genic application. However, when carbon is baked the resistivity de-
creases and these changes are irreversible (Mrozowski [52]).
The thin film carbon thermometers got their desired electrical resis-
tance by a final heat treatment at 150°C for one hour in vacuum. This
anneal temperature was empirically determined after various anneal
processes at different temperatures. The resistance of the thermo-
meters was then about 250 Ω at 300 K and about 2600 Ω at 4.2 K with
little variations between the various sensors. The reproducibility
after cycling a few times between room temperature and 4.2 K was
good, no noticeable changes occurred.

From transmission-electron-microscopy observations it was seen that
the deposited carbon films were highly amorphous in character. For
doing these observations a few films were deposited on glass sub-
strates, so that they could be easily floated off.
Annealing the carbon film reduces the electrical resistance, but its
amorphous character did not vanish. This effect was also observed by
other authors, e.g. Kupperman et al. [53]. Hauser and Platel [54]
explain the changes of the electrical properties by stating that
amorphous carbon contains a mixture of graphite bonds and diamond
bonds. The localized conduction states in amorphous carbon are situa-
ted in the graphite bonds. It is found by Hauser [55] that during the
annealing process the film recrystallizes to a greater part in the
graphite configuration. Hence, there will be more localized conduc-
tion states and a reduced electrical resistivity.

The carbon film is a rectangle of 2 × 4 mm, on the short side for
1 mm overlapped by the copper contacts. The effective resistor is
thus a square film of 2 × 2 mm (Fig. 4.3).
Insulated copper wires of 0.05 diameter were attached to each copper
terminal with the aid of colloidal silver[*]. This allowed for a four
point resistance measurement.

_____

[*] Manufacturer: Acheson, see Appendix C.

4.3. Characteristics of the thermometer at low temperatures

4.3.1. Temperature-resistance correlation

The resistance of the carbon thin films was measured by a four wire potentiometric system. Excitation currents of 1 μA and 10 μA supplied by a constant current source were passed through the films. The potential difference across the films was measured by digital voltmeters. Two calibrated carbon glass and one germanium thermometer (Lake Shore[**], model CGR-1-1000, GR-200A-1000) were used as temperature standards.

All thermometers were mounted on a copper block. Four stainless steel wires (diameter 0.2 mm) and three nylon spacers were used to keep the calibration block in its proper position inside a vacuum vessel. This vessel was surrounded with liquid helium of 4.2 K to minimize the heat input by radiation. The vessel was evacuated to about $5 \cdot 10^{-4}$ Pa after which it has been cooled down by liquid helium. The potential differences across the various thermometers were scanned at normal and inverted polarities by a cryogenic multiplexer. [84, 85].

Figure 4.4 shows the calibration block as it is mounted before assembling the cryostat.

Figure 4.5 shows plots of the resistance versus temperature for a few carbon thin film thermometers. The resistance temperature curves of the thermometers can be correlated by the commonly used logarithmic function

$$\ln R = A_0 + A_1 \ln T + A_2 (\ln T)^2 \qquad (4.4)$$

or reversely

$$T = \exp \frac{- A_1 - \sqrt{A_1^2 - 4A_2(A_0 - \ln R)}}{2A_2} \quad . \qquad (4.5)$$

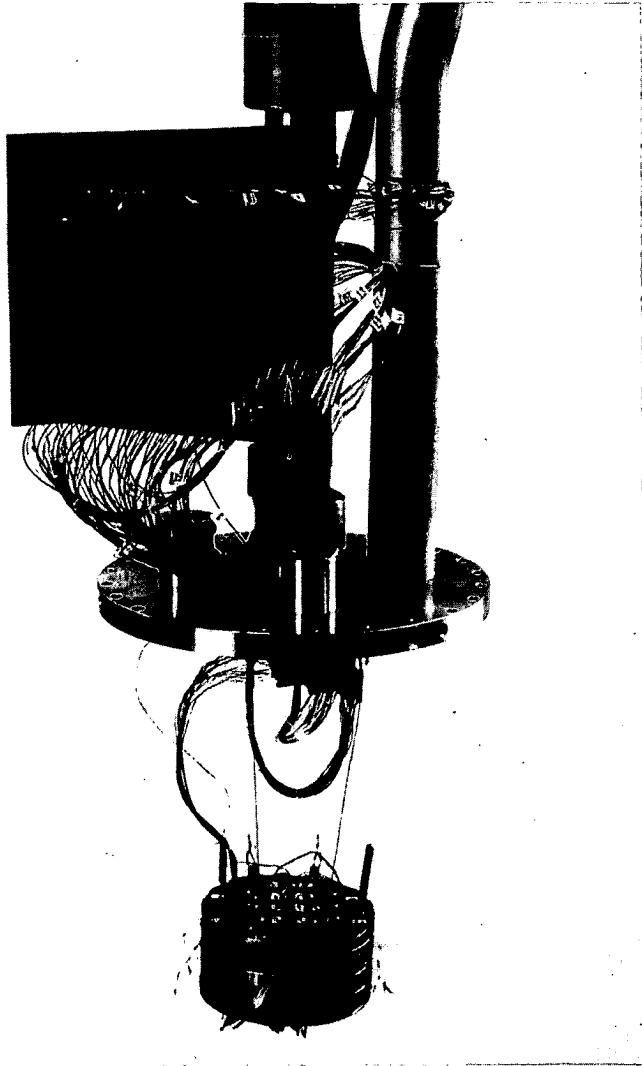[**] address, see Appendix C

- 78 -

Figure 4.4   View on the calibration block for the thin film
             thermometers (demounted vacuum vessel). The cryogenic
             multiplexer has been mounted on the pump tube above the
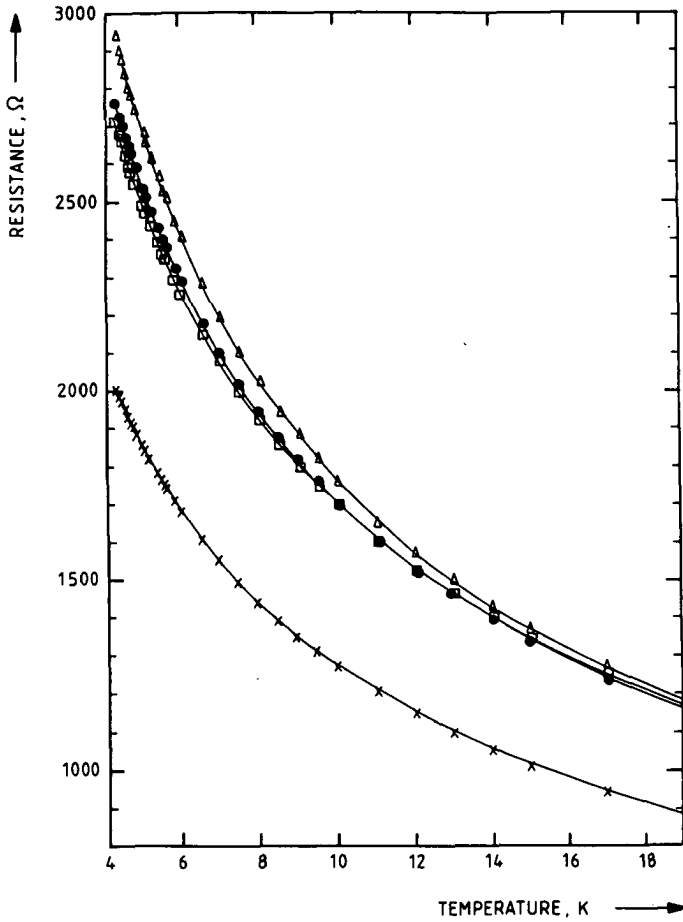   flange on the left side (the print has been marked with
             TE 1514).

Figure 4.5   Resistance versus temperature for a few carbon thin film
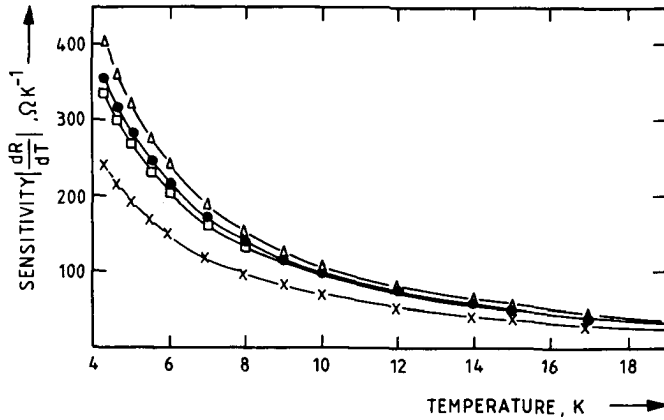   thermometers.

Figure 4.6   The sensitivity $S = \left|\dfrac{dR}{dt}\right|$ versus temperature for a few thin film thermometers.
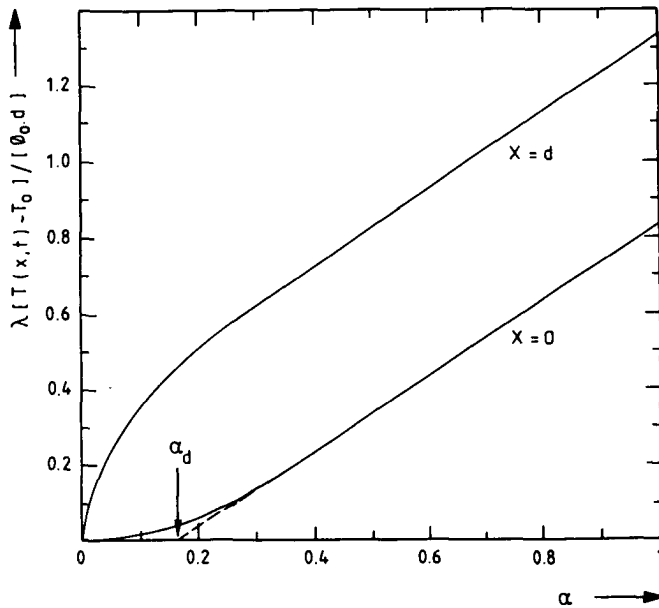
Figure 4.7   The nondimensional temperature rise of two parallel planes of an infinite slab as a function of the Fourier parameter $\alpha = at/d^2$, when a constant heat flux ϕ_0 is flowing into the slab at $x = d$. At $x = 0$ the slab is thermally insulated.

The coefficients A_0, A_1 and A_2 were computed for each thermometer from the calibration data by the least square method.
The sensitivity S, defined as $S = \left|\frac{dR}{dT}\right|$ of the carbon films is plotted in Fig. 4.6.

The thermometers were exposed to more than 30 thermal cycles from helium temperature up to about 15 K and a few cycles up to room temperature. No noticeable resistance chance occurred; the reproducibility is better than 0.1%.
Influences of liquid helium and gaseous helium, air and moisture on the film resistance have not been noticed.

4.3.2. Method of response time measurement

For the use as temperature probe the sensor will be soldered or glued onto experimental test sections. The temperature variations have to pass the alumina substrate before they are registered by the thermal sensitive carbon layer. The thermal relaxation time of the alumina slab, as defined by eq. (4.3), determines the response time of the thermometer. In first instance the influences of the carbon-, copper and glass film on the response time are neglected because these layers are very thin in comparison with the alumina substrate.
As indicated in paragraph 4.2.1 in first approximation the thermal behaviour of the sensor is comparable with the behaviour of an infinite slab of thickness d. Because it is very difficult to create a well-defined temperature jump, the method of response time measurement by registrating the temperature response as function of time according to eq. (4.2) is unsuitable.

When no heat transfer is possible at the side of the sensor where the carbon film is situated (carbon film side) and the temperature variations are imposed on the other side (copper side) by a constant heat flux, it is possible to determine the response time. The constant heat flux can be generated by an electrical current through the thin copper film on the mounting side of the sensor (copper side) because the electrical resistivity is practically constant at low temperatures. When the whole slab is placed in vacuum, the heat generated by

the current can only flow into the alumina substrate.
The temperature of the slab will rise, because there is also no heat
transfer at the carbon side (thermally insulated by vacuum).
Again considering an infinite slab, the temperature distribution
$T(x,t)$ when a constant heat flux ϕ_0 is flowing into the slab at $x = d$
(copper side) (at $x = 0$ is the carbon film side) is given by [19]:

$$T(x,t) = T_0 + \frac{\phi_0 t}{\rho\, c_p\, d} + \frac{\phi_0 d}{\lambda} \left\{ \frac{3x^2 - d^2}{6d^2} + \right.$$

$$\left. - \frac{2}{\pi^2} \sum_{n=1}^{\infty} \frac{(-1)^n}{n^2} \exp(-a\, n^2 \pi^2 t/d^2)\, \cos(n\pi x/d) \right\} \quad . \qquad (4.6)$$

The physical properties λ, ρ and c_p are considered as being constant.
The Fourier parameter α is defined as $\alpha = at/d^2$. Rewriting formula
(4.6) for the temperatures at the carbon film- and the copper sides
results in:

$$\frac{\lambda\, [T(0,t) - T_0]}{\phi_0 d} = \alpha + \left\{ -\frac{1}{6} - \frac{2}{\pi^2} \sum_{n=1}^{\infty} \frac{(-1)^n}{n^2} \exp(-\alpha\, n^2 \pi^2) \right\} \qquad (4.7)$$

(carbon film side, insulated, $x = 0$),

and

$$\frac{\lambda\, [T(d,t) - T_0]}{\phi_0 d} = \alpha + \left\{ \frac{1}{3} - \frac{2}{\pi^2} \sum_{n=1}^{\infty} \frac{1}{n^2} \exp(-\alpha\, n^2 \pi^2) \right\} \qquad (4.8)$$

(copper side, constant heat flux, $x = d$).

Calculated values of both temperatures are shown in Fig. 4.7. From
this figure it can be seen that after some time the curves given by

eq. (4.7) and (4.8) are linear with α since the exponential terms are quickly approaching zero. The linear temperature difference $T(0,t) - T_0$ of the carbon side extrapolated to zero

$$\frac{\lambda \left[T(0,t) - T_0 \right]}{\phi_0 \, d} = \alpha - \frac{1}{6} \qquad (4.9)$$

gives an apparent delay expressed by the Fourier parameter α_d, which corresponds to a delay time $\tau_d = \alpha_d \, d^2/a$.
It is clear from eq. (4.7) that α_d equals $\frac{1}{6}$, thus $\tau_d = d^2/(6a)$.
Considering the case that the constant heat flux ϕ_0 is only supplied during a limited period of time: t_p (pulse time), the total absorbed heat is then $E = \phi_0 \, t_p$. The same amount of heat can be delivered during various pulse times t_p at appropriate flux levels $\phi_0 = E/t_p$.
For a long time t_p eq. (4.9) is valid. In that case the temperature $T_p = T(0,t_p)$ at the carbon side is given by

$$\frac{\lambda}{d}(T_p - T_0) \Rightarrow \lim_{t_p \to \infty} \frac{\lambda}{d}(T_p - T_0) = \lim_{t_p \to \infty} \phi_0 (a \, t_p/d^2 - \frac{1}{6})$$

$$\qquad (4.10)$$

$$= \lim_{t_p \to \infty} (\frac{aE}{d^2} - \frac{E}{6 \, t_p}) = \frac{aE}{d^2} = \frac{\lambda}{d}(T_\infty - T_0) \quad .$$

The final temperature T_∞ will always prevail in the slab after absorption of an amount of heat E, independent of the manner of how the heat is supplied and assuming there are no heat losses. On the other hand the amount of heat E (per unit area) is given by

$$E = \int_{T_0}^{T} \frac{\rho \, c_p \, V}{A} \, dT \qquad (4.11)$$

where A is the surface of the slab and V its volume.
When equal energy E is absorbed at $x = d$ during a short time t_p, there will still exist a nonlinear temperature gradient in the slab. Neglecting the heat losses, during the time t_p the momentary value of $T(0,t)$ is given by (4.7). After time t_p the temperature at $x = 0$ will rise until it reaches the final value as given by formula (4.10). This behaviour allows a second method for measuring the response of
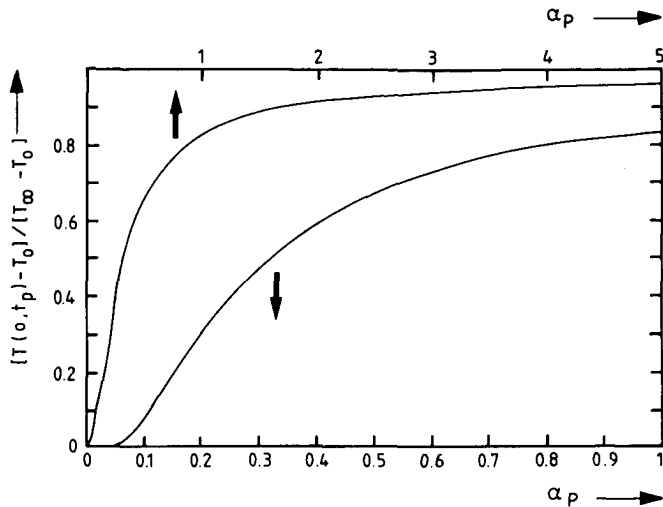
Figure 4.8   Plot of the temperature ratio $[T(0,t_p)-T_0]/[T_\infty-T_0]$
as a function of the Fourier parameter α_p as given in
formula (4.12).

the thermometer. It is possible to vary experimentally the pulse time
t_p and the heat flux ϕ_0 in such a manner that the total amount of
absorbed heat is constant.

During the heat pulse the temperature $T(0,t)$ rises until the value
$T(0,t_p)$ is reached at the end of the pulse. After the pulse the tem-
perature at $x = 0$ will rise still further until it has reached the
final temperature T_∞ as given by (4.10); then the temperature profile
in the sensor has leveled out completely. The ratio between $T(0,t)_p$
and T_∞ can be derived from (4.7) and (4.10) for various pulse times
t_p:

$$\frac{T(0,t_p)-T_0}{T_\infty-T_0} = 1 + \left\{ -\frac{1}{6} - \frac{2}{\pi^2} \sum_{n=1}^{\infty} \frac{(-1)^n}{n^2} \exp(-n^2\pi\,\alpha_p)\right\} /\alpha_p. \quad (4.12)$$

The right hand side of (4.12) depends only of $\alpha_p = a\,t_p/d^2 = t_p/\tau_r$
and is a unique function of the response time $\tau_r = d^2/a$. Formula
(4.12) has been plotted in Fig. 4.8. The ratio $[T(0,T_p) - T_0] /$
$[T_\infty - T_0]$ can be derived from the temperature curve which is measured
on the carbon side for various heat pulses. At the ratio 0.84 the
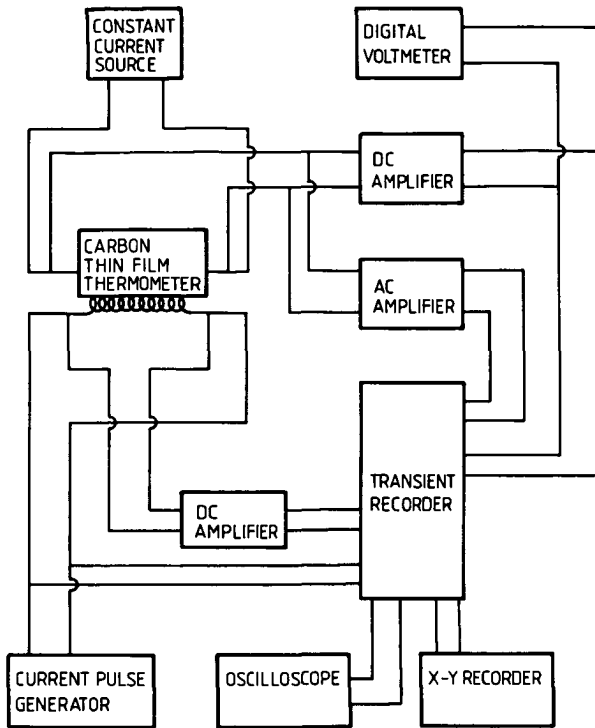response time τ_r is found. During the measurements the temperature

Figure 4.9   Response time measuring circuit and data acquisition
              system.

increase should be small in order to keep the physical properties λ,
ρ and c_p sufficiently constant.

4.3.3. Response time measurements

One of the carbon thin film thermometers was mounted inside a vacuum
vessel which was surrounded by liquid helium of 4.2 K, for determin-
ing its response time. The thin copper film on the backside of the
alumina substrate was used as heater. The current leads were stripped
monofilament NbTi wires (diameter 0.2 mm), the leads to measure the
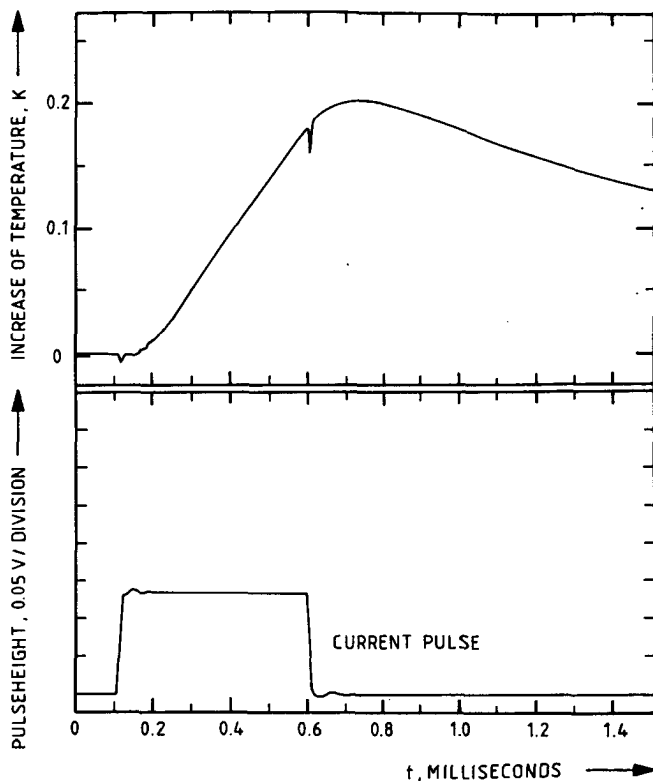
Figure 4.10   Temperature response of a carbon thin film thermometer
on a heat pulse. The heating current causing the pulse
was monitored across 0.595 Ω resistor. The resistance of
the copper film heater was 0.011 Ω.

voltage drop across the heater were two constantan wires (diameter
0.04 mm) with synthetic fibre insulation. The leads of the heater
were soldered on the copper film with indium.
Copper wires (insulated with enamel on poly-urethane base, diameter
0.05 mm) were attached on the copper terminals of the carbon film
with colloidal silver. Constant currents of 10 µA and 100 µA through
the carbon film were supplied by a battery.

The signals across the film were amplified by a d.c. as well as an
a.c. amplifier and recorded on a transient recorder (Data Lab) with a
sample rate of 5 µs.
The transient recorder had been equipped with four memories, each
memory had a capacity of 4096 data points (recorded time range for a
measurement: 4096 * sample rate). During a measurement the memories
were loaded parallel with the various measuring signals.
A pulse generator could supply heat pulses up to 400 W (20 A, 20 V)
with pulse times in the range from 0.1 ms to 9 s. The pulse generator
was especially developed for the experiments (leading edge, rise time
1 µs; trailing edge, fall time 1 µs). The current causing the heat
pulse was monitored across a 0.595 Ω resistor. Figure 4.9 shows the
schematic diagram of the measuring circuit and data acquisition
system.

As mentioned the thermal relaxation time τ_r can be derived from the
measured temperature response to a heat pulse. During a series of
measurements the total heat input was kept constant for various pulse
durations, starting at 0.1 ms and increasing in steps of 0.1 ms to a
maximum time of 1 ms. The behaviour of the sensor to a 0.5 ms pulse
is shown in Fig. 4.10. Also the current pulse is shown. Figure 4.11
shows a few records of temperature responses on different heat pulses
of constant time but different power. Extrapolation of these curves
gives a delay time τ_d of about 70 µs. Following the theory of the
thermal delay time ($\tau_r = 6 \, \tau_d$) the response time is 0.42 ms.

The second method of determining the response time was based on mea-
suring the temperature ratio $[T(0,t_p) - T_0] / [T_\infty - T_0]$. The tempe-
rature $T(0,t_p)$ of the carbon film is reached at the end of the pulse
and T_∞ is the constant final temperature of the thermally insulated
thermometer. During the experiment small heat losses to the environ-
ment causes a temperature decrease and thus T_∞ will not be reached
as can be seen from Fig. 4.10.
In order to estimate the temperature T_∞, experiments with small
values of the heat flux and large pulse times (> 5 ms) were carried
out. During the pulses there exists a negligible temperature gradient
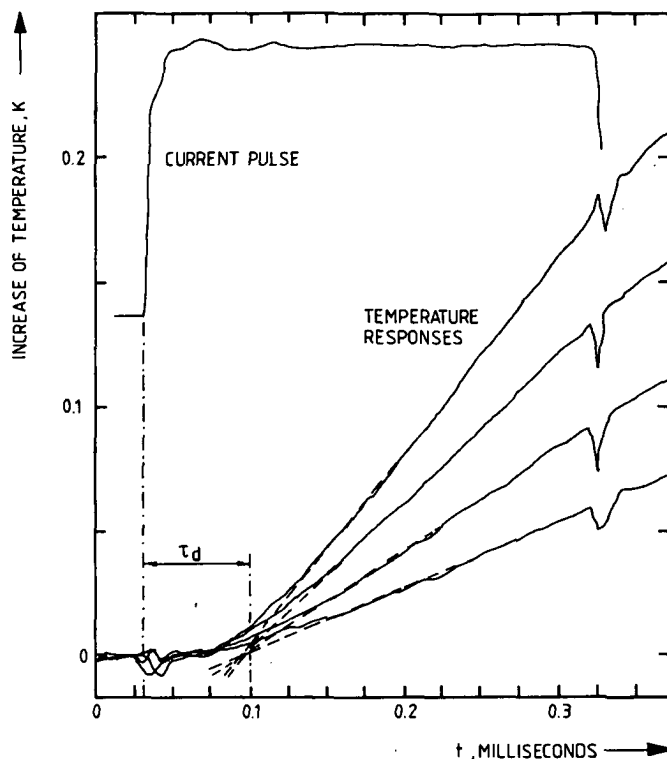
Figure 4.11 The determination of the delay time from different
temperature responses to different current pulses at
constant pulse time.

in the slab. The results showed that the temperature decrease at the
end of the pulse started after an additional 70 μs, which is identi-
cal to the reported delay time τ_d. This time is necessary to build up
the temperature gradient belonging to the losses and from this it can
be concluded that the heat leaked from the copper side and not from
the carbon side. This conclusion is confirmed by the fact that the
relatively thick superconducting wires were connected to this copper
side.

A value of T_∞ might be derived by backward extrapolation of the tem-
perature curve after the pulse to the time t_p. This temperature
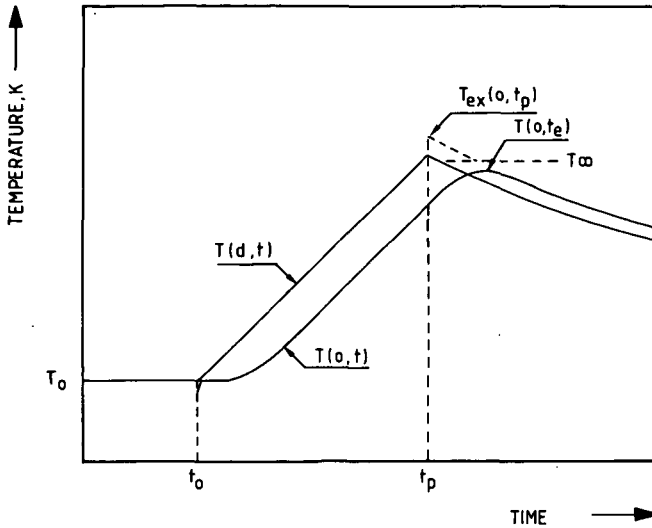
Figure 4.12   The temperatures of the thin film thermometer at the heater side [T(d,t)] and carbon side [T(0,t)] during and after a heat pulse starting at t = t_0 and ending at t = t_p.

T_{ex} $(0,t_p)$ (Fig. 4.12) will be higher than the average sensor temperature, because during the losses the carbon side temperature T(0,t) is higher than the copper side temperature T(d,t). On the other hand the maximum measured temperature $T(0,t_e)$ will be lower than the theoretical value of T_∞ due to the fact that the heat losses occur immediately when the temperature of the sensor starts to rise.

On this line of argument it follows that $T(0,t_e) < T_\infty < T_{ex}$ $(0,t_p)$. When T_∞ is replaced by these boundaries in the temperature ratio $[T(0,t_p) - T_0] / [T_\infty - T_0]$ an interval estimation of the thermal response time τ_r is possible. From Fig. 4.13 it can be seen that τ_r is lying between 0.4 ms and 0.6 ms, which confirms the results derived from the delay time (τ_r = 6 τ_d = 0.42 ms). These results show that the response time of the thin film carbon thermometer is indeed lower than 1 ms.

The measured τ_r is a factor 50 worse than the theoretically calculated value of paragraph 4.2.2. It is likely that the heat transfer
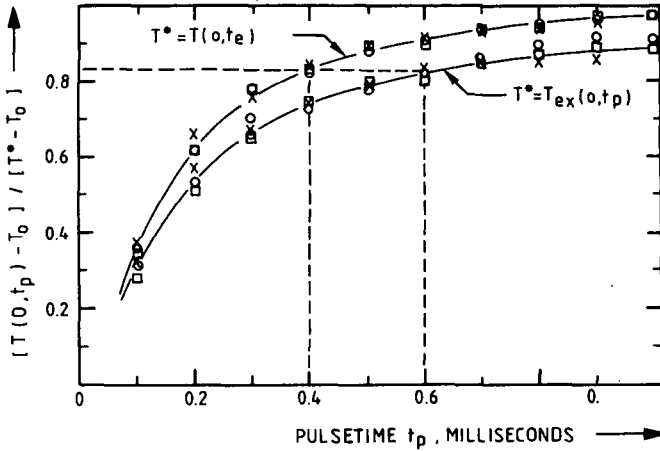
Figure 4.13 Plot of the measurement results of the temperature
ratios $[T(0,t_p)-T_0]/[T_{ex}(0,t_p)-T_0]$ and
$[T(0,t_p)-T_0]/[T(0,t_e)-T_0]$ versus the pulse time t_p. The
thermal relaxation time is defined by the temperature
ratio of 5/6.

(conductivity) apart of the influences of the other layers, is limi-
ted by the grain boundaries of the sintered slab.

It is noted that the same order of response time might be expected
at temperatures higher than 4.2 K, because the thermal conductivity
and the specific heat of sintered alumina increase in the same way
when the temperature rises (see e.g. Fig. 4.1 and 4.2), thus
$a = \lambda/(\rho\, c_p)$ is nearly constant.

4.3.4. Magneto-resistance

For one of the fast response thermometers the resistance was deter-
mined as a function of the magnetic field at 4.2 K. The thermometer
was mounted in the bore of a small superconducting magnet which was
submerged in a bath of liquid helium. The direction of the current,
flowing through the thin carbon film, was perpendicular on
the field ($\vec{I}_{thermometer} \perp \vec{B}$). The results are shown in Fig. 4.14.
At higher magnetic field the resistance is also higher.
The error introduced by the presence of a field is of the same order,
or somewhat smaller, than measured for carbon glass resistors [56].
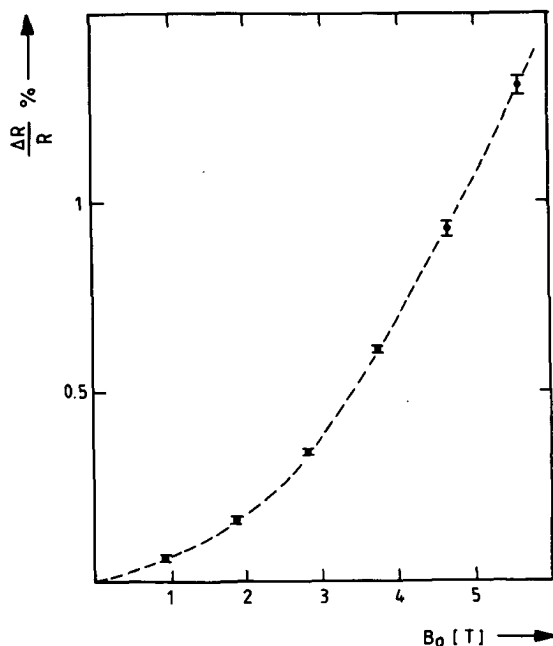
Figure 4.14 The relative error according to the resistance of the
thermometer at zero field as a function of the applied
magnetic field.

Figure 5.1A

Schematic view of the supercritical helium loop
 1. Purified helium gas storage (high pressure)
 2. Orifice flow meters
 3. Counter flow heat exchanger (300 K - 80 K)
 4. Cryostat filled with liquid nitrogen and
    containing carbon filter bed and heat exchanger
 5. Second counter flow heat exchanger (80 K - 4 K)
 6. Cryostat filled with liquid helium and containing
    vacuum vessel, V, and test section, T
 7. Helium gas holder (atmospheric pressure)
 8. Compressor
 9. Polluted helium gas storage (high pressure)
10. Compressor
11. Helium purifier

CHAPTER 5

EXPERIMENTAL EQUIPMENT

5.1. Blow down loop

5.1.1. General

The supercritical helium flow was acquired by deflating a high pres-
sure helium gas stock through a system of pressure reducing valves
and cooling this flow to 4.2 K using heat exchangers and liquid
nitrogen and helium baths.
The blow down loop was designed for a maximum helium flow of 3 g/s.
In first instance the helium gas, which was used, was stocked in a
battery of high pressure bottles. The available volume of the bottles
limited the duration of a 3 g/s flow to 30 minutes. Because tempera-
ture, pressure and flow adjustments, and also the read out of the
various measuring data took considerable time, it was necessary to
extend the maximum time of the experiments. By using the purified
helium gas stocks of the helium liquefier the available volume of
helium was enlarged to 350 m³ NTP (1 bar, 293 K). Then a mass flow of
3 g/s could hold for over 5 hours.
The helium had to be purified extensively, otherwise the cold tubes
were clogged up with frozen gases and fluids (i.e. water, oil, air).
The outlet of the loop was connected with a gas holder (at a pressure
of about 1 bar). The gas holder was emptied at intervals by a com-
pressor into the polluted helium gas stocks (high pressure).
Figure 5.1A shows schematically the blow down loop after some essen-
tial modifications, which will be described in the next paragraph.
The picture of 5.1B shows the counter flow heat exchanger with
mounted transfer tube.
After constructing the links with the liquefier and some primary ex-
periments, the transfer tube (par. 5.1.3), the handling and regula-
ting valves and the flow meters (par. 5.1.4) were modified. The large
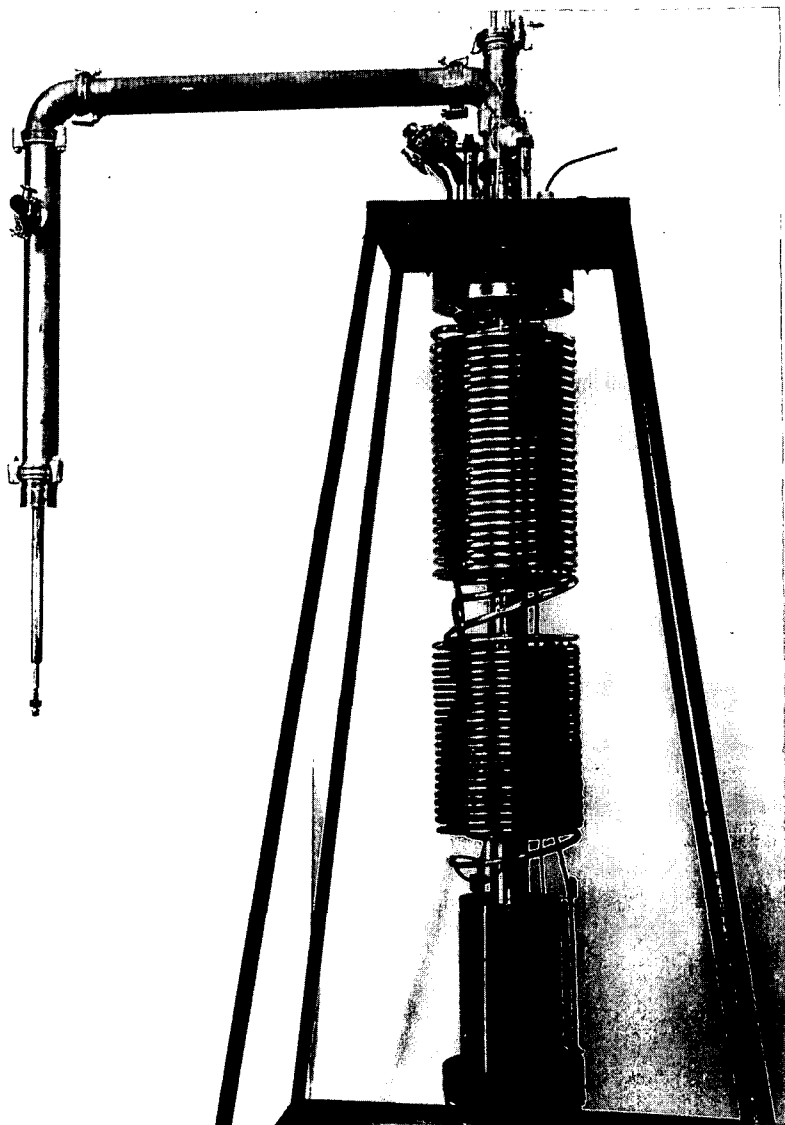counter flow heat exchanger in the first cryostat consists of 3 spi-

Figure 5.1B Picture of the counter flow heat exchanger
(80 K - 4 K) with mounted transfer tube. At the bottom
of the heat exchanger is the 10 m copper tube heat
exchanger which makes contact with liquid helium. Length
of heat exchanger insert: upper flange - bottom (copper
spiral): 1.74 m.

ralized parts. The bottom counter flow spiral has been replaced by a spiralized copper tube (tube length ~ 10 m). During the initial experiments the helium flow leaving the heat exchanger to the experiments did not get a constant temperature of 4.2 K. The copper heat exchanger submerged in liquid helium stabilized the temperature. In the second He-cryostat the insert with test section was mounted. Before entering the large counter flow heat exchanger of the first He-cryostat the helium flows through a carbon filter submerged in liquid nitrogen (77 K). This served as an extra purifier.
The compressors, the gas holder, the helium stocks and purifier were part of the helium liquefier infrastructure. The helium evaporation from the cryostats was also collected in the gas holder.

5.1.2. Insert of the second helium cryostat (He 2)

For the experiments a special cryostat insert was designed and constructed. For the heat transfer experiments it was necessary to minimize the heat transport (leakage) from the test tube to the environment. This was realized by mounting the test tube in a large vacuum vessel which would be submerged in liquid helium of 4.2 K. The insert consisted of the vacuum vessel, pumping tube and the joints for the in- and outlet for the supercritical helium flow.
Special attention was given to the radiation shields in the pumping tube (a shield situated at the 77 K link and one at 4.2 K) and the electrical feed-throughs. These latter had to be helium and vacuum tight. The feed-throughs (Fig. 5.2) were based on those developed by Mathu and Meyer [57], only they were scaled up in size (32 copper wires insulated with poly-urethane enamel, diameter 0.3 mm).

INSULATED COPPER WIRE, ⌀ 0,3mm
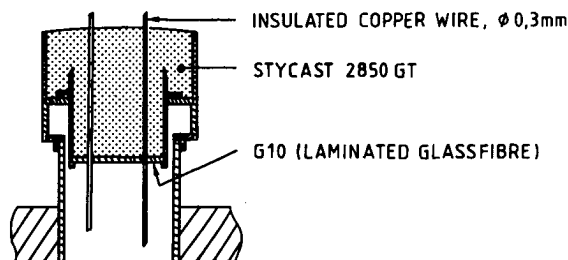
STYCAST 2850 GT

G10 (LAMINATED GLASSFIBRE)

Figure 5.2   Schematic view of an electrical lead through
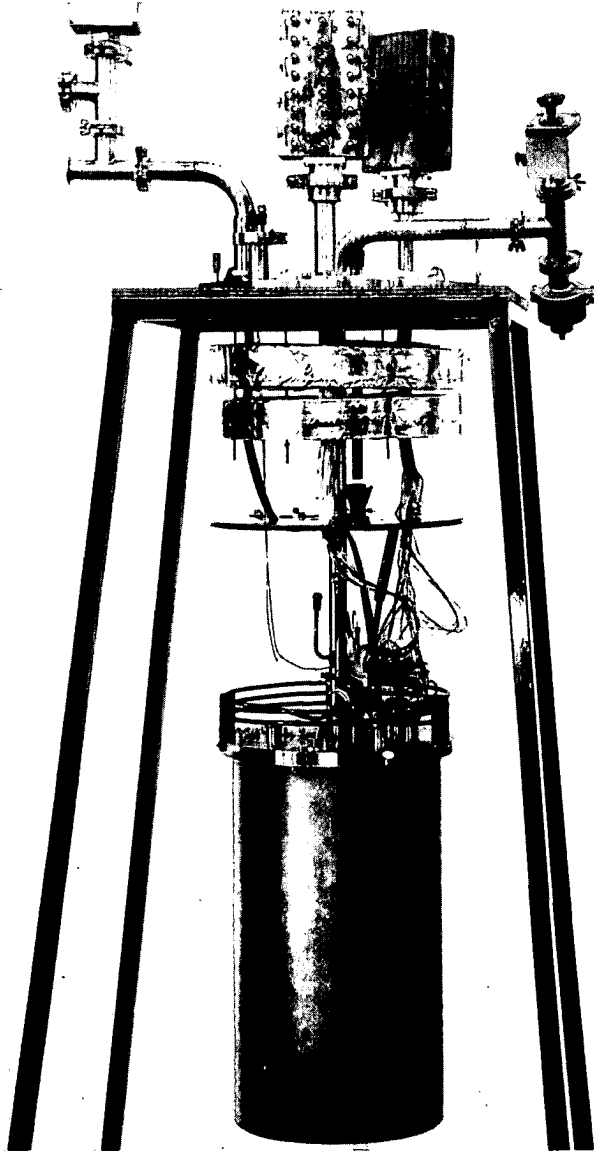(in reality containing 32 wires).

Figure 5.3A Picture of the insert of the second cryostat.
The central tube is the pumping tube for the vacuum
vessel (mounted). At the middle of the tube a large
radiation shield was soldered (gold plated copper)
which made contact with the liquid nitrogen vessel.
The tube on the left side on the upper flange was for
the helium boil-off.
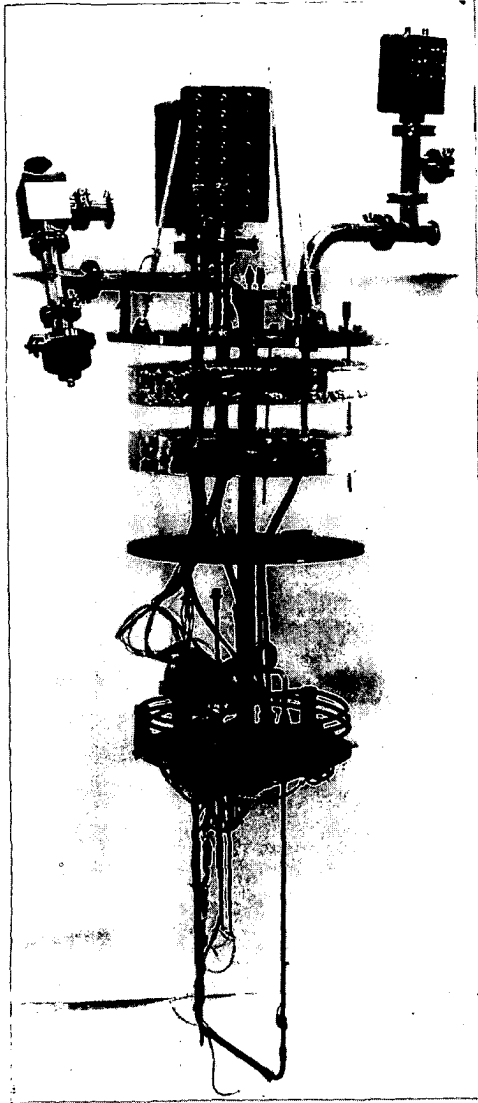Length insert: upper flange - bottom vacuum vessel: 112 cm.

Figure 5.3B Picture of the insert of the second cryostat with demounted
             vacuum vessel. On the top of the vacuum flange a copper
             spiral was mounted as an extra heat exchanger for the
             incoming supercritical helium flow. On the left side along
             the downward conduit in the vacuum vessel the stationary
             preheater was realized.
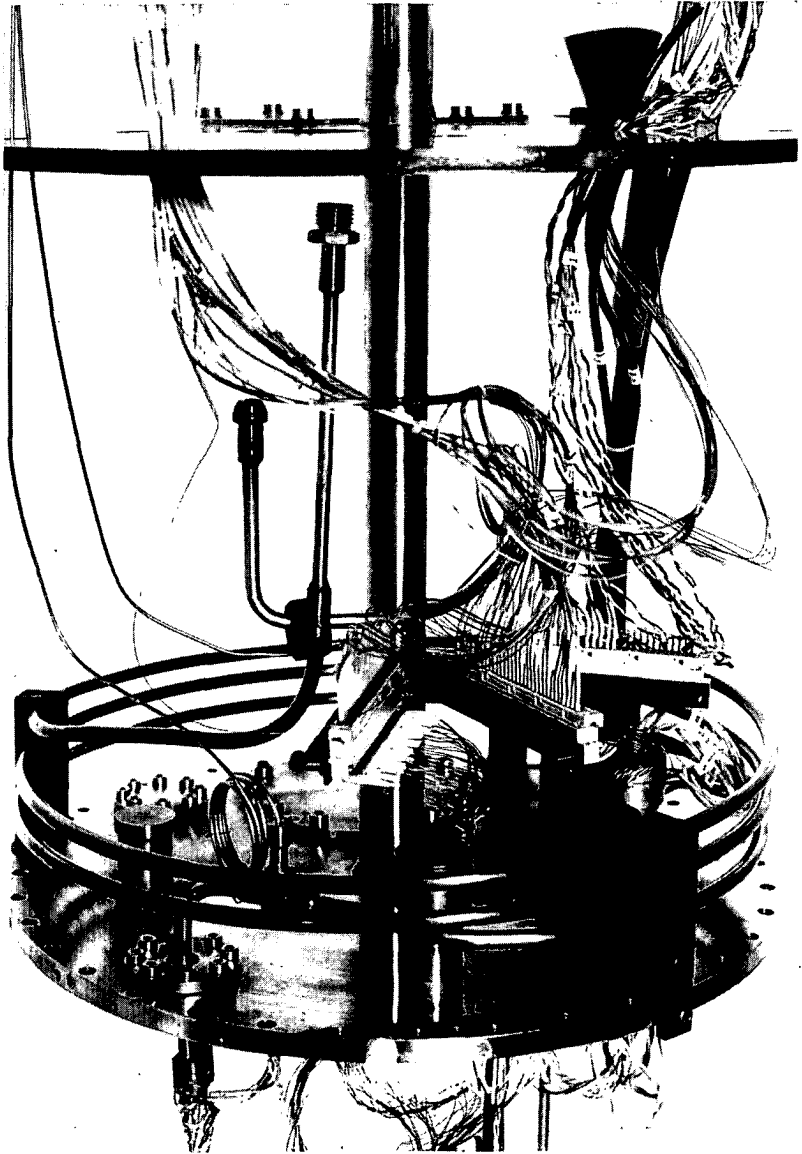
Figure 5.4   Picture of a detail of the flange of the vacuum vessel
             (copper spiral heat exchanger, electrical lead throughs,
             connectors supercritical helium conduit).

To minimize the helium evaporation a copper shield was soldered on
the pumping tube, which made contact with the 77 K link of the inner
helium bath. To avoid oxidation the shield had been gilt. Figure 5.3
shows the insert with mounted and demounted vacuum can and Fig. 5.4
shows a detail of the upper flange of the vacuum vessel.
In the supercritical helium conduit an extra heat exchanger was con-
structed, situated on the top of the vacuum vessel. This exchanger
had to be submerged in liquid helium, which surrounded the vessel,
and compensated the heat inleak of the transfer tube.
In the vacuum vessel a stationary heater was mounted. This heater
made it possible to increase the inlet temperature of the helium flow
before entering the test section. The heater consisted of a copper
tube (length 300 mm, inner diameter ~ 4 mm, outer diameter ~ 6.35 mm)
wrapped around with insulated zeranin resistance wire (zeranin, alloy
of 88% Cu, 6% Ge, 6% Mn, from Isabellenhütte, Appendix C). The wire
was glued with GE 7031 varnish (Oxford Instruments) on the tube. A
few layers of super-insulation had been wrapped around the heater-
tube-section to reduce the heat radiation.
The temperature of the supercritical helium conduit was monitored by
four carbon glass resistors (Lake Shore, model CGR-1-1500). An extra
CGR was mounted on the upper flange of the vacuum vessel. The resis-
tors were mounted in small copper blocks with the aid of Apiezon N
grease, the four insulated wires of each sensor were attached to the
copper blocks with GE 7031 varnish, thus heat leakage or input
through the wires could not influence directly the thermometers. The
picture of Fig. 5.5 shows a detail of the construction.

5.1.3. Transfer tube

In first instance the two cryostats were linked with two transfer
tubes, one for the in- and one for the outcoming flow, but these
tubes showed a bad performance during the first tests (bad vacuum,
large heat leakage).
A new transfer tube consisting of concentric tubes was designed.
Through the inner stainless steel tube supercritical helium flowed to
the experiment. This stainless steel conduit was surrounded by a cop-
per tube and on this "shield" a small copper tube was soldered in
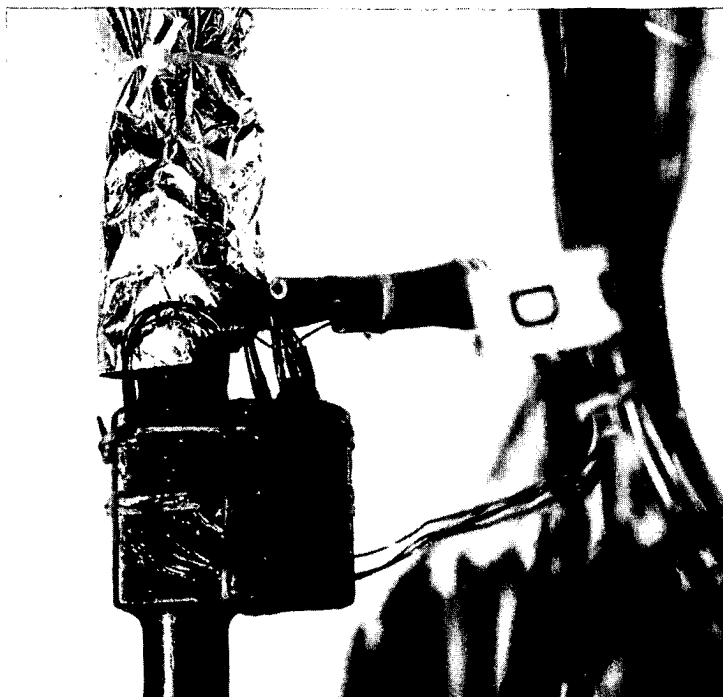
Figure 5.5   Picture of the small copper block in which the carbon
              glass resistor was mounted with the aid of Apiezon N
              grease. The grease was required for good thermal contact
              between thermometer and copper. The electrical wires
              were glued onto the copper with GE 7031 varnish and kept
              in their position with dental flosh.

which the return flow of helium passed. Around the second tube an-
other copper shield was situated which was cooled with liquid nitro-
gen. The whole was enclosed in a stainless steel housing. All the
three inner tubes were wrapped around with super-insulation. The
tubes were kept in position by small nylon spacers. Figure 5.6 shows
the cross section of the transfer tube.

The space between the shields was evacuated. After evacuating with a
small oil diffusion pump, a vacuum of 10^{-6} - 10^{-5} mbar was realized
during the experiments. From separate preliminary experiments it was
concluded that the heat leakage was about 0.5 W (mass flow 0.2 g/s).
For these measurements the extra heat exchanger in the second He-
cryostat was not mounted.

The transfer tube was connected to the heat exchanger and the insert of the second He-cryostat with conical stainless steel connectors. They were soldered or welded onto the tubes. To reduce the probability of helium leakage very thin indium foil was laid inside the connectors on the closing surfaces (Fig. 5.7).
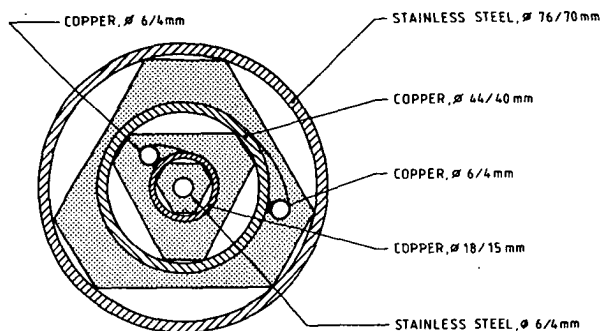

Figure 5.6   Cross section of the transfer tube. The inner stainless steel tube is for the incoming helium flow (direction to experiment). The small copper tube on the second copper shield is for the outcoming flow (from experiment). The third shield is the 77 K shield (liquid nitrogen flows through small copper tube on shield. The shields are spacered by thin triangular nylon plates.
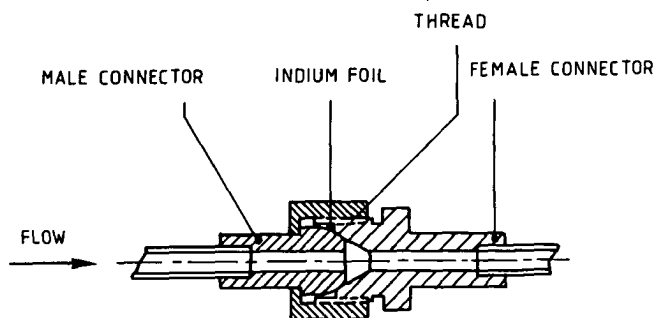
Figure 5.7   Longitudinal section of the connectors of the supercritical helium conduit.

5.1.4. Flow meters

The blow down loop had been equipped with an orifice flow meter which
had been mounted at the outlet of the circuit. But inaccuracies were
introduced in the flow measurements by small pressure oscillations
caused by a back pressing valve. This valve was necessary because the
helium evaporation from other experiments were also linked with the
gas holder. Otherwise the loop would be damaged if somewhere a super-
conducting magnet would quench (causing suddenly a pressure wave by
the enormous evaporation of liquid helium).
When this flow meter at the outlet position would be working at a
pressure of a few bars the problem would be solved. However, it would
then not be possible to create a pressure of 3 bar at the test sec-
tion for large flows (because of the pressure drop over the heat ex-
changer).
For these reasons a new flow meter was placed at the high pressure
side of the loop (15 bar). Small pressure fluctuations would not
introduce large errors, because the density of helium increases with
a factor 15 (10 mbar at 1 bar is 1%, at 15 bar 0.07%). Operating the
flow meter at 15 bar limited the pressure drop over the blow down
loop, although a flow of 3 g/s at a pressure of 10 bar at the test
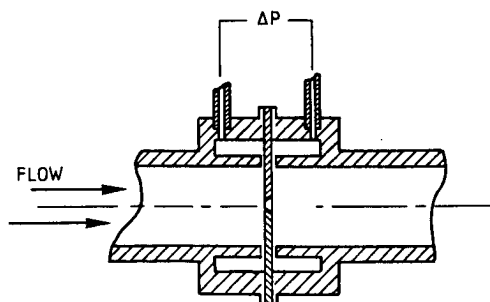section was still possible.

Figure 5.8   Longitudinal section of the orifice flow meters.
The gap between the orifice-plate and the orifice
support is 0.4 mm. The minitubes for the pressure
measurement have an inner diameter of 1 mm (outer
diameter 2 mm). The edge of the orifice in the plate is
45 degrees.

5.1.4.1. Design

The orifice flow meters were designed following the standards of the
Verein Deutsche Ingenieure (VDI – Durchflussmessregeln DIN 1952
[58]). When flow meters are designed by these standards and the cal-
culated dimensions are in the range of the standards, then it is not
required to calibrate the flow meters.
The correlation between mass flow $\dot{m}$ and the pressure drop Δp over the
orifice is

$$\dot{m} = \alpha \ \varepsilon \ \delta \ D^2 \sqrt{2 \ \rho \ \Delta p} \qquad\qquad (5.1)$$

with α the coefficient of discharge, ε the expansion factor, δ the
ratio between the orifice diameter d and tube diameter D ($\delta = d/D$)
and ρ the density of the fluidum. For helium at 15 bar $\rho = 2.39$ kg/m^3
and for ε the value 1 was taken . Although $\varepsilon = 1$ for noncompressible
fluids, the flow meters were designed for this value of ε, since it
was still necessary to calibrate the flow meters, because their di-
mensions validity range was at the limits of the VDI standards.
The maximum permissible pressure drop Δp is determined by the maximum
flow $\dot{m}_{max}$ through the orifice and the maximum of the range of the
pressure transducer used. $\Delta p_{max} = 250$ mbar (1 mbar = 100 Pa) was cho-
sen, thus

$$\alpha \ \delta = \frac{\dot{m}_{max}}{346 \ D^2} \ . \qquad\qquad (5.2)$$

On the other hand the Reynolds number Re $= 4 \ \dot{m}/(\pi D \eta)$ is important.
For the maximum mass flow it is given by

$$Re = 6.2 \ 10^4 \ \frac{\dot{m}_{max}}{D} \qquad\qquad (5.3)$$

with using $\eta = 204.8 \ 10^{-7}$ kg/(ms) for helium at 15 bar and 293 K.

Following the directives of DIN 1952 an optimum has to be found be-
tween α and δ using Re. It was not possible to measure the mass flow

	$\dot{m}$ (g/s)	Δp (mbar)
small orifice flowmeter $D = 6 \ 10^{-3}$ m $d = 1.5 \ 10^{-3}$ m	1 0.5 0.3 0.1	1126 281 101 11.3
large orifice flowmeter $D = 15 \ 10^{-3}$ m $d = 3.8 \ 10^{-3}$ m	3 2 1 0.5	244 108 27 6.8

Table 5.1. Pressure drop over the orifice
as a function of the mass flow.

range 0 - 3 g/s with one flow meter. Finally two orifice flow meters
with some overlap were chosen with the following dimensions:

    small flows :   0 - 0.3 g/s $\alpha = 0.6$, $\delta = 0.63$
                                       $D = 6 \ 10^{-3}$ m
                                       $d = 1.5 \ 10^{-3}$ m

    large flows :   0 - 3   g/s $\alpha = 0.6$, $\delta = 0.65$
                                       $D = 15 \ 10^{-3}$ m
                                       $d = 3.8 \ 10^{-3}$ m

In Table 5.1 the expected pressure drop as a function of the mass
flow is given. Because the flow meters operated at the boundaries of
the DIN 1952 standard, it had been necessary to calibrate the flow
meters (e.g. the standards of the orifice plate thickness were not
realized). In Fig. 5.8 a drawing of the longitudinal cross section of
one of the orifice flow meters is shown.

5.1.4.2. Calibration of the flow meters

The flow meters were calibrated with helium gas at a pressure of 15
bar (293 K). Helium from a high pressure bottle (volume 50 liter,
maximum pressure 200 bar) was adjusted to the desired flow with regu-
lation valves at the in- and outlet of the orifice flow meters. Both
flow meters have been constructed with an entrance and outtrance
length of 0.7 m.

The pressures were measured with bourdon pressure gauges, except the
pressure difference over the orifice, which was measured with an
electrical pressure transducer (Schlumberger). The helium volume,
which passed through the flow meter, was registered by a gas meter
(Schlumberger, working pressure at 1 bar). At the volume gas meter
the temperature of the helium was measured. Figure 5.9 shows schema-
tically the experimental equipment.

The mass flow is determined by

$$\dot{m} = \frac{\text{passed volume (of gas meter)} * \rho_{He}(P_3, T)}{\Delta t} \quad . \tag{5.4}$$

The time Δt was measured with a stopwatch. To minimize the read er-
rors of stopwatch and passed volume, the calibrations dured for long
flow times Δt. A lot of the adjusted flows were once or twice repeat-
ed with different Δt. During the measurements time and flow were
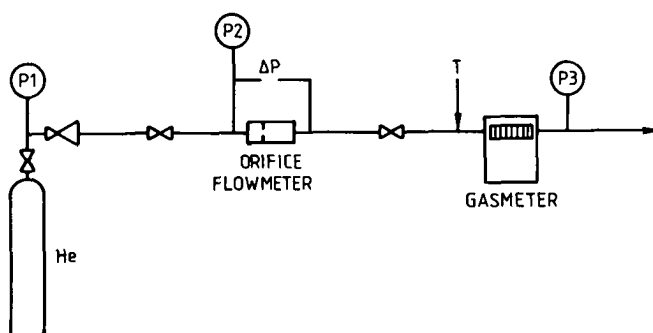

Figure 5.9   Schematical view of calibration experiments of the
orifice flow meters, P_1 - P_3 pressure gauges,
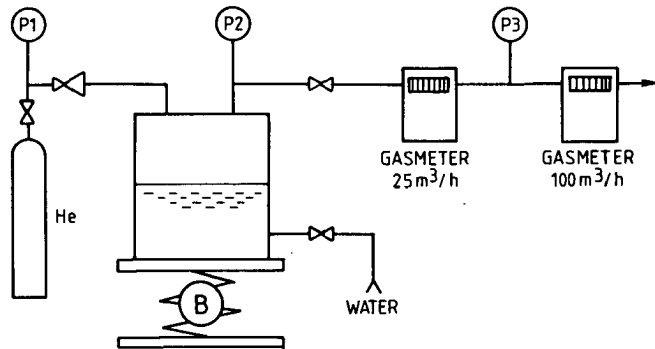T thermometer.

Figure 5.10   Experimental setup of the calibration of the gasmeters.
B is the balance, the vessel on the balance has a volume
of 500 ℓ.

also recorded at intervals. The calibration experiments were very
well reproducible. For small flows a gas meter with a maximum capa-
city of 25 m³/h was used, for large flows 100 m³/h. The uncertainty
of the orifice flow meters was given by the uncertainty of the gas
meters.

The gas meters were calibrated by a flow of helium, which was induced
by a flow of water. A large vessel of 500 liter was filled with
helium gas. When a valve was opened, water flowed into the vessel and
the helium was pressed out the vessel through the gas meters. The
displaced volume of gas was measured by the increase of the weight of
the water volume (Fig. 5.10). The balance had an error of 0.5 kg.
From the calibration experiments it was concluded that the gas meters
had an uncertainty of 1%.
In Fig. 5.11 the final calibration curves of both orifice flow meters
have been plotted. The pressure drop over each orifice was measured
with a differential pressure transducer. The output signal of these
transducers had a maximum of 2 V; the output voltage has been plotted
along the x-ordinate. It has to be noted that for the large orifice
flow meter a pressure transducer was used with a maximum pressure
range of 600 mbar instead of 250 mbar. The reproducibility of the
plots of Fig. 5.11 was good. The flows in the heat transfer measure-
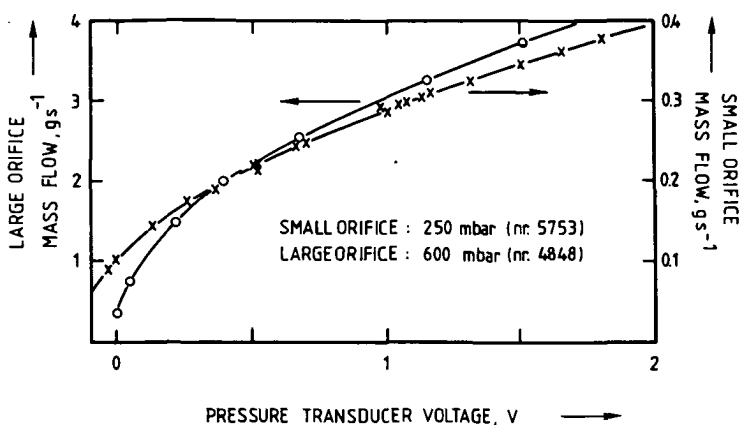ments were adjusted with these graphs.

Figure 5.11 Final calibration curves of the orifice flow meters
(working pressure 15 bar absolute).
Curves can be described with:
small orifice $\dot{m} = 0.27 \sqrt{V + 0.1^4}$
large orifice $\dot{m} = 0.0587 + 2.971 \sqrt{V + 0.01}$

A comparison between calculated and measured pressure drops shows a discrepancy (see Table 5.2).
This discrepancy is caused by the fact that the flow meters had been designed at the limits of the DIN 1952 standards, and that the orifice discs had not the desired thickness as laid down in these standards.

	$\dot{m}$ (g/s)	Δp (mbar)	
		calculated	measured
small orifice	0.1	11.3	15
	0.3	101	120
	0.38	180	209
large orifice	1	27	34
	3	244	340

Table 5.2. Comparison between measured and calculated
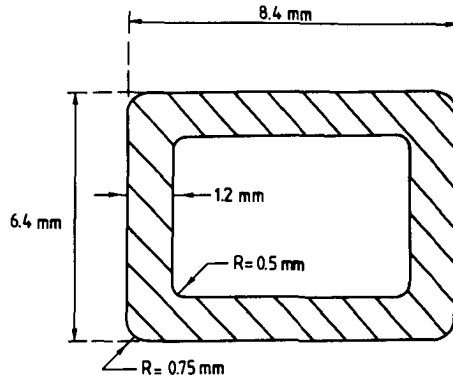pressure drop over the orifice flowmeters.

Figure 5.12 Cross section of the rectangular copper tube of the
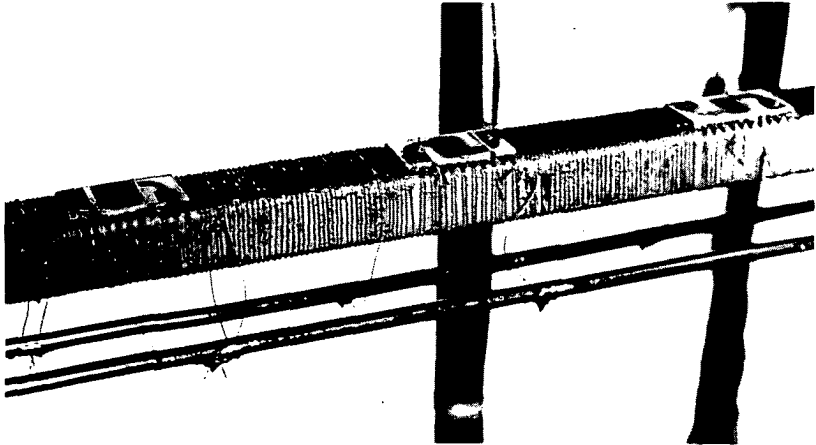test sections.

Figure 5.13 Test section with wound zeranin wire as heater (glued
with colloidal silver). Along the section the + and −
electrical terminals were mounted for the small heaters
(all the wound heaters were connected parallel and each
heater was wound contra-circulary to its neighbour).
The fast response thermometers were soldered on the
upper side of the tube. Under the thermometers were
small grooves in which also the heater wires were glued.

5.2. Test sections

The test sections were made of rectangular OFHC copper tubes, which
also have been used in the SULTAN 8 T inner coil [48, 59]. The dimen-
sions of the cross section of the tube are given in Fig. 5.12.
The advantage of this tube was the easy soldering of the thermometers
(flat surfaces). The final construction handlings were the soldering
of the fast response thermometers and the mounting of the heater.
When the test sections had been completed (with thermometers, heater
and electrical leads) they were soldered between the joints of the
supercritical helium loop in the vacuum vessel of He-cryostat 2.

5.2.1. Fast response heater

Special attention was required for the construction of an electrical
fast response heater. The produced heat must readily flow into the
copper, the heat pulse may not be distorted.
An option could be direct heating of the copper tube by an electrical
current, but the electrical resistance of the tube per unit length at
4.2 K is about 3.4 $\mu\Omega$. Thus, to generate heat fluxes of a few watts
large currents are required (more than 1000 A). Secondly, these cur-
rents have to be pulsed and because of the desired well-defined con-
stant heat fluxes it is required that the current pulses have a
square form. To realize large current block pulses is very diffi-
cult and thus the possibility of indirect electrical heating with
the aid of insulated resistance wires and foils has been considered.

Basically four heater constructions were tested.

1a. Stainless steel foil (thickness 10 μm, width 10 mm) was electri-
    cally insulated from the tube with thin paper (thickness
    40 - 45 μm). Stainless steel and paper foil were glued on the
    tube with use of GE 7031 varnish. At 77 K and 4.2 K bubbles oc-
    curred between stainless steel foil, paper and tube. This might
    be caused by bad drying of the solvent of the varnish.

1b. Instead of stainless steel nichrome (NiCr) ribbon had been used. No bubbles, but the attachment was bad.

2. Commercially available Scotch 850 Argent tape was wrapped around the tube (tape: mylar foil of 50 µm thickness on which a silver film of 0.03 µm thickness had been deposited. The adhesive layer had been applied on the silver film). The electrical insulation at 4.2 K was perfect, only a response time of 200 ms was measured, possibly caused by partly coming off of the tape from the tube by shrinkage.

3. Insulated zeranin wires (diameter 0.1 mm, insulation thickness of about 15 µm) were glued onto the tube with colloidal silver. The attachment at 4.2 K was very good. First experiments showed a response time of 0.5 ms. After constructing a complete test section it was not possible to reproduce this response time. When finally response time experiments were repeated with the use of gold-chromel thermocouples it became clear that the heat transfer through the silver layer (on micro-scale existing of a lot of silver grains) was the limiting factor. From a few experiments with different heater constructions it followed that in all cases the response times were in the order of 2 ms. A detail of one of these "slowly" heated test sections is shown in Fig. 5.13.

4. Manganin foil of 10 µm thickness and 2 mm width was electrically insulated from the tube with very thin paper (paper thickness of 25 µm). Manganin and paper foil were glued onto the four sides of the rectangular tube with special strain-gauge bond (M-bond 610 of Micro Measurements). For drying the bond and getting the desired strength it was required to apply a heat treatment. The whole test tube was annealed in an oven (at 1 bar in an atmosphere of air) during 4.5 hours at a temperature of 100°C. This anneal temperature did not influence the thermometers (change of calibrations; this was measured afterwards), because this temperature was less than the anneal temperature of the fast response

thermometers (150°C).

The heat strips were attached to the copper test tube side for
side, thus the test sections were annealed totally 4 times.
The thermometers were soldered on the tube before the heater was
glued, because the soldering temperature (160°C) might damage the
paper (scorched paper).
The manganin foil was especially delivered by Billiton and the
paper foil was commercially available cigarette paper. From the
available cigarette paper brands one package was bought at a
typically Dutch tobacconist's shop. At the laboratory the thick-
ness of the various cigarette papers was measured and the thin-
nest one was chosen to be applied (cigarette paper from
S.D. Mondiano (made in Italy), thickness 22 – 25 μm). A detail of
this type of heater is shown in Fig. 5.15.

The response time of the various constructed heater sections was
measured in the same way as the response time of the thermometer.
One of the fast response thermometers was soldered with indium on
the tubes. For the measurements the tubes were mounted in a vac-
uum vessel and the vessel was submerged in liquid helium. During
the experiments at 4.2 K the vacuum in the vessel was kept at
10^{-6} mbar and in the tube at 10^{-4} mbar. Small heat pulses were
released in order to keep a region of nearly constant material
properties and the temperature response was measured.
The same formalism of paragraph 4.3.2 was used for determining
the response time.
The results of the measurement on the fourth type of heater con-
struction (manganin foil/thin paper) showed the same characteris-
tics as the thermometer response time measurements.
The response time of the heater must therefore be better than the
thermometer response time (τ_r < 0.6 ms).
An estimation of the response time can be made by using some
literature values. For example, when the paper that has been
soaked with bond, it can be regarded as a filled epoxy, the λ
and c_p of this kind of materials can be used [60].
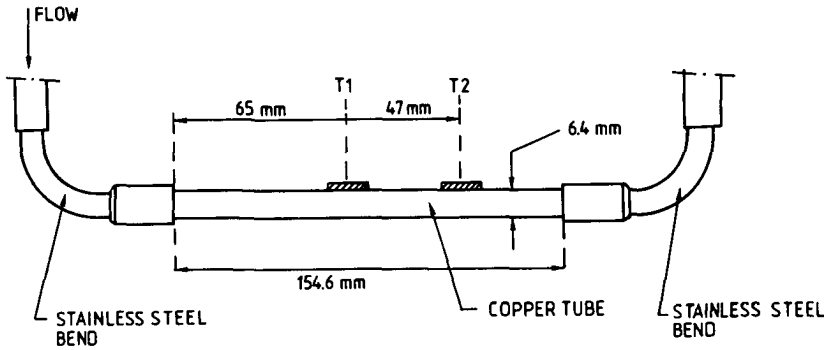
Figure 5.14   Dimensions of test section 1 and the positions of the
              thermometers T_1 and T_2.
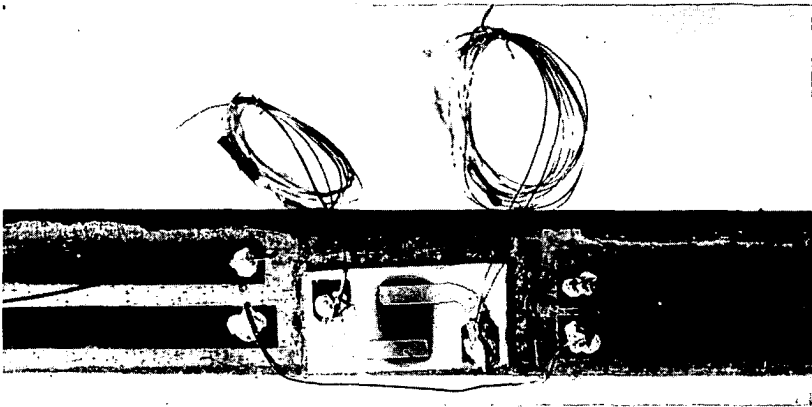

Figure 5.15   Details of the copper test tube (test section 1). The
              thermal sensitive carbon film is in the centre on the
              aluminum substrate of the fast response thermometer.
              On both sides of the thermometer two strips of manganin
              foil were glued onto the tube, electrically insulated
              from the tube with thin paper.

With λ = 0.05 W/(mK), ρ = 2000 kg/m³, c_p = 2 J/(kgK) and a rela-
tively large thickness d = 50 µm, the response time is of the
order of

$$\tau = \frac{d^2}{a} = \frac{\rho\ c_p\ d^2}{\lambda} = 0.2\ \text{ms}\ . \tag{5.5}$$

Due to its best performance the fourth type of construction was
accepted.

5.2.2. Test section 1 for heat transfer measurements

After constructing various test sections with the different kind of
heaters, the final test section for the transient heat transfer mea-
surements to a flow of supercritical helium was made of the
SULTAN 8 T inner coil copper tube. A length of about 155 mm of the
copper tube was soldered between two 90° bends of stainless steel
tube. The circular inner diameter of the steel tubes had the same
hydraulic diameter as the copper tube D = 5 mm).
The use of stainless steel minimizes the axial heat conduction
through the wall. At 4.2 K the thermal conductivity of stainless
steel is about 1 W/(mK) and the thermal diffusivity is about 6.25
10^{-5} m²/s (copper: 0.33 m²/s).
The positions of the fast response thermometers were determined on
the basis of the thermal entrance length. The entrance length is de-
fined as the length of pipe required to reach a Nusselt number that
is 95% of the fully developed flow value. An entrance length of 8 - 9
hydraulic diameters is required (Mills [61]). The same order of
length is required after a bend, a narrowing or widening section
[62]. The thermometers were soldered on the tube with indium. Indium
was used as solder because of:
1. The good thermal conductivity at low temperatures (at 4.2 K in the
   order of 800 W/(mK) [63]. Radebaugh [64] measured the thermal con-
   ductance of indium soldering joints. At 4.2 K he found for a
   Cu-In-Cu joint a conductance of 300 kW/(m²K).
2. Superconductivity occurs below a T_c of 3.4 K (deterioration of the
   thermal conductivity in the superconducting state).

3. Melting temperature is 156.6°C, this is slightly higher than the
   anneal temperature of the fast response thermometers (150°C). It
   was seen from a few experiments (and also after constructing the
   various test sections with soldered thermometers) that the solder-
   ing did not influence the calibration. The thermometers were lift-
   ed up in temperature above the annealing temperature during only
   a few seconds while soldering.

On the four sides of the tube the foils of the fast response heater
type 4 were mounted. Figure 5.14 shows the dimensions of the test
section and the positions of the thermometers. The picture of
Fig. 5.15 shows a detail of the test section.

5.2.3. Test section 2 for axial heat transfer and pressure waves

A second test section was developed to analyse the heat transfer in
axial direction, and to detect the existence of a hot gas volume and
to follow it in the flow in addition to pressure waves. These pressu-
re waves are caused by releasing heat pulses.
Pressure waves in a flow of supercritical helium were predicted by
Cornelissen [65] with the aid of a numerical simulation model.
Induced pressure waves have an important influence on the propagation
velocity of forced flow cooled superconductors. A numerical study by
Cornelissen and Hoogendoorn [66] showed that the mechanism inducing
the pressure wave has to be found in the expansion of the heated
fluid near the wall. This expansion leads to a pressure rise and a
motion of the fluid. At the hot spot of the conductor, caused by the
released heat pulse, the electrical current flows through the copper
stabilizer and the quenched superconducting wires of the conductor.
Heat is generated by the current and the normal zone of the conductor
grows, the flow velocity and pressure get higher and higher, and the
coolant is forced out of the cooling channel at both ends.
As mentioned before, it is quite difficult to simulate a complete
forced flow cooled superconductor, because large electrical currents
are required when no magnetic field is available. For example, the
SULTAN 8 T inner coil conductor was designed for a transport current
of 1860 A at 8 T. To create a quench at 0 T a very large current

(~ 23 kA) would be required.

The existence of pressure waves could be detected by releasing heat pulses on a tube in which supercritical helium is flowing. The pressure waves propagate with the velocity of sound, and this latter is in the range of 100 - 300 m/s for supercritical helium at low temperatures [67]. Thus the detection of pressure changes should happen at a distance from the heater, so that it would take some time before the pressure wave arrives. When two pressure sensors are mounted with some distance between them, also the velocity of sound can be measured (in addition to determining the existence of the pressure waves), thus verifying the nature of the pressure waves.

5.2.3.1. Pressure transducers

The static pressure in the test section was measured with bourdon pressure gauges. These pressure gauges are too slow for detection of the pressure waves. The response of the pressure transducers have to be within a few milliseconds. In addition long tubes, which link the test section with the pressure transducers cannot be applied. The problem was solved by using small electronic pressure transducers which could be mounted on the test conduit. Only, they had to operate at 4.2 K. Breimesser et al. [68] did some experiments with small pressure sensors based on the piezo resistive character of a sensitive thin film. They used the sensor at 1 bar and 4.2 K in an experimental test rig rotating at 3000 r.p.m.

The mentioned pressure transducers are commercially available and for the experiments the Sensym LX 0520 AD sensor was chosen. The manufacturer guarantees response times less than one millisecond and can be used in the range of 6.8 bar without any harm. They can eventually be used up to 13.6 bar. All the specifications and guarantees of the manufacturer are given in the temperature range of −40°C +105°C.

At room temperature the sensitivity of the LX 0520 AD sensors was about 5 mV/bar, at 77 K about 10 mV/bar and 4.2 K about 100 mV/bar. Thus the sensitivity increases with a factor 20 and from ohmic measurements it was concluded that the resistance of the sensitive film increases from 1.8 kΩ at 293 K up to larger than 10 MΩ at 4.2 K.
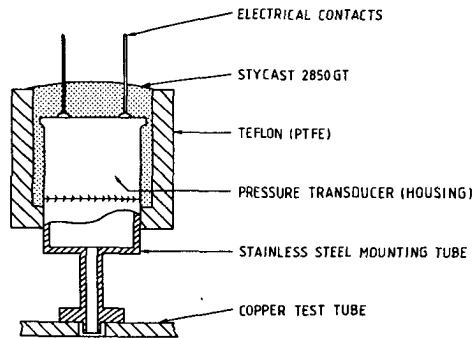
Figure 5.16A Schematical view of the mounting construction of the fast response pressure transducers. Diameter of the transducer is 9 mm, diameter of the small part of the stainless steel mounting tube is 2/1 mm.
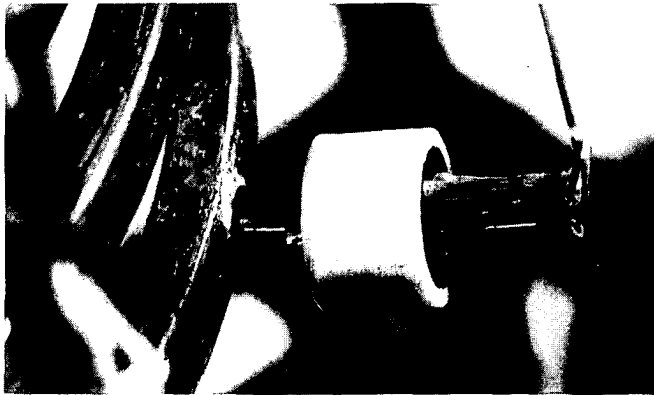

Figure 5.16B Picture of mounted fast response pressure transducer.

This latter value had the consequence that the input impedance of the
amplifiers had to be adapted (paragraph 5.3).

It was found from some introducing experiments on a small test sec-
tion (a conduit filled with static supercritical helium) that the
sensors were not quite reliable and that the calibration curves
change between the various cool down runs. But, when the sensors were
calibrated at the start of the runs at 4.2 K and they were kept at
helium temperatures, there were no variations in the calibration
curves.

Because the sensors were mounted on the test tube filled with super-
critical helium in an environment of vacuum (at 4.2 K), they had to
be absolutely vacuumtight for the high helium pressures at these low
temperatures. The sensitive film of the sensor was mounted in a small
stainless steel cap with an orifice (inlet for the fluid) which was
sealed with a slab with the electrical contacts. To ensure against
leakage, the sensor was embedded in stycast 2850 GT (supplied by
Emerson and Cuming). To make soldering on the test conduit possible,
the sensor was welded on a small stainless steel holder.

Figure 5.16A shows schematically the final construction and the pic-
ture of 5.16B shows a mounted pressure transducer.

5.2.3.2. Design and construction of test section 2

For the heat transfer measurements a special tube was constructed
existing of the rectangular copper tube with parts of rectangular
stainless steel tubes between it. The heated section was made of
copper tube with a fast response thermometer soldered and a type four
fast response heater glued on it. At a distance of 17.5 mm and
42.5 mm from the heated section two fast response thermometers were
soldered on copper tube sections of 15 mm length. Between the heated
and thermometer sections stainless steel tubes of 14 mm length had
been soldered. These stainless steel sections minimized heat transfer
through the wall of the tube, so the two thermometer sections would
measure the fluid temperature. At a mass flow of 3 g/s the average
velocity is about 1 m/s, thus it lasts about 20 ms when the hot
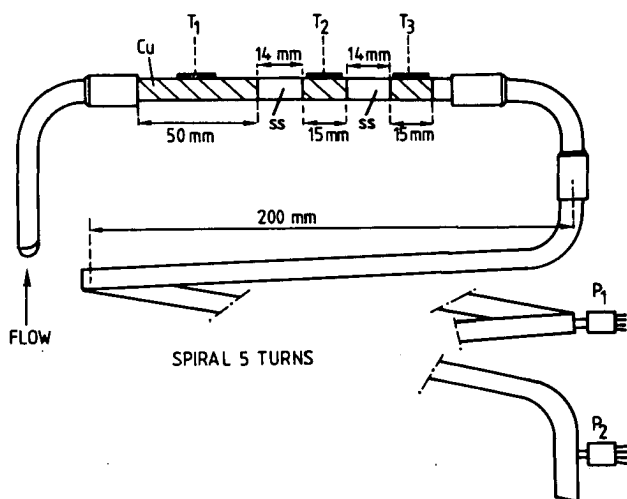volume of gas passes thermometer 2.

Figure 5.17   Dimensions of test section 2 and the position of the
thermometer T_1, T_2 and T_3. Cu is rectangular copper
tube, SS is stainless steel rectangular copper tube.
P_1 and P_2 are the fast response pressure transducers.

The various sections of the tube were soldered with silver-copper
solder. Because the solder attaches badly to stainless steel, the end
sides of these tubes were plated with a thin nickel layer. On the end
sides of the copper sections small cams had been milled to create a
well-defined slit (0.02 mm) for the soldering foil. To keep the var-
ious sections in position during the soldering process a boron ni-
tride fitting was inserted in the tubes. The tube was soldered in a
vacuum oven at a temperature of about 800°C. The rectangular holes in
the stainless steel tubes were made by a sparking method and the
holes were polished afterwards. Thus the test section had over its
total length the same cross section and the same wall roughness.
At the outlet of the heater thermometer section a large spiral of
copper tube was mounted. The total length of the spiralized tube was
4 m. Halfway and at the end of the spiral the pressure sensors were
soldered. The distance between them was 1.945 m. Figure 5.17 shows
the dimensions of the test section and the picture of 5.18 shows the
test section mounted in the insert of the second cryostat.
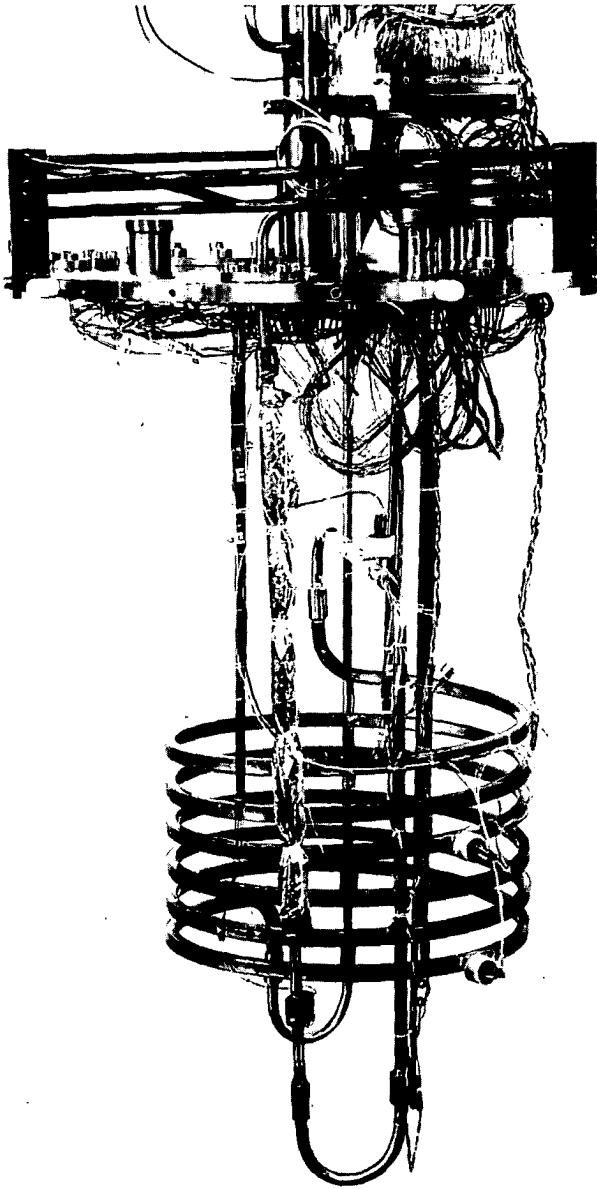
Figure 5.18 Picture of mounted test section 2. Halfway the flange
            and the spiral is the horizontal heater thermometer
            section. On the left side is the vertical stationary
            preheater (wrapped with super insulation). The fast
            response pressure transducers have been soldered on the
            spiral (halfway and bottom, right side).

5.3. Measuring circuits and data acquisition

5.3.1. Electronic circuits

The central measuring unit was a transient recorder of Data Lab with
8 memory modules, in which the signals of the fast response thermome-
ters, the fast pressure transducers and the current and voltage pulse
across the fast response heater were stored.
The resistance of the carbon thin film thermometers was measured by a
four wire potentiometric system. Excitation currents of 10 μA sup-
plied by a constant current source were passed through the films.
This constant current source exists of a cascade of thirty 4.5 V bat-
teries. The thermometers were part of a bridge circuit, so apart from
the total resistances also the changes with regard to e.g. the 4.2 K
level could be recorded.
To minimize the influences on the excitation current, when the carbon
film resistance decreases because of the temperature rise during a
heat pulse, large resistors were put in series with the thermometers.

Figure 5.19 Electronic circuit for the excitation current of the
thermometers and the manner of measuring the voltage
of the thermometers. The power of the current source has
been supplied by a battery bank (serial connection of
thirty 4.5 V batteries).

Figure 5.19 shows schematically the used current source. The uncertainty in the measured 10 µA was determined by the uncertainty in the 10 kΩ resistors (1% resistors).
The output voltages of the thermometers were amplified by special DC-amplifiers.The amplified signals were recorded on the transient recorder.
The amplifiers were developed at ECN for these measurements and they have a maximum bandwidth of 30 kHz. Gain and bandwidth could be selected (gain 50 - 10^4, bandwidth 20 Hz - 30 kHz).

Also the carbon glass resistors were fed by the constant current source. The output signals were amplified and recorded on a 6 pens paper recorder (Rikadenki). This recorder registered also the relevant pressures of the orifice flow meters. The orifice flow meter signals were also measured by a digital multimeter.

The same pulse generator as mentioned in paragraph 4.3.3 was used for the fast response heaters. The current- and voltage pulses were recorded on the transient recorder. Differential amplifiers were used to separate groundings. It was then possible to chose the point of grounding of the circuit. Figure 5.20 shows schematically the used electronic circuit of measuring the voltage and current of the released heat pulse.

For the fast response pressure transducer a special high impedance buffer had been developed. At 4.2 K the output resistance of the sensor is about 20 MΩ which is larger than the input impedance of the memory modules of the transient recorder (1 MΩ). In the high impedance buffer an input impedance was realized of 1000 GΩ by using JFET's. The gain was 1 and the bandwidth of the buffer was 600 kHz. The voltage supplies of the sensors (+4 V, +8 V) were realized by using standard voltage and current suppliers (Delta E 030-1).
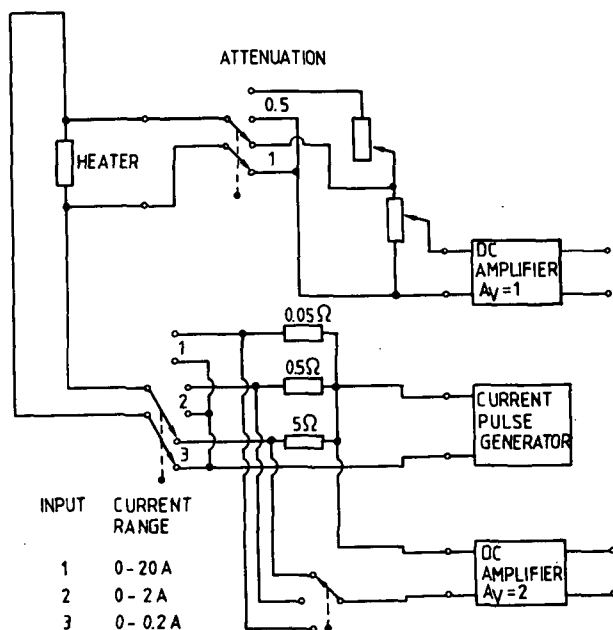
Figure 5.20 Electronic circuit and method of measuring the released
heat flow by the heater by means of $\phi = VI$.

5.3.2. Data record and handling

Every memory module of the transient recorder could store 4096 data
points with a resolution of 10 bits. The sample rate of the recorder
was in the range of 5 µs - 0.2 s (time base: 20.48 ms - 819.2 s). The
input amplifiers of the memories had a bandwith of 70 kHz and an in-
put impedance of 1 MΩ.

After a measurement the data of the memories were digitally stored on
diskettes for permanent record by a LSI-11 computer system (large
scale integrator). A small pre-analysing program could be used on
this LSI computer. It was possible to get the physically relevant
data like released heat flow, maximum reached temperature and inlet
temperature.

At a later stage, the data from the diskettes were processed on a
PDP-11 computer. In first instance the data of the thermometers were
translated to temperatures by the aid of the calibration curves of
the various thermometers. The released heat flux was computed from
the registered current and voltage pulses. The time was calculated
with the aid of the sample rate. Other important parameters, such as
the wetted surface of the tube, which has been required for deter-
mining the heat transfer coefficient, and the heat capacity of the
tube as a function of temperature, were written down in the computer
program.

The heat absorption by the heated tube

$$\phi_{tube} = m \, c_p \frac{dT}{dt} \tag{5.6}$$

had to be determined, because the heat flux to the supercritical
helium flow was given by the released heat flow minus ϕ_{tube}. The dif-
ferential coefficient dT/dt was numerically computed by the midpoint
rule

$$\frac{dT}{dt} = \frac{T_{i+1} - T_{i-1}}{t_{i+1} - t_{i-1}} \, . \tag{5.7}$$
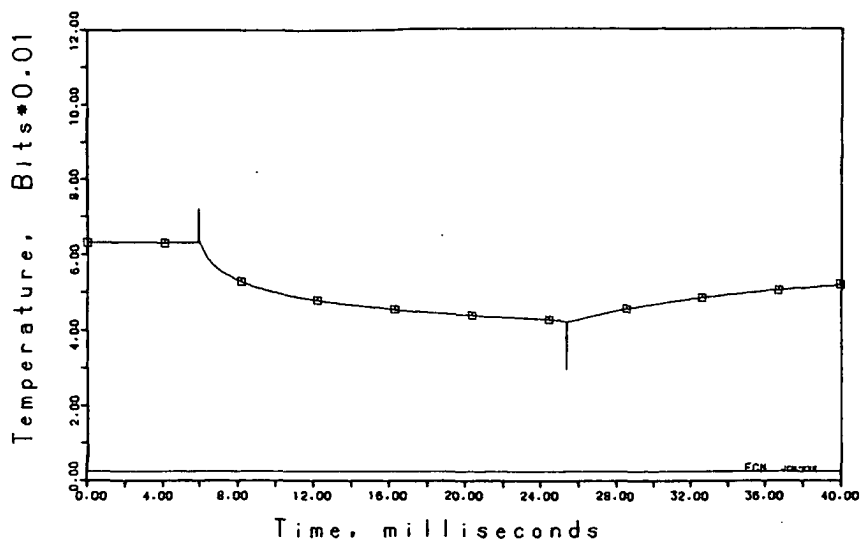
Figure 5.21A Originally recorded temperature signal. During temperature rise the resistance of the thermometer decreases (see e.g. Figure 4.5). Zero volt correponds with 25 bits.
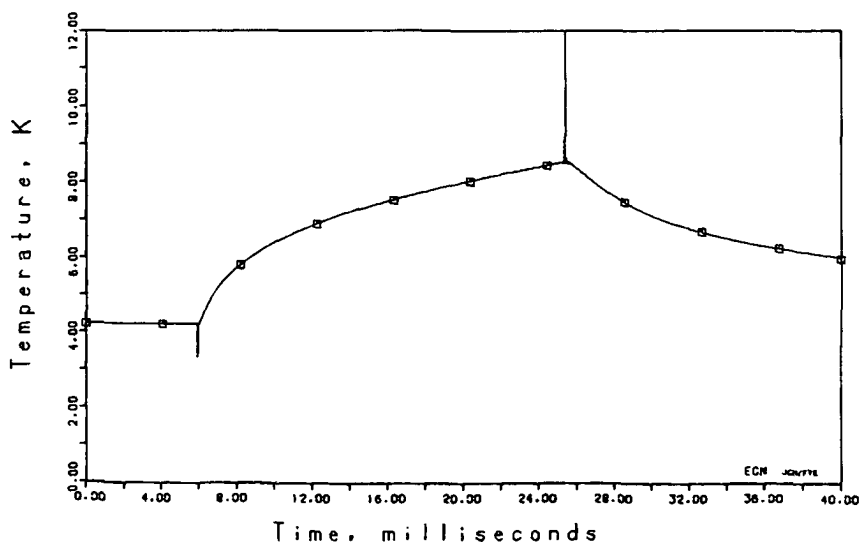

Figure 5.21B Computed temperature from recorded data. The smoothed temperature has been plotted too, but equals the original temperature curve.

Because of the discrete numerical levels (from the resolution of the transient recorder memories) numerical instabilities could occur (dT/dt gets zero and very large values). For this reason the temperature results were smoothed. The average temperature was determined over a time interval (time slice). The width of the time slice was at most 100 data points on the time ordinate and the time slice ran along the time ordinate with steps equal to the sample rate. When the sample rate was large (long registration time of the transient recorder) and the temperature responses became temperature peaks, the time slice became smaller because otherwise the peak would vanish by the smoothing.

Most of the experiments were sampled with rates of 5 and 10 μs, thus the recorded time window was 20.48 ms and 40.96 ms respectively. On these time scales the heat transfer phenomena lasted milliseconds, thus the smoothing had very small influences on the physical reality. For example, Fig. 5.21 shows one record with the originally recorded signal, the computed primary temperature signal and the smoothed temperature.

After computing the primary physical data T, Δp and ϕ, they were plotted as a function of time. These data were stored on Winchester disks. Later on these data were used to calculate the heat transfer coefficients. After the numerical and plotting procedures the data were stored on tape for permanent record. Figure 5.22 shows a diagram of the data recording and handling circuits.
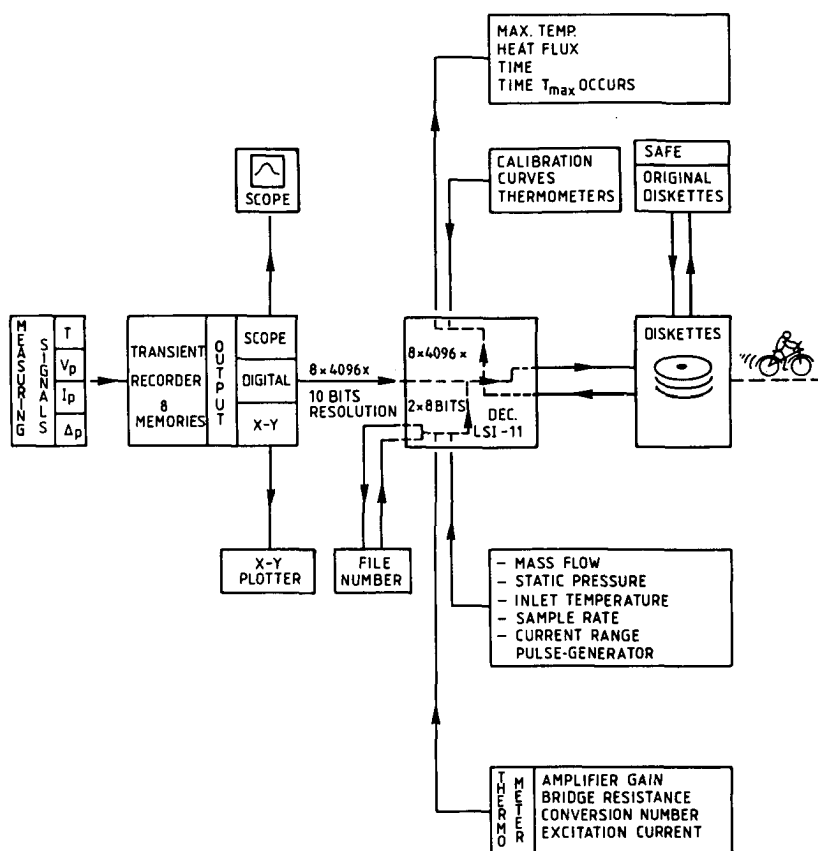
Figure 5.22 (left) Scheme of data handling (laboratory).
Primary measuring signals recording and data dumping on
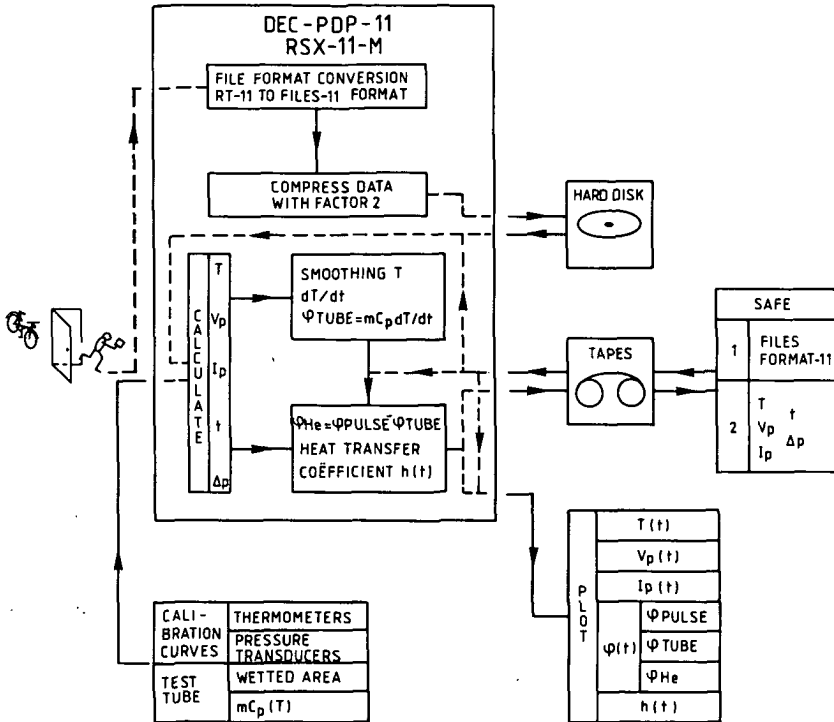diskettes.

Figure 5.22 (right) Scheme of data handling (office).
          Computing of the physical relevant data with the
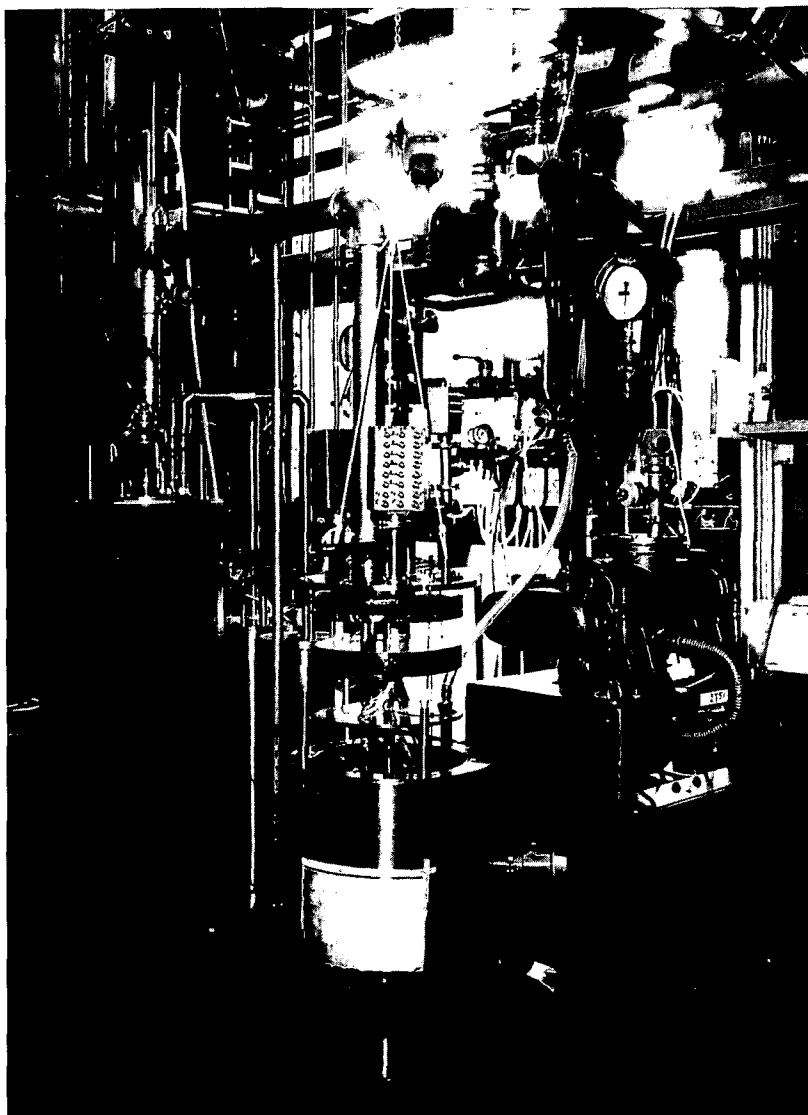   DEC-PDP-11 computer.

Figure 5.23   Picture of the heat exchanger and test cryostat.
A part of the insert of the test cryostat can be seen.
On the right side a molucular turbo vacuum pump is
standing. Between the two large cryostats two small
cryostats can be seen, one containing the 300 - 80 K
heat exchanger and the other liquid nitrogen and the
molecular filter bed. The transfer tube has been mounted
between the two cryostats.

CHAPTER 6

EXPERIMENTAL RESULTS[*]

6.1. Method of determining the heat transfer coefficient

The physical properties which were measured were temperature and heat
flow. The heat flow was released on the copper wall of the conduit
and the temperature of the wall was recorded. It was impossible to
measure directly the temperature of supercritical helium layer close
to the wall. It was not possible to insert a fast response thermome-
ter inside and free from the wall in the conduit.
All the heat transfer phenomena were related to the temperature dif-
ference of the wall temperature and the fluid bulk temperature. Be-
fore a heat pulse was released the bulk temperature was measured by
1) the standard carbon glass resistor thermometers and 2) the fast
response thermometers.
As was seen in chapter 3 the thermal diffusivity of helium is very
small (a_{He} at 4.2 K is about $5 \ 10^{-8}$ m²/s) and thus the penetration
depth is, on the millisecond time scale, of the order of tens of
micrometers. For example, in case of a well-defined temperature jump
at the wall, the penetration depth is given by (eq. (2.11))

$$\delta_T = \sqrt{\pi \ at} \ .$$

(6.1)

For example, for t = 10 ms the penetration depth is about 40 μm.
The hydraulic diameter of the tube was 5 mm, thus during the heat
pulses (even up to 100 ms) the bulk temperature of the helium flow
was basically the same as the inlet temperature of the flow.
The transient recorder was used in the "standby-mode"; it was record-
ing continuously.

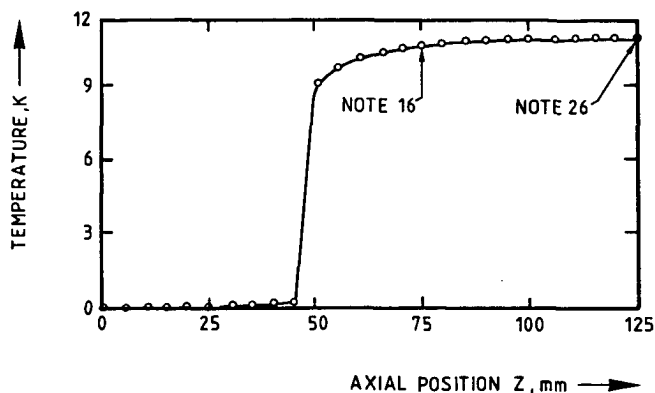*) Parts of chapter 6 and 7 have been published [81], [82]

Figure 6.1A Temperature along a test section, both ends consisting of 50 mm stainless tube and in the middle a length of 150 mm copper tube (axial symmetry at 125 mm). In the numerical model has been calculated with a heat release of 33.3 kW/m² and a heat transfer coefficient to the coolant (in the tube) of 3 kW/(m²K).
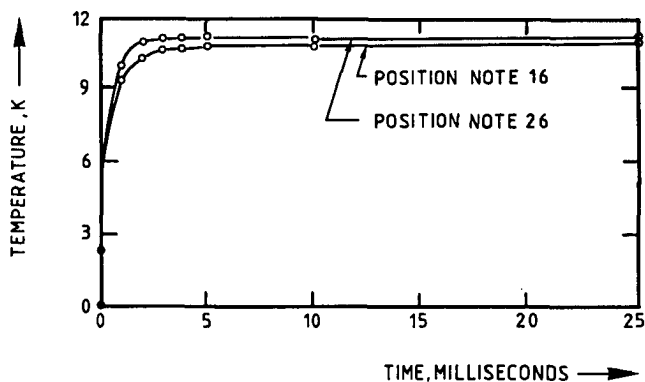

Figure 6.1B Temperature as a function of time at 75 mm of the entrance of the test section (note 16) and the middle of the test section (note 26) (see Figure 6.1A).

The transient recorder was adjusted at a delay time of 596 * sample
rate. When a heat pulse was released, the recorder was triggered and
started to memorize the signals from time ordinate point 596. The
first 596 points stored the pre-triggering signals, leaving 3500 data
points for the response on the heat pulse.

From the stored signals during the pre-triggering time the bulk tem-
perature (or inlet temperature) could be determined. Thus during an
experiment the temperature response as well as the bulk temperature
was measured by the same thermometer. The heat pulse was only re-
leased when the whole test tube was in thermal equilibrium, because
only then the wall temperature was equal to the helium- and thus bulk
temperature.

The heat transfer coefficient h was defined as

$$h = \frac{\phi_{He}}{A(T - T_b)} \quad .$$
(6.2)

Here A is the wetted surface inside the tube, T_b the bulk temperature
of the fluid before the heat pulse was released (and also during the
pulse because δ_T is small on the regarded time scale), T the measured
copper wall temperature and ϕ_{He} the heat flow, which flows from the
wall into the helium. All the heat transfer coefficients are correla-
ted to inlet bulk temperatures, which is common in the heat transfer
research.

To calculate the heat flow to the helium flow, ϕ_{He}, the total heat
flow released by the heater had to be corrected with the $mc_p(T)\frac{dT}{dt}$
(heating up) of the copper tube at every temperature:

$$\phi_{He} = \phi_{released} - m \, c_p(T) \, \frac{dT}{dt} .$$
(6.3)

The mc_p, which is a function of temperature, was taken at temperatu-
re T which occurred at time t.

The $\phi_{released}$ was computed from the recorded data as the product of
the current and voltage across the heater during the pulse. The re-
sistance of the thin film thermometers was calculated from the re-
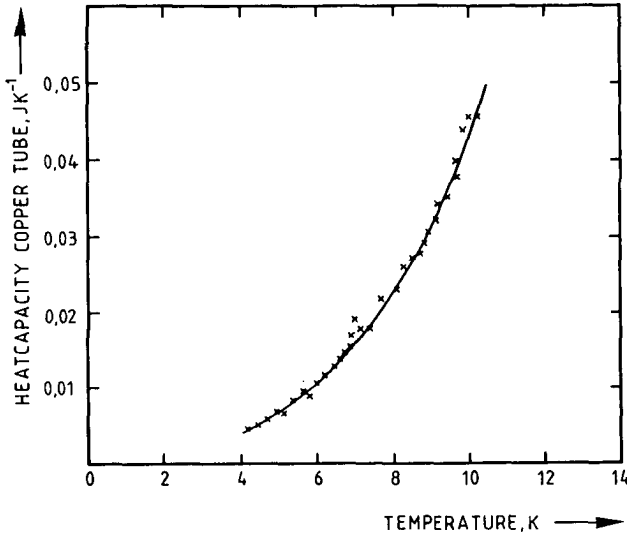corded voltage, the excitation current of 10 μA and the amplifier

Figure 6.2   Heat capacity of the copper test tube (test section 1)
             as a function of temperature.

T (K)	copper tube c_p (J/(kg K))	literature $c_p(1)$ (J/(kg K))	c_p (2) (J/(kg K))
4	0.096	0.108	0.1
5	0.165	0.166	0.16
6	0.262	0.247	0.24
7	0.396	0.361	0.35
8	0.571	0.498	0.48
9	0.793	0.679	0.64
10	1.068	0.895	0.86

Table 6.1. The specific heat of the copper tube and some
           literature values of the specific heat of copper.
           (1) copper with 5% Fe, ref. [70].
           (2) OFHC copper, ref. [83].

gain. From these ohmic results the temperatures were computed via the calibration curves of the thin film sensors.

The heat capacity of the tube mc_p was experimentally determined as a function of temperature. Because at every time t the temperature T was known, the quotient $\frac{dT}{dt}$ could be determined. Then with the aid of the $mc_p(T)$ function and the released heat flow, $V_p I_p$, the heat transfer coefficient according to eq. (6.2) was computed.

The axial heat conduction from the copper tube to the environment has been neglected in eq. (6.3). The stainless steel bends have a very low thermal conductivity ($\lambda \approx 0.1 - 1$ W/(m²K)). The wall cross section was about 30 mm², thus at every side of the tube the axial heat flow through the wall was of the order of

$$\phi_{ax} = 3 \ 10^{-5} \ \frac{dT}{dz} \quad W \tag{6.4}$$

Thus, for a large dT/dz, e.g. 5 K/mm, $\phi_{ax} = 0.15$ W; ϕ_{ax} can be neglected in addition to the released heat flows $\phi_{released} = 15$-30 W. Some numerical calculations have been employed to estimate the axial heat transport. In the numerical model a copper tube with a length of 15 cm was heated up with a heat flux of 33 kW/m². At both ends of the copper conduit two stainless steel tubes of 5 cm were situated. The heat transfer coefficient to supercritical helium was 3000 W/(m²K) and constant. From the numerical results it was seen that the temperature profile along the copper tube is quite constant and dT/dz at the copper-steel boundaries is of the order of 1.8 K/mm. An example of the calculations is shown in Fig. 6.1A and B.

6.2. Test section 1.

6.2.1. Heat capacity of the tube

For the heat capacity measurements the tube was mounted in its definite position in which it also would be used for the heat transfer measurements. Only instead of connecting the transfer tube to the supercritical in- and outlet a vacuum connection was used. In this

way it was possible to evacuate the inner of the tube.

The inside of the copper tube and the vacuum vessel were evacuated to 10^{-4} mbar and cooled down to 4.2 K by filling the second He-cryostat with liquid helium. To quicken the cool down of the tube a small amount of helium contact gas was released in the vacuum vessel. When the test section was 4.2 K, the vacuum in the vessel was restored up to 10^{-6} mbar.

The temperature at which the heat capacity had to be determined was realized by heating up the tube with the fast response heater. Because of the small axial heat leaks through the walls, the tube cooled down again, but very slowly (due to the stainless steel bends). With the fast response heater small heat pulses were released, and the tube rised slightly in temperature. The temperatures were measured with the fast response thermometers and the signals were recorded on the transient recorder and finally plotted with a x-y plotter. During the registered time range of 20 ms no temperature decrease was noticeable; the temperature jump caused by the small heat pulse was constant.

From the released (and also recorded) heat pulse and the temperature rise ΔT it was possible to determine the heat capacity by

$$\phi \; t_p = m \; c_p \; \Delta T \tag{6.5}$$

with t_p the duration of the heat pulse (a few milliseconds). The temperature rise ΔT was kept small (0.1 K - 0.2 K), so that c_p was nearly constant. In this way c_p was determined for temperatures up to 10 K. The results are shown in Fig. 6.2, and the heat capacity of the copper tube can be expressed by the correlation

$$m \; c_p = (4.0 \; T^3 + 33.44 \; T) \; * \; 10^{-5} \quad J/K , \tag{6.6}$$

where the uncertainties in the factors are respectively:
4.0 ± 0.08 and 33.44 ± 0.85.

In Table 6.1 the results are compared with two literature sources.

It must be said that eq. (6.6) counts for the complete test tube, thus including heater, thermometers and wires. However, the contributions of the latter parts are calculated to be small compared to the copper tube.

For test section 1 the wetted surface as used in eq. (6.2) was $33.3 * 10^{-4}$ m². (The wetted perimeter was 19.14 mm and the length of 174 mm of the copper tube included the ends which were soldered in the stainless steel bends.)

6.2.2. Inlet temperature 4.2 K

Most of the experiments were carried out at an inlet bulk temperature of 4.2 K. The experiments included determination of the heat transfer when pressure, heat flux and mass flow were varied.
Three pressures were chosen: 3 bar, 6 bar and 10 bar. The pressure of 3 bar is near the critical pressure of 2.27 bar. The influence of pressure (and temperature) on the volume heat capacity ρc_p of helium is shown in Fig. 6.3. Near 4.2 K the helium volume heat capacity is nearly the same for the three pressures. An energy release can have dramatic results on the temperature rise in the 3 bar case when the transposed critical temperature of 5.6 K is passed. At 10 bar the temperature increase will be more gradual.
The mass flow was in the range from zero to 3 g/s. In most experiments flows of 0.1, 0.3, 1 and 3 g/s were chosen. When it was found that the region from 1 to 3 g/s was the most interesting one, some more measurements were carried out with other mass flows, namely 1.5, 2 and 2.5 g/s.
The heat pulses had durations of 10 and 20 milliseconds. For studying the heat transfer becoming stationary, pulses of 0.1 s were released. The markers on the curves identify the various measuring runs. The data points (measuring points) of a measuring run were related to the sample rate of the transient recorder (see paragraph 5.3.2).
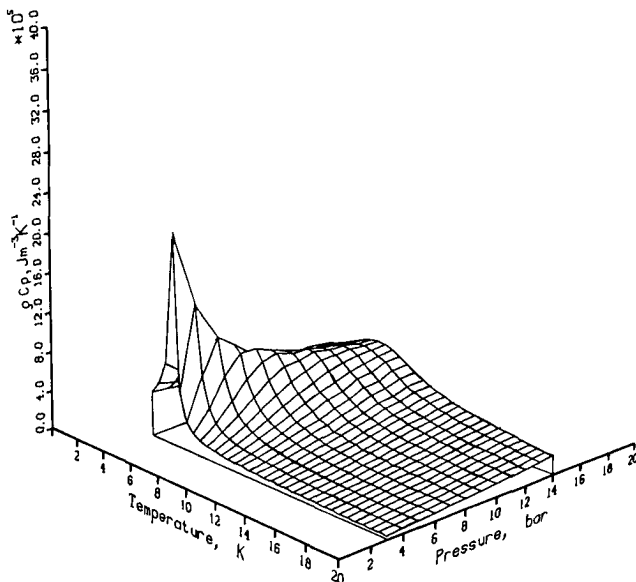
Figure 6.3   Volume heat capacity, ρc_p, of helium as a function of temperature and pressure.

6.2.2.1. Pressure variation

In Figs 6.4, 6.5 and 6.6 the results are shown for three fixed mass flows 0.3, 1 and 3 g/s respectively at different pressures.

There is no strong difference in the results and not much improvement from 3 to 10 bar. Noted is the different time scale of Fig. 6.5. The dip at the end of the pulse in the heat transfer coefficient is caused by i) the induction peak in the temperature signal (caused by the decrease of the heater current) and ii) the differential quotient dT/dt (used in eq. (6.3)) crosses zero because the temperature reaches a maximum at the end of the heat pulse. It must be remarked that the two thermometers on the copper tube registered basically the same temperature. The temperature difference between the two thermo-meters was less than 0.2 K (for large temperature rises). The ratio of this difference and the temperature rise was less than 3%.
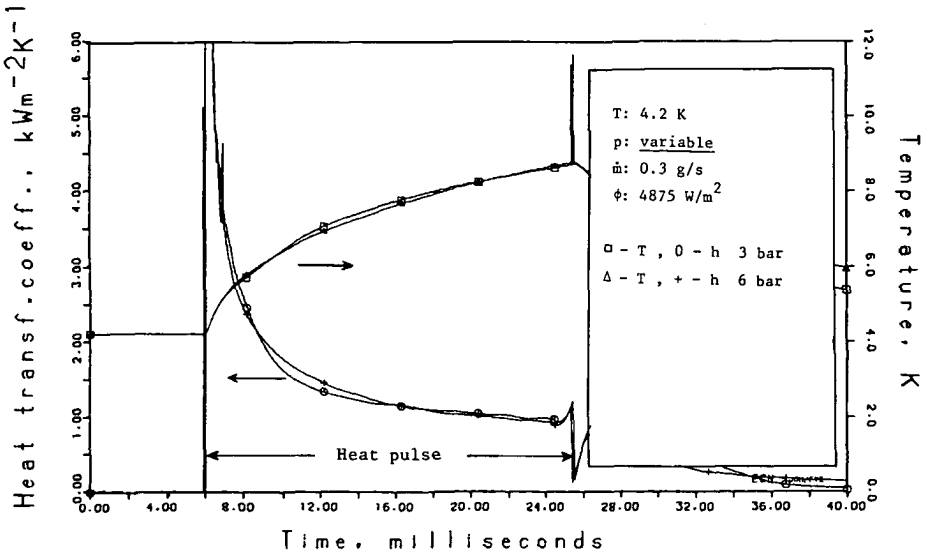
Figure 6.4   Heat transfer coefficient and temperature as a function
of time at 4.2 K; pulse started at 5.96 ms.
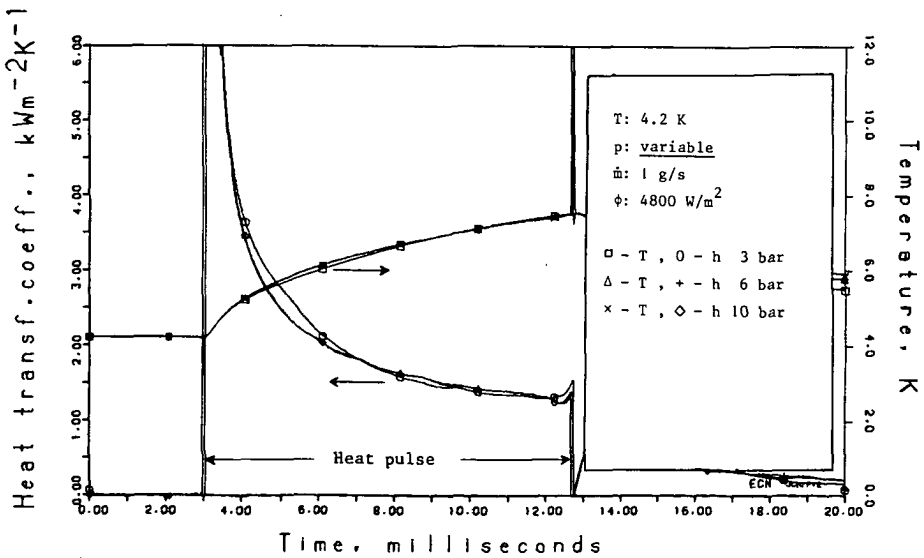
Figure 6.5   Heat transfer coefficient and temperature as a function
of time at 4.2 K; pulse started at 2.98 ms.
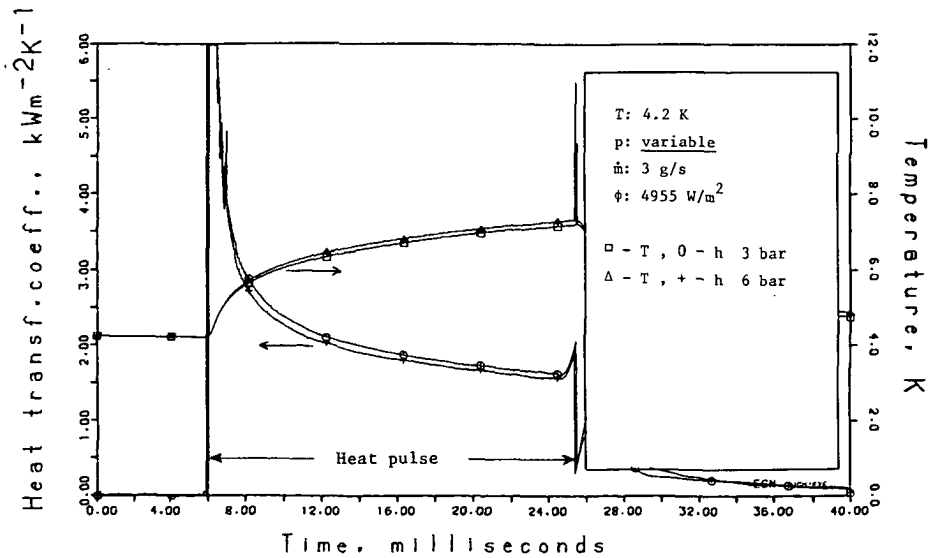
Figure 6.6   Heat transfer coefficient and temperature as a function
of time at 4.2 K; pulse started at 5.96 ms.
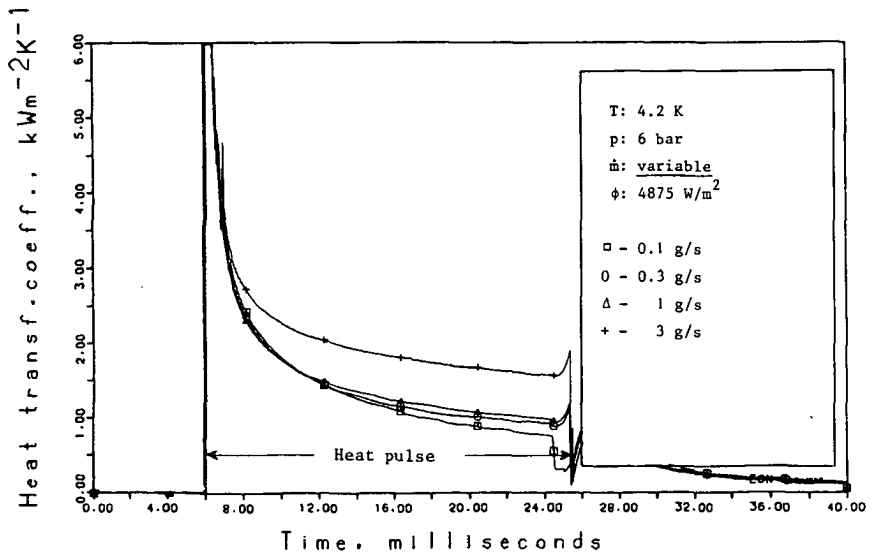
Figure 6.7 A. Heat transfer coefficient as a function of time at four
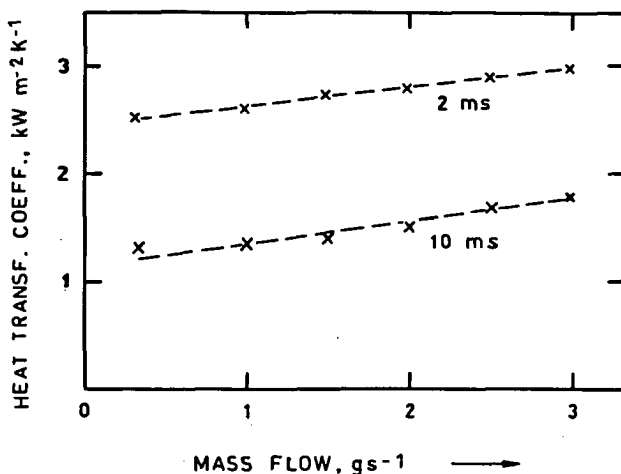different mass flows at 4.2 K; pulse started at 5.96 ms.

Figure 6.7B   Heat transfer coefficient at two times after the start of
the heat pulse as a function of mass flow at 4.2 K and
10 bar.

6.2.2.2. Mass flow variation

When the mass flow is increased there is an improvement of the heat
transfer for higher mass flows as can be seen from Fig. 6.7A. From
the experiments it had been seen that the improvement occurred at all
the three pressures (see e.g. Fig. 6.4 - 6.6). A gradual linear im-
provement of the heat transfer coefficient had been measured with
increasing mass flows. Some results at 10 bar are gathered in
Fig. 6.7B. As was seen in paragraph 6.2.2.1. there was no pressure
influence on the heat transfer. Similar results of Fig. 6.7B occur-
red at different pressures (3 bar and 6 bar).

For long heat pulses the heat transfer becomes stationary. It has to
be noted that for large mass flows the steady state value of the heat
transfer is reached sooner than for small flows. This can be ex-
plained by the fact that during the first milliseconds the heat
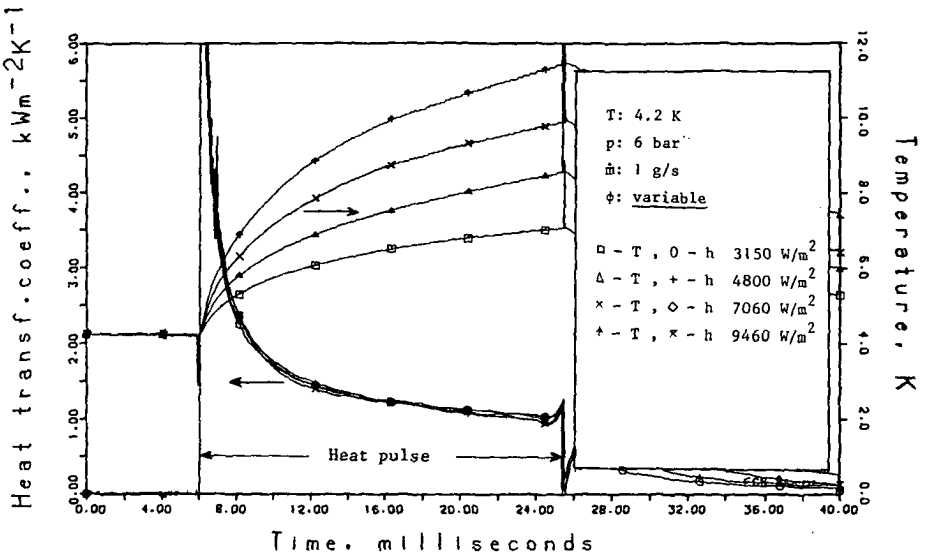
Figure 6.8 — Heat transfer coefficient and temperature as a function of time for different heat releases at 4.2 K; mass flow 1 g/s, pressure 6 bar, pulse started at 5.96 ms.
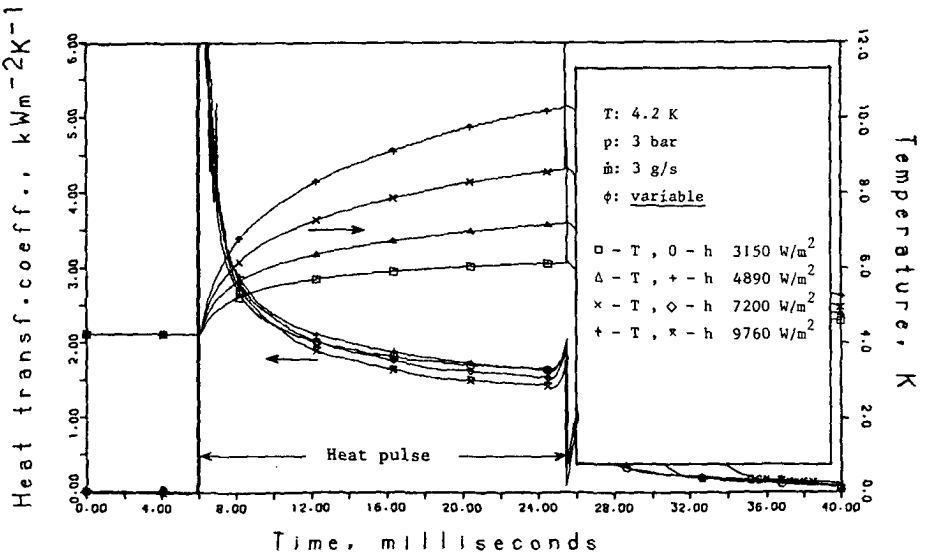

Figure 6.9 — Heat transfer coefficient and temperature as a function of time for different heat releases at 4.2 K; mass flow 3 g/s; pressure 3 bar; pulse started at 5.96 ms.

transfer is dominated by heat conduction in the laminar sublayer.
This layer is thinner for large flows, thus the time of noting the
turbulence influences becomes shorter for these large flows.

6.2.2.3. Heat flow variation

The heat transfer coefficient is hardly dependent on various heat
fluxes during the experiments as can be seen from Figs 6.8 and 6.9.
It must be remarked that the plots of Fig. 6.9 are from measurements
at 3 bar. The lowest heat transfer coefficients belong to the highest
temperature curve (largest heat input).

6.2.3. Inlet temperature 5 K

Higher inlet bulk temperatures were realized with the use of the sta-
tionary heater of 300 mm length (paragraph 5.1.2). This heater was
mounted upstream the test section. The carbon glass resistor thermo-
meters which controlled the helium temperatures were recorded on a
multipen paper recorder.
At an inlet temperature of 5 K also pressure, mass flow and heat flow
were varied.

6.2.3.1. Pressure variation

In Fig. 6.10 heat transfer coefficients and temperature responses are
shown of measurements with a mass flow of 3 g/s and a heat flux of
5100 W/m^2.
The 3 bar heat transfer results are slightly higher than the 6 and
10 bar results.

6.2.3.2. Mass flow variation

At 5 K there is also an improvement of the heat transfer when the
mass flow is increased, as can be seen from the plots of Figs 6.11
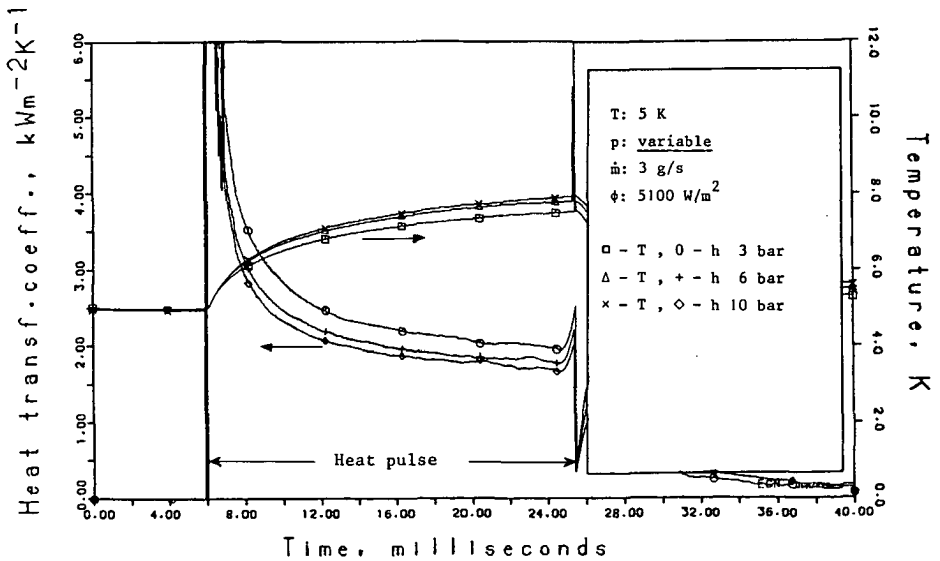(10 bar) and 6.12 (6 bar).

Figure 6.10   Heat transfer coefficient and temperature as a function of time at 5 K; pulse started at 5.96 ms.
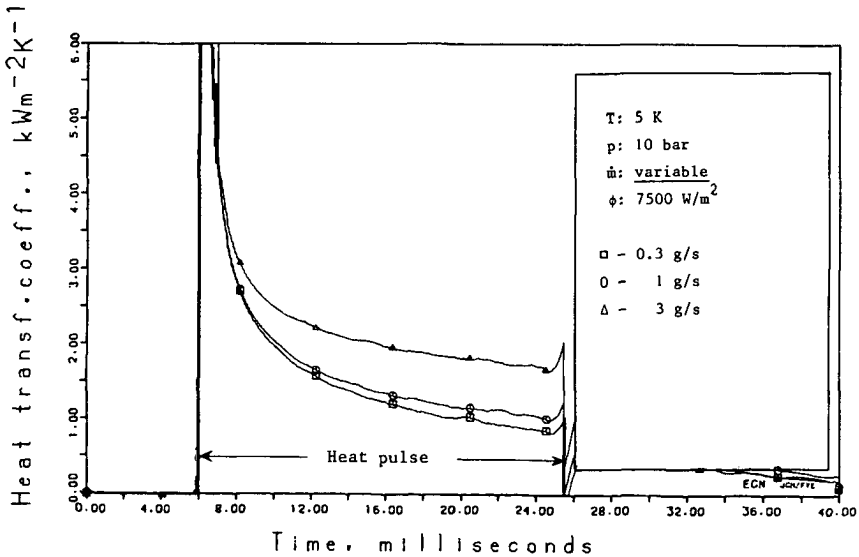

Figure 6.11   Heat transfer coefficient as a function of time at three different mass flows at 5 K; pulse started at 5.96 ms.
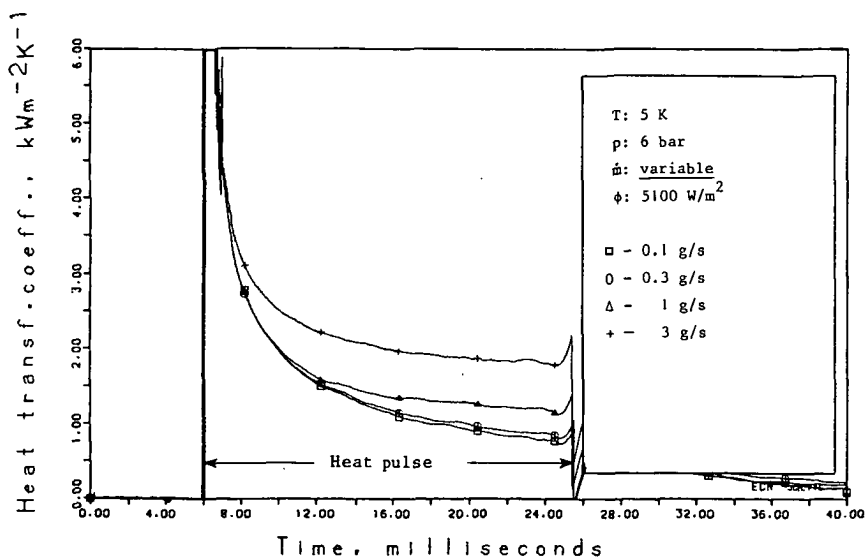
Figure 6.12 Heat transfer coefficient as a function of time at four different mass flows at 5 K; pulse started at 5.96 ms.
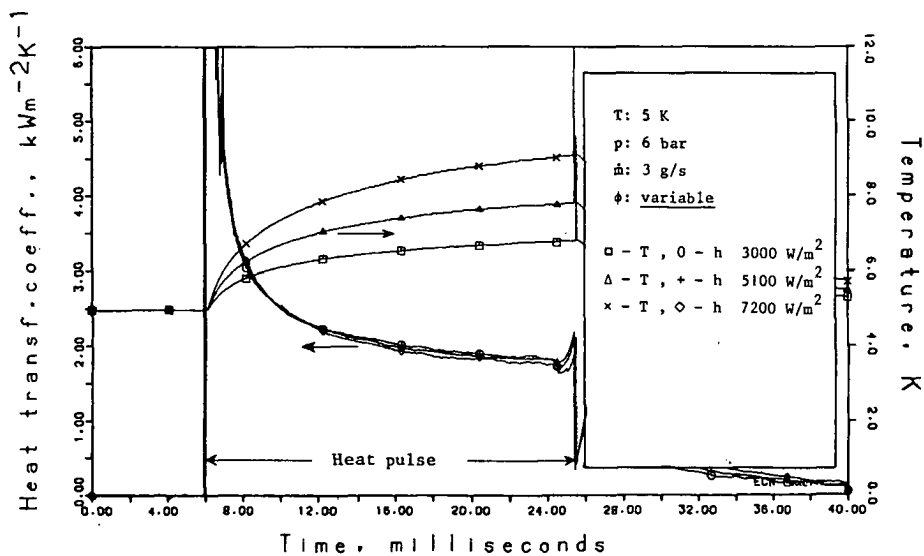

Figure 6.13 Heat transfer coefficient and temperature as a function of time for different heat releases at 5 K; mass flow 3 g/s; pressure 6 bar; pulse started at 5.96 ms.
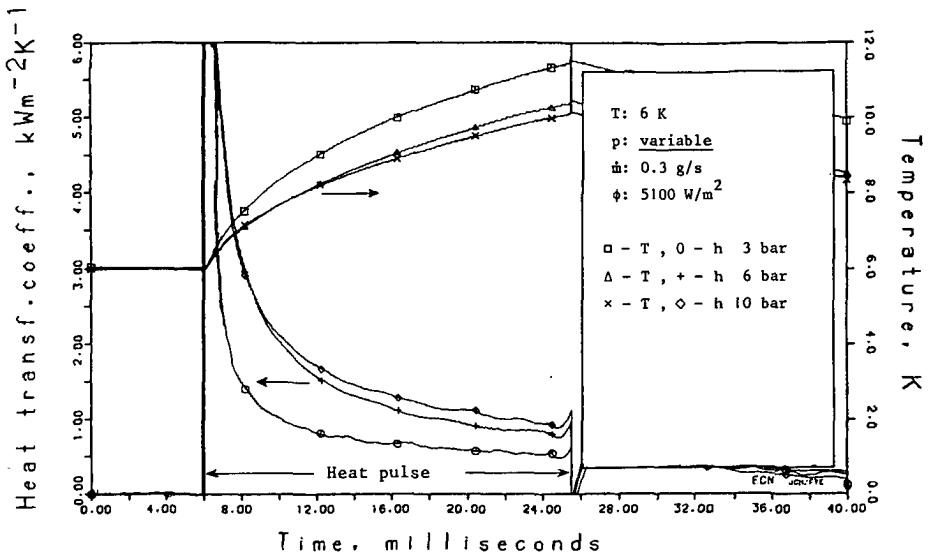
Figure 6.14   Heat transfer coefficient and temperature as a function
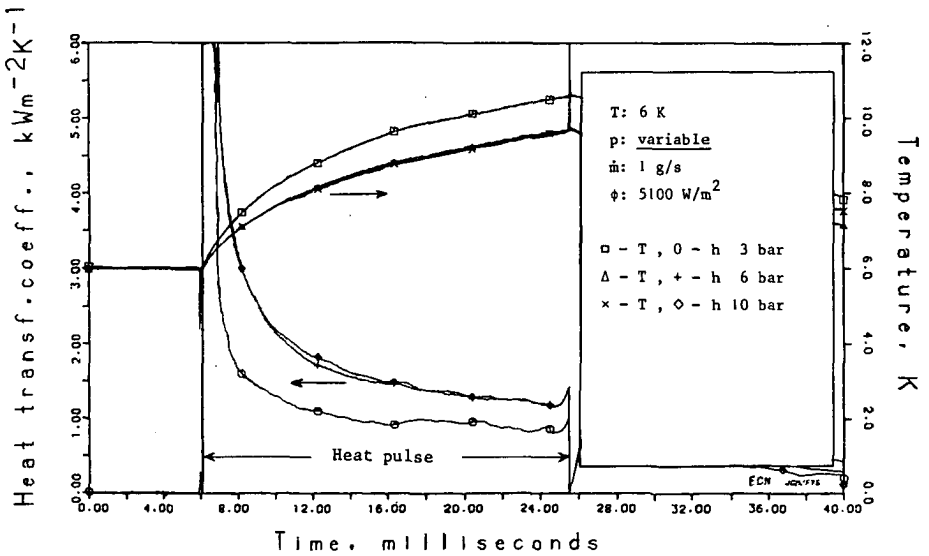   of time at 6 K; pulse started at 5.96 ms.

Figure 6.15   Heat transfer coeffient and temperature as a function of
              time at 6 K.

6.2.3.3. Heat flow variation

At the bulk inlet temperature of 5 K no significant differences occur
on the heat transfer coefficient at different heat flows as can be
seen from Fig. 6.13.

6.2.4. Inlet temperature 6 K

For high mass flows and low pressures it was a problem to realize
high inlet temperatures, even up to 6 K. For example the heat flow
which was required to get an inlet temperature of 6 K at 3 g/s was
about

$$\dot{\phi} = \dot{m} \, \Delta H = 3 \cdot 10^{-3} \ (17460 + 4433) \ W = 65.7 \ W . \qquad (6.7)$$

The stationary heater could not resist currents larger than 1.2 A,
leaving the maximum inlet temperature at 5.6 K for a flow of 3 g/s.
On the other hand these large heat flows required for the higher
inlet temperatures caused a larger helium boil-off in the cryostat
with the counter flow heat exchanger. Regularly liquid helium supply
was necessary.

6.2.4.1. Pressure variation

At 3 bar the inlet temperature of 6 K is higher than the transposed
critical temperature of 5.6 K. From Figs 6.14 and 6.15 it can be seen
that the heat transfer deteriorates considerably in the 3 bar case
compared with 6 and 10 bar.

6.2.4.2. Mass flow variation

From Fig. 6.16 it can be seen that a considerable improvement of the
heat transfer occurs when the mass flow is increased. This phenomenon
manifests also at 3 bar; this can be seen from comparing the 3 bar
measurement of Fig. 6.14 (0.3 g/s) and the 3 bar measurement of Fig.
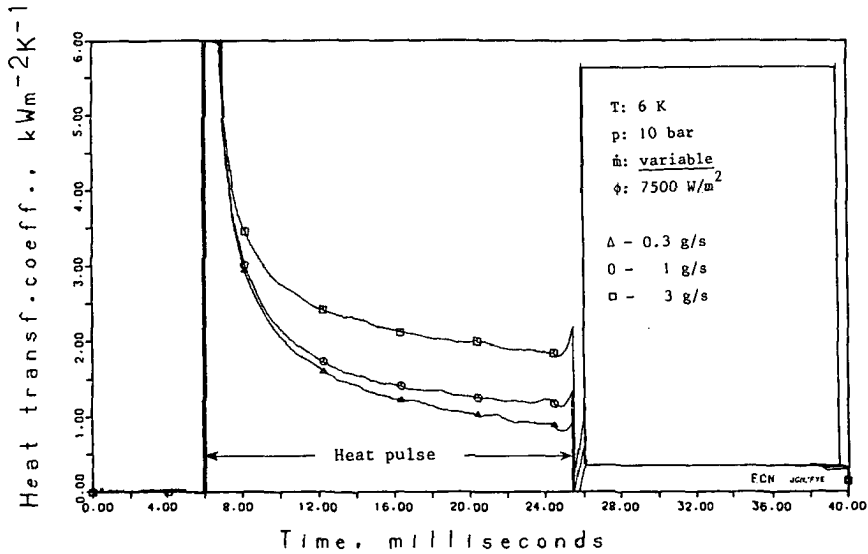6.15 (1 g/s).

Figure 6.16   Heat transfer coefficient as a function of time at
three different mass flows at 6 K; pulse started at 5.96 ms.
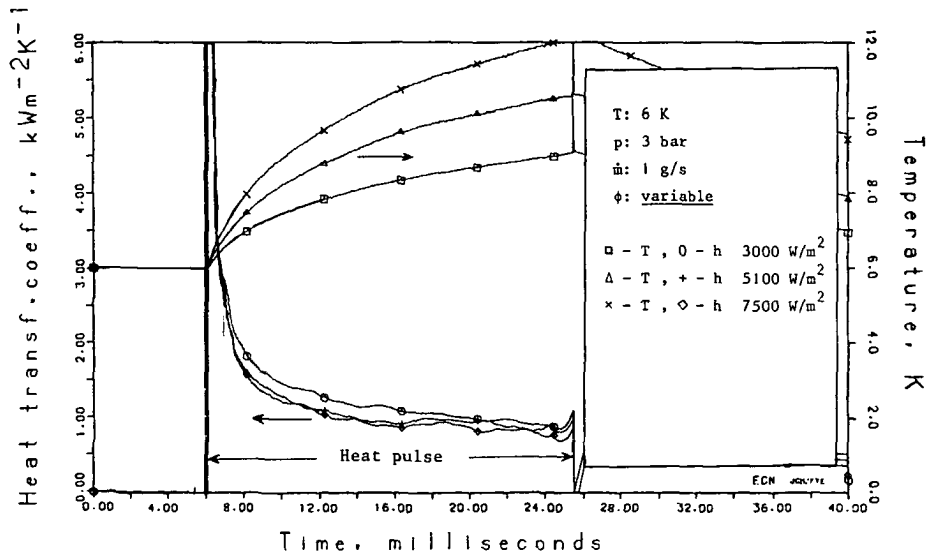

Figure 6.17   Heat transfer coefficient and temperature as a function
of time for different heat releases at 6 K;
mass flow 1 g/s; pressure 3 bar; pulse started at 5.96 ms.

6.2.4.3. Heat flow variation

At 6 K the heat transfer coefficients are nearly the same for diffe-
rent heat flows. From Fig. 6.17 it can be seen that this also occurs
at 3 bar. In case of a heat flux of 7500 W/m² the maximum temperature
rise at the end of the pulse is 12.15 K, and that is out of the range
of the temperature ordinate.

6.3. Test section 2

6.3.1. Heat capacity

The heat capacity of the second test section was measured in the same
way as test section 1. Here the heat capacity is related to the heat-
ed section of 5 cm length of copper tube. The heat capacity of the
tube can be expressed by the correlation

$$m \, c_p = (1.046 \, T^3 + 15.24 \, T) * 10^{-5} \quad J/K \, , \tag{6.8}$$

where the uncertainties in the factors are respectively:
1.046 ± 0.025 and 15.24 ± 0.45.
The results are shown in Fig. 6.18. In Table 6.2 they are compared
with those of test section 1. The ratio of the two heat capacities
increases with temperature, this can be caused by the fact that test
section 1 contains more insulating materials (paper, glue, two ther-
mometers) than test section 2. These components have another tempera-
ture-specific heat correlation than the bulk material of copper. This
might introduce the differences in the heat capacity ratio at higher
temperatures.
The wetted surface inside the copper tube of the heated section was
9.57 10^{-4} m². This value was used in eq. (6.2).

6.3.2. Pressure transducers

As mentioned in paragraph 5.2.3.1 the calibration curves of the fast
response pressure transducers changed slightly when the sensors were
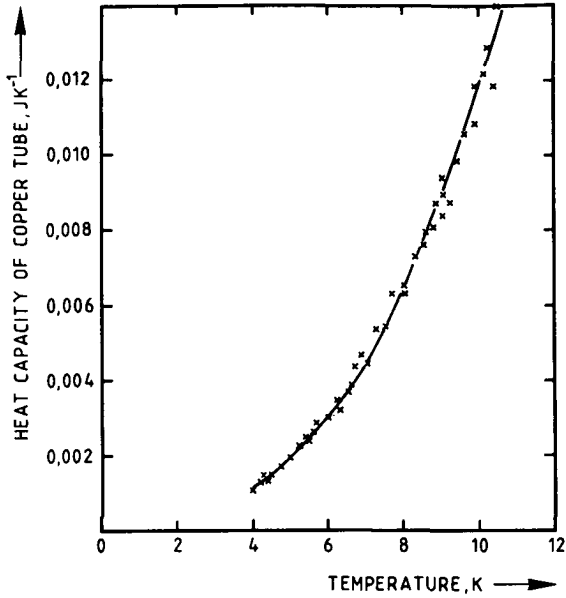cycled between 4.2 K and room temperature.

Figure 6.18 Heat capacity of the heated section (copper tube) of
test section 2 as a function of temperature.

T (K)	mc$_p$ (J/K)		$\dfrac{mc_p(1)}{mc_p(2)}$
	test sect. (1)	test sect. (2)	
4	0.0039	0.00128	3.05
5	0.0067	0.00207	3.24
6	0.0106	0.00317	3.34
7	0.0161	0.00465	3.46
8	0.0232	0.00657	3.53
9	0.0322	0.009	3.58
10	0.0433	0.01198	3.61

Table 6.2. Ratio of the heat capacities of the test sections
1 and 2 as a function of temperature.

In the first instance the sensors were calibrated with the aid of a
precision manometer up to 11 bar with helium. It was found that at
4.2 K the output voltage of the sensors was directly proportional
with the pressure (also at 293 K and 77 K). That means that when the
sensors were calibrated for the next time at 4.2 K only a few cali-
bration points were required.

When the test section had been mounted in the supercritical helium
loop the calibration pressures were taken from the bourdon pressure
gauges of the loop. Precise absolute pressure measurements were not
required, the sensors were used for detecting pressure waves and not
for measuring absolute pressures, so a small error of less than 5%
was not important. These latter pressures were measured with the
bourdon pressure gauges.

6.3.3. Pressure waves

It was possible to detect the existence of pressure waves if the tube
was pulse-heated. In Fig. 6.19 three results are shown at 3 bar, 6
bar and 10 bar. The start of the pressure step (wave) is marked by an
arrow. The oscillations on the pressure steps are probably pressure
reflections at the bends of the test section (e.g. the 90° bends,
Fig. 5.17).

Because the steady state voltage output of the transducers were com-
pensated in an electrical bridge circuit, only pressure differences
were measured. The pressure difference with regard to the steady
state pressure has been plotted on the vertical ordinates.

The released heat pulses lasted 2 ms and started at $t = 6$ ms. The
energy release was 68.8 mJ over the entire heated section of 5 cm
$(\phi_{released} = 34.4$ W).

During some measurements the blow down loop was prone to pressure
oscillations. These oscillations (with frequencies of 1.6 Hz and
16.7 Hz) occurred when the cryostat with the 80 - 4 K heat exchanger
was filled up with liquid helium. Some of the effects of the oscilla-
tions is seen in the figures. The slow variations in Fig. 6.19 are
related to these oscillations. No influences of the various mass
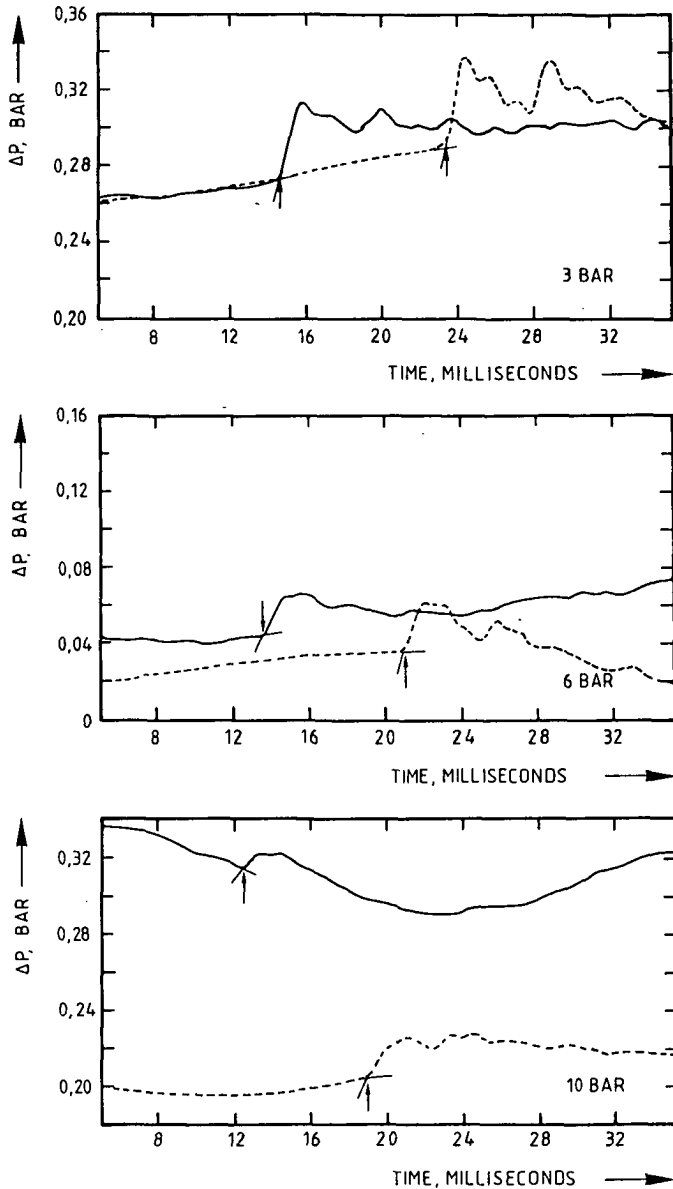flows on the pressure responses have been noticed.

Figure 6.19   Pressure response of the pressure transducers after a
heat release of 68.8 mJ (released during 2 ms) at
different static pressures. Temperature was 4.2 K.
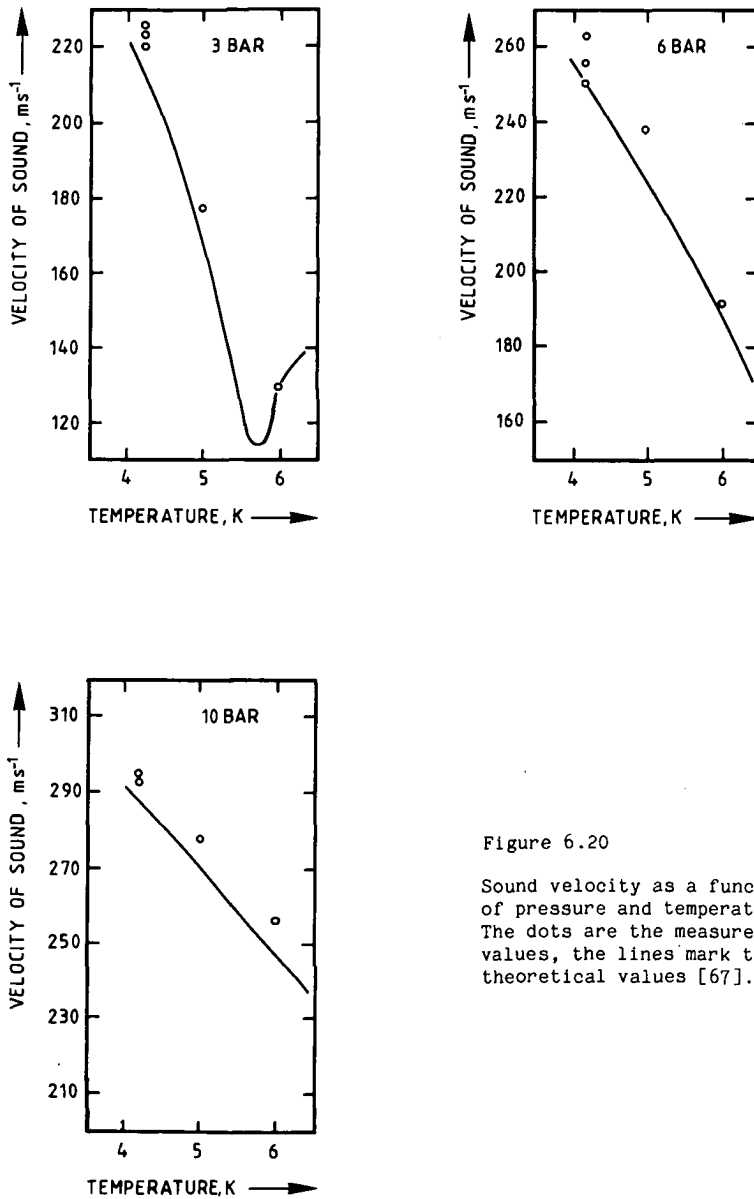Dotted line is response of transducer 2.

Figure 6.20

Sound velocity as a function
of pressure and temperature.
The dots are the measured
values, the lines mark the
theoretical values [67].
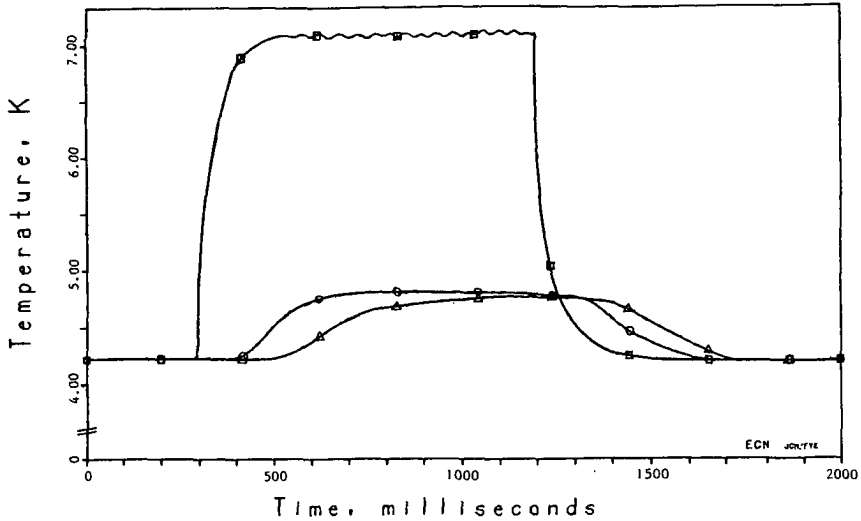
Figure 6.21   Temperature responses of test section 2 on a heat pulse
             of 1.6 W as a function of time. Heat pulse started at
             0.298 s and lasted 0.88 s; mass flow 1 g/s;
             pressure 6 bar; inlet temperature 4.2 K;
             □ - thermometer 1 (heated section); 0 - thermometer 2;
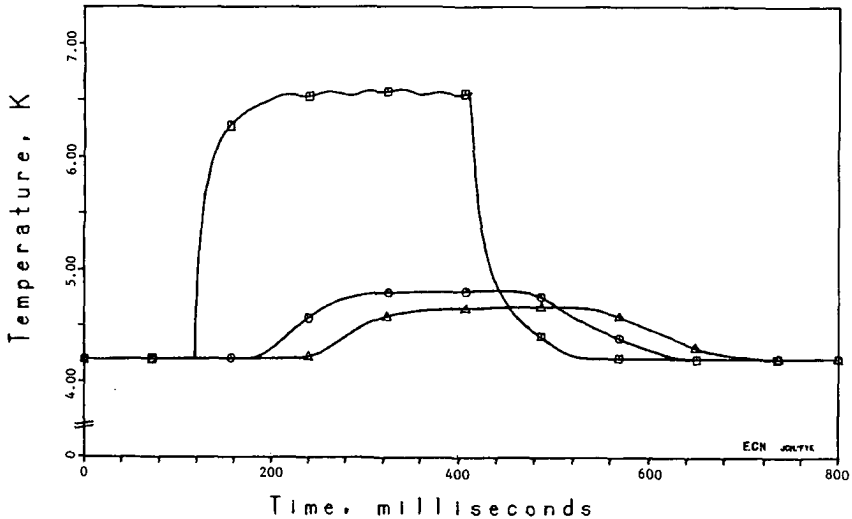   Δ - thermometer 3.

Figure 6.22   Temperature responses of test section 2 on a heat pulse
             of 1.98 W as a function of time. Heat pulse started at
             0.1192 s and lasted 0.29 s; mass flow 2 g/s;
             pressure 10 bar; inlet temperature 4.2 K;
             □ - thermometer 1 (heated section); 0 - thermometer 2;
             Δ - thermometer 3.

From the time difference between the two starts of the two pressure
rises and the distance between the two pressure transducers (1.945 m)
it was possible to calculate the velocity of sound in supercritical
helium for three pressures and three temperatures. The results are
shown in Fig. 6.20 and compared with numerically computed values by
Mc Carthy [67]. He computed the speed of sound from an equation of
state of helium. This equation of state was verified by comparing
computed and measured values of different helium properties. He
compared the speed of sound with measurements in the range of
98 - 423 K, with pressures up to 100 bar, the difference between ex-
perimental and calculated velocities of sound in this region was less
than 0.1% (see [67]).
The deviation in the 3 bar case is 9.5%, in the 10 bar case 4%. The
measured values are larger than the theoretical values. Notice the
difference of the scales of the velocity ordinates.

6.3.4. Steady state heat transfer

With test section 2 some steady state heat transfer measurements were
carried out. The two thermometer sections downstream the heated sec-
tion monitored the fluid temperature and from these temperatures the
heat absorption by the flow could be determined. The measured down-
stream temperatures were much lower than the wall temperature of the
heated section.
From the time difference between the temperature rises of the thermo-
meters and the distance between them, the mass flow could be calcu-
lated. For example, in case of Fig. 6.21 it takes about 0.1 s when the
heated helium flows from T_2 (thermometer section 1) to T_3 (thermo-
meter section 2). The distance between the two thermometers is 29 mm,
thus the flow velocity is of the order of 0.29 m/s. This velocity of
0.29 m/s corresponds with a mass flow of

$$\dot{m} = A_{He} \, \rho \, v$$

$$= 23.8 \; 10^{-6} * 143.2 * 0.29 = 0.988 \; 10^{-3} \; \text{kg/s} .$$
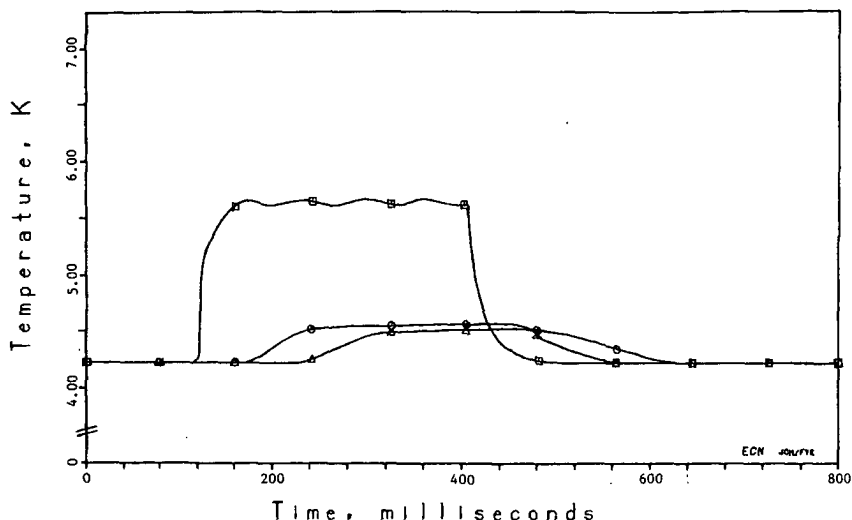
(6.9)

Figure 6.23 Temperature responses of test section 2 on a heat pulse
of 1.6 W as a function of time. Heat pulse started at
0.1192 s and lasted 0.29 s; mass flow 2 g/s;
pressure 3 bar; inlet temperature 4.2 K;
□ - thermometer 1 (heated section); 0.- thermometer 2;
△ - thermometer 3.

This flow is of the same order as the mass flow of 1 g/s according to
the orifice flow meters. The measurements showed that the time range
of the temperature effects was larger than the time range of the
pressure waves. The heat transfer phenomena became stationary within
0.1 - 0.2 s.

The heated helium flowed through the conduit as a distinguished vol-
ume. The duration of the pulse can be found in the length of the
heated volume. The temperature is leveling out a bit, the measured
temperature T_2 of the second sensor is somewhat lower, but the time
that the temperature is higher than 4.2 K lasts longer (larger time
base; e.g. Fig. 6.21 section one Δt_{T_1} = 120 ms, section two
Δt_{T_2} = 125 ms).

The effect of the temperature widening is caused by the heat capacity
of the wall (heating up and cooling) and the velocity profile of the
helium flow.

CHAPTER 7

ANALYSIS OF THE RESULTS

7.1. Heat penetration

It may be expected that during the first milliseconds the heat trans-
fer is determined by heat conduction in the boundary layer of the
supercritical helium flow. Because the thermal diffusivity of helium
is small, the results of heat penetration can be described with the
theory of heat transfer from a flat plate to a semi-infinite medium.
The analytical solution for a constant heat flux, ϕ/A, starting at
$t = 0$, and constant helium properties, is [19]

$$T(y,t)-T_b = \frac{2\phi/A}{\lambda} \left\{ (\frac{at}{\pi})^{\frac{1}{2}} \exp[-y^2/(4at)] - \frac{y}{2} \, \text{erfc}[y/(2\sqrt{at})] \right\} \quad (7.1)$$

where T_b is the helium bulk temperature at $t = 0$, y the distance in
the fluid perpendicular on the wall and a the thermal diffusivity of
helium.
From eq. (7.1) the heat transfer coefficient $h = \phi/(A\Delta T)$, with
$\Delta T = T(0,t) - T_b$, can be derived:

$$h = \frac{1}{2} \sqrt{\pi \, \lambda \, \rho \, c_p/t} \, . \quad (7.2)$$

Except for time t, h is completely determined by the helium proper-
ties λ, ρ and c_p. The product of these quantities, $\varepsilon = \lambda \, \rho \, c_p$, is a
kind of volumetric heat absorption coefficient. ε of helium is shown
in Fig. 7.1 as a function of pressure and temperature.
The heat transfer coefficient of eq. (7.2) has been computed using
the He-properties related to the measured wall temperatures. The
He-quantities were taken from literature [67], [71], [72].
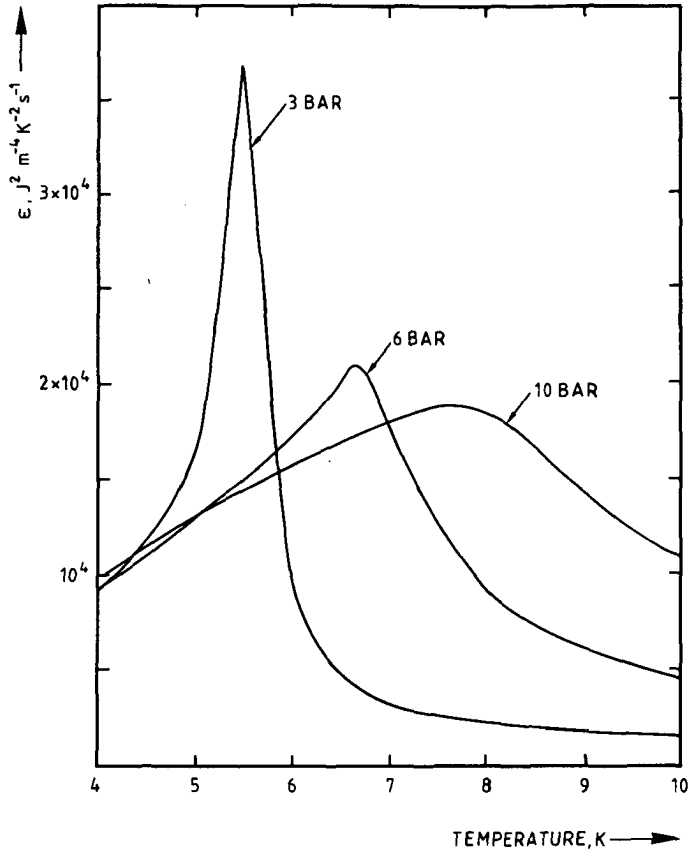Some of these computed results are shown in Table 7.1. It must be

Figure 7.1   Product $\varepsilon = \lambda \rho c_p$ of helium as a function of temperature and pressure.

realized that eq. (7.2) counts for constant properties. The results
of Table 7.1 are a qualitative comparison. During the first milli-
seconds the approximation is good. For pressures near the critical
pressure, e.g. 3 bar, the model introduces errors. At this pressure
the difference becomes larger with increasing time. This can be
caused by the effect that ε is determined from the temperature at the
wall and that the growing thickness of the heated helium film is not
taken into account and thus the changing He-properties. For long
times h from eq. (7.2) goes to zero, but in reality h approaches a
stationary value. So, for long times the discrepancy between the mea-
sured and the computed value of h becomes greater. For the 3 bar data
this is very true, for the 6 bar measurement it is already consider-
ably less, and for the 10 bar data it is not yet apparent after
10 ms.

It is remarkable that the temperature increase during a heat pulse is
nearly the same for the three pressures at 4.2 K (results paragraph
6.2.2.1). At an inlet temperature of 5 K the heat transfer in the
3 bar case improves (results paragraph 6.2.3.1) and at 6 K the 3 bar
results deteriorates with respect to the 6 and 10 bar results (re-
sults paragraph 6.2.4.1). At these higher inlet temperatures the 6
and 10 bar results are nearly the same. Looking at the function of ε
in Fig. 7.1, at 4.2 K ε is of the same order for the three pressures,
at 5 K ε at 3 bar is larger than ε at 6 and 10 bar. These two latter
values are nearly the same. At 6 K the value of ε at 3 bar is lower
than ε at 6 and 10 bar.
With the aid of ε it is possible to predict qualitatively the heat
transfer as a function of temperature and pressure. As was seen, when
ε is nearly the same at one inlet bulk temperature and different
pressures the heat transfer will be the same. On the other hand, when
ε changes, the heat transfer coefficient will behave in a different
way. For example, in Figs 7.2, 7.3 and 7.4 the results are shown for
different pressures and different bulk temperatures for a fixed mass
flow. In the 6 and 10 bar cases with the same bulk temperature the

	3 bar				6 bar				10 bar			
t	T_m	$\varepsilon \cdot 10^{-4}$	h_c	h_m	T_m	$\varepsilon \cdot 10^{-4}$	h_c	h_m	T_m	$\varepsilon \cdot 10^{-4}$	h_c	h_m
(ms)	(K)	$(J^2 m^{-4} K^{-2} s^{-1})$	$(Wm^{-2}K^{-1})$	$(Wm^{-2}K^{-1})$	(K)	$(J^2 m^{-4} K^{-2} s^{-1})$	$(Wm^{-2}K^{-1})$	$(Wm^{-2}K^{-1})$	(K)	$(J^2 m^{-4} K^{-2} s^{-1})$	$(Wm^{-2}K^{-1})$	$(Wm^{-2}K^{-1})$
1	5.2	2.26	4213	3900	5.2	1.37	3280	3600	5.11	1.34	3244	3600
2	5.6	3.06	3466	2800	5.7	1.59	2499	2500	5.56	1.46	2394	2510
3	6	0.88	1518	2200	6.05	1.76	2147	2100	5.9	1.54	2008	2070
4	6.4	0.5	991	1850	6.3	1.89	1926	1850	6.15	1.61	1778	1815
5	6.6	0.4	793	1650	6.6	2.09	1812	1700	6.4	1.66	1615	1640
6	6.8	0.34	667	1500	6.8	1.98	1610	1550	6.6	1.71	1496	1517
7	7.05	0.3	580	1400	6.95	1.8	1421	1500	6.75	1.75	1401	1430
8	7.25	0.27	515	1350	7.15	1.58	1245	1425	6.9	1.78	1322	1340
9	7.4	0.26	476	1300	7.3	1.4	1105	1350	7.05	1.81	1257	1275
10	7.5	0.25	443	1250	7.4	1.34	1026	1300	7.2	1.84	1202	1230

Table 7.1. Measured heat transfer coefficient h_m compared with the computed
heat transfer coefficient h_c (equation (7.2)) at three pressures.
T_m is the measured temperature. The released heat flux was
4800 W/m^2 and the mass flow was 1 10^{-3} kg/s.
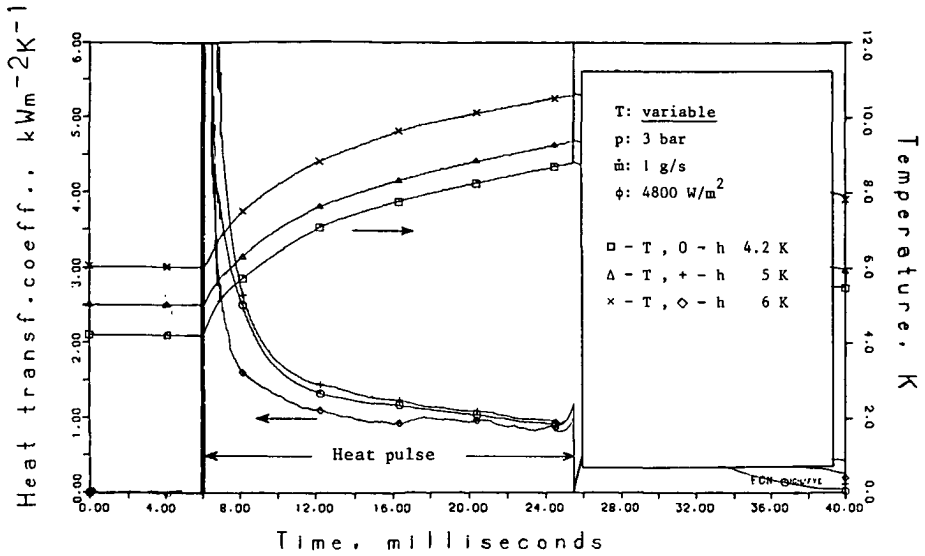
- 159 -

Figure 7.2   Heat transfer coefficient and belonging measured
             temperature curves as a function of time.
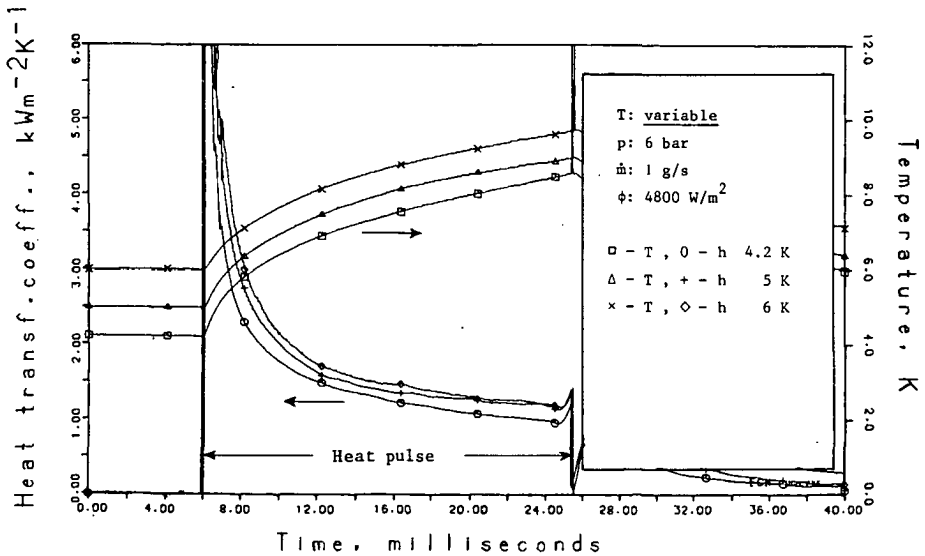

Figure 7.3   Heat transfer coefficient and belonging measured
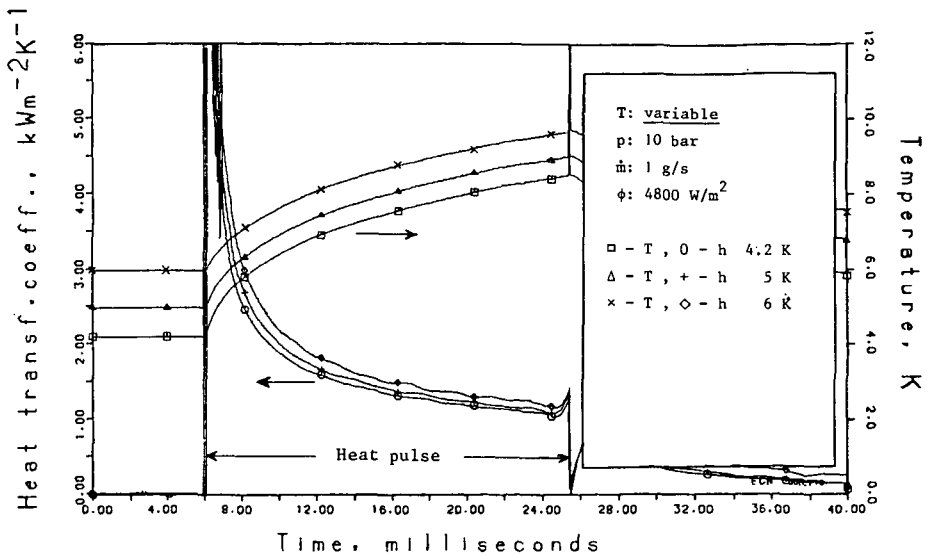   temperature curves as a function of time.

Figure 7.4   Heat transfer coefficient and belonging measured
temperature curves as a function of time.

temperature rise is the same. At 3 bar and 6 K the deterioration of
the heat transfer occurs, according to the lower value of ϵ.
It can also be noted that at higher inlet bulk temperatures the heat
transfer coefficient is somewhat higher than at 4.2 K in the 6 and
10 bar cases. For higher pressures ϵ is relatively large at high
temperatures. For a stable performance of forced flow cooled super-
conductors it seems therefore favourable to operate rather at high
pressures than at low pressures. As was seen from the measurements at
4.2 K (paragraph 6.2.1.1) there is no advantage to work at low pres-
sure; the peak of ϵ does not manifest in the results (i.e. lower tem-
peratures because of the peak).

From the results of chapter 6 it can be seen that when the mass flow
was increased, there was an improvement of the heat transfer for
higher mass flows. During the first milliseconds of the heating pro-
cess the heat transfer takes place in a thin layer of helium along
the wall of the heated conduit. The heat transfer phenomenon is ruled
by heat penetration.

The heat transfer mechanism based on penetration is after a few milliseconds taken over by convection caused by turbulence of the supercritical helium flow. It is possible to make a rough estimation of the time when this happens.

During the time that the heat transfer can be described by the heat penetration theory, a penetration depth δ_T can be defined

$$\frac{T_b - T(0,t)}{\delta_T} = \left. \frac{d(T(y,t) - T_b)}{dy} \right|_{y=0} . \tag{7.3}$$

In case of the fixed heat flux at the wall, eq. (7.1), the penetration depth is

$$\delta_T = \sqrt{4at/\pi} . \tag{7.4}$$

When a temperature step T_w at $t = 0$ is realized at the wall, then the temperature profile in the semi-infinite medium is given by [19]:

$$T(y,t) - T_b = (T_w - T_b)\, \mathrm{erfc}\left(y/(2\sqrt{at})\right) \tag{7.5}$$

and then the penetration depth is

$$\delta_T = \sqrt{\pi at} . \tag{7.6}$$

The model of the semi-infinite medium counts during the first milli-seconds because δ_T is of the order of micrometers (thermal diffu-sivity of helium at 4.2 K: $a \approx 5\ 10^{-8}$ m²/s) and the hydraulic diame-ter D_h is 5 mm.

When the penetration depth δ_T reaches the thickness of the laminar boundary layer, then the influence of the turbulence becomes notice-able and an improvement in the heat transfer may be expected in comparison with the heat transfer coefficient according to eq. (7.2). For reasons of simplicity, the turbulent flow is represented by an effective layer of laminar flow (so that the momentum transport to

Re \ t_t	4.2 K			5 K			6 K		
	0.3 g/s	1 g/s	3 g/s	0.3 g/s	1 g/s	3 g/s	0.3 g/s	1 g/s	3 g/s
3 bar	$2.08 \ 10^4$ / 116	$6.9 \ 10^4$ / 19.2	$2.08 \ 10^5$ / 3.7	$2.46 \ 10^4$ / 153	$8.2 \ 10^4$ / 24.2	$2.46 \ 10^5$ / 4.8	$3.8 \ 10^4$ / 67.5	$1.27 \ 10^5$ / 11.1	$3.8 \ 10^5$ / 2.1
6 bar	$1.8 \ 10^4$ / 124	$6 \ 10^4$ / 20.3	$1.8 \ 10^5$ / 3.9	$2 \ 10^4$ / 127	$6.8 \ 10^4$ / 20.9	$2 \ 10^5$ / 4	$2.4 \ 10^4$ / 137	$7.9 \ 10^4$ / 22.5	$2.4 \ 10^5$ / 4.3
10 bar	$1.56 \ 10^4$ / 129	$5.2 \ 10^4$ / 21.2	$1.56 \ 10^5$ / 4.1	$1.74 \ 10^4$ / 126	$5.8 \ 10^4$ / 20.8	$1.74 \ 10^5$ / 4	$1.95 \ 10^4$ / 125	$6.5 \ 10^4$ / 20.5	$1.95 \ 10^4$ / 4

Table 7.2. Reynolds number and take-over-time t_t (milliseconds) as a function of temperature, pressure and mass flow.
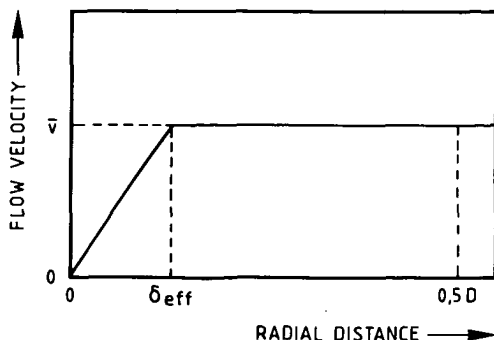
Figure 7.5A Simplified velocity profile of a turbulent flow existing of an effective layer of laminar flow and a turbulent core with average velocity $\bar{v}$.

the wall remains the same) and a turbulent core with average velocity $\bar{v}$ (Fig. 7.5A). The velocity profile in the effective layer follows from Newton's law of friction

$$\tau_w = \eta \frac{dv}{dy} \qquad (7.7)$$

where τ_w is the wall shear stress.

The thickness of the effective layer, δ_{eff}, is given by

$$\frac{dv}{dy} = \frac{\Delta v}{\Delta y} = \frac{\bar{v}}{\delta_{eff}} \ . \qquad (7.8)$$

Using Newton's law

$$\delta_{eff} = \bar{v} \frac{\eta}{\tau_w} \qquad (7.9)$$

The wall shear stress τ_w is a function of the friction factor f:

$$\tau_w = \frac{1}{2} f \rho \bar{v}^2 \ . \qquad (7.10)$$

According to measurements by Daney and Ludtke [73] and Junghans [74] there is no significant difference between the friction factor for supercritical helium at low temperatures and for classical fluids.

For those fluids the expression for the friction factor is (Knudsen and Katz [75])

$$f = 0.076 \ Re^{-0.25} \ . \tag{7.11}$$

From (7.9), (7.10) and (7.11) and using $Re = \rho \ \overline{v} \ D/\eta$ follows for the thickness of the effective layer

$$\delta_{eff} = \frac{2D}{0.076 \ Re^{0.75}} \quad . \tag{7.12}$$

When the temperature penetration depth δ_T approaches the thickness of the effective layer influences of turbulence may occur on the heat transfer. From (7.6) and (7.12) a take-over-time t_t can be defined when this happens;

$$t_t = \frac{\pi}{a} \ (\frac{D}{0.076})^2 \ Re^{-1.5} \ . \tag{7.13}$$

In Table 7.2 some values of t_t as a function of temperature, mass flow ($Re = 4 \ \dot{m}/(\pi \eta D)$) and pressure are given. Well below the take-over-time heat transfer is determined by heat penetration, which is mass flow independent. This effect has been demonstrated by the measurements for low mass flows, where the take-over-time is larger than the interval of time of the measurements, see e.g. Figs 6.7, 6.11 and 6.12. From Table 7.2 it can be seen that the pressure dependence of t_t for a given mass flow is small at 4.2 K.

7.2. Correlation for transient heat transfer coefficient

From the experiments it can be concluded that the transient heat transfer coefficient h_{tr} is a function of Reynolds number, time, bulk temperature and in less extent of pressure.

$$h_{tr} = f(Re,t,p,T_b) \ . \tag{7.14}$$

For small mass flows at defined pressure p and bulk temperature T_b the transient heat transfer coefficient can be described by eq. (7.2). The only problem is to fit the varying helium properties λ, ρ and c_p as a function of time when during a heat pulse the tempe-

- 165 -

p (bar)	T_{bulk} (K)	$\dot{m}$ (g s^{-1})	Re	t_t (ms)	h_{tt} (W/m^{2}K)	λ/D (W/m^{2}K)	Nu_{tt}	b_0	$\bar{b}_0$
3	4.2	1	6.92 10^4	19.2	950	3.93	241.7	0.057	
		3	2.08 10^5	3.7	2500	3.93	636.1	0.065	
	5	1	8.20 10^4	24.1	850	3.96	214.6	0.044	
		3	2.46 10^5	4.8	2800	3.96	707.1	0.064	0.058
	6	1	1.27 10^5	11.1	925	3.03	305.3	0.045	
		3	3.82 10^5	2.1	3250	3.03	1072.6	0.070	
6	4.2	1	5.99 10^4	20.4	1000	4.28	233.6	0.061	
		3	1.8 10^5	3.9	2300	4.28	573.4	0.066	
	5	1	6.77 10^4	20.9	1100	4.46	246.6	0.059	
		3	2.03 10^5	4.0	2550	4.46	571.7	0.060	0.061
	6	1	7.93 10^4	22.5	1200	4.37	274.6	0.058	
		3	2.38 10^5	4.3	3000	4.37	686.5	0.064	
10	4.2	1	5.2 10^4	21.3	1075	4.64	231.7	0.067	
		3	1.56 10^5	4.1	2225	4.64	479.5	0.061	
	5	1	5.79 10^4	20.7	1150	4.92	233.7	0.063	
		3	1.74 10^5	4.0	2400	4.92	487.8	0.057	0.061
	6	1	6.51 10^4	20.5	1250	5.03	248.5	0.061	
		3	1.95 10^5	3.9	2750	5.03	546.7	0.059	

Table 7.3. The coefficient b_0 as a function of pressure
and Reynolds number.

rature increases. We have tried to fit the measured heat transfer curves with a power law, $h \sim t^i$, with a single value of the exponent i. Let us first consider the heat transfer coefficient h_{tt} at the take-over-time t_t, using eq. (7.2).

$$h_{tt} = \frac{1}{2} \sqrt{\pi \lambda \rho c_p / t_t} \ . \tag{7.15}$$

If the helium properties are related to the bulk temperature, from (7.15) and (7.13) and using the expression of the thermal diffusivity $a = \lambda/(\rho c_p)$ the following relation of h_{tt} can be derived

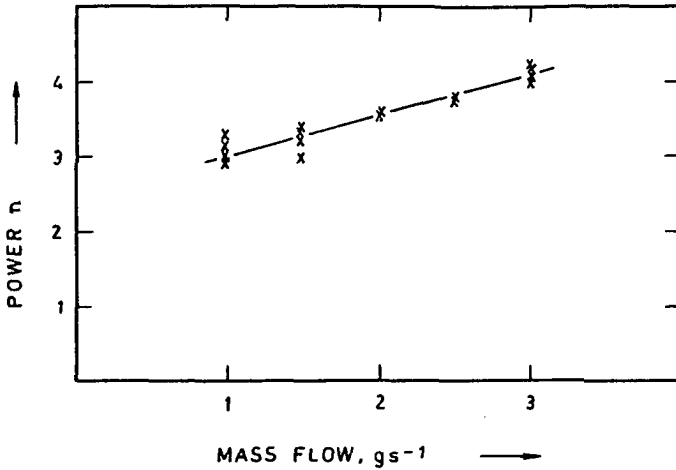$$h_{tt} = 0.038 \frac{\lambda}{D} Re^{0.75} \tag{7.16}$$

Figure 7.5B   Determination of the exponent of the power law
               of the time function.

or with the Nusselt number $Nu = hD/\lambda$

$$Nu_{tt} = 0.038 \ Re^{0.75} .$$

(7.17)

From the experimental results the quotient $b_0 = Nu_{tt}/Re^{0.75}$ was de-
termined. This was done by computing t_t with eq. (7.13) and then h_{tt}
at time t_t was taken from in the measured curves. The thermal conduc-
tivity λ of helium was taken at the inlet bulk temperature and with
the formula $Nu_{tt} = h_{tt}D/\lambda$ the Nusselt number was computed (Table 7.3).
According to Table 7.3 it can be seen that the constant 0.038 of
eq. (7.17) is a factor 1.58 too small. The average value of b_0 is
0.06 with a standard deviation of 0.007.
Assuming the power law $(c/t)^i$ for the time dependency and realizing
that at t_t $h_{tr} = h_{tt}$ or $Nu_{tr} = Nu_{tt}$, the transient heat transfer

is described with

$$Nu_{tr} = Nu_{tt} \ (t_t/t)^i \ . \tag{7.18}$$

After analysing the data it was concluded that the parameter i had to be a function of the mass flow to avoid large discrepancies between measured and computed h_{tr}, Fig. 7.5B. It was found that the transient heat transfer, $h_{tr} = \lambda Nu_{tr}/D$, can be predicted within 10% by

$$Nu_{tr} = 0.06 \ Re^{0.75} \ (t_t/t)^{1/n} \tag{7.19}$$

with

$$n = 500 \ \dot{m} + 2.5 \tag{7.20}$$

and $\dot{m}$ in kg/s and ranging from 1 to 3 g/s (see Fig. 7.5B). The time range of eq. (7.19) is from $2 \ 10^{-3}$ s up to 0.1 s. In Figs 7.6 - 7.11 some measured and computed results (eq. 7.19) are compared. In Appendix A results at higher inlet bulk temperatures and with mass flows of 2 g/s are gathered and compared.
Only in case of high inlet temperatures at 3 bar there are differences between experimental and computed values. This can be explained by the fact that the helium properties vary a lot when the temperature rises (variations of b_0, Table 7.3).

7.3. Steady state heat transfer

Some experiments, with test sections 1 and 2, were carried out with long pulse times (pulse times up to 900 ms). From these experiments it could be seen that within 100 - 300 ms the heat transfer becomes stationary (Fig. 6.21 - 6.23).
From the measured steady state heat transfer coefficients the Nusselt numbers were computed. The thermal conductivity of helium was related to the inlet bulk temperatures. The Reynolds- and Prandtl numbers calculated for the given conditions allow us to determine the quo-
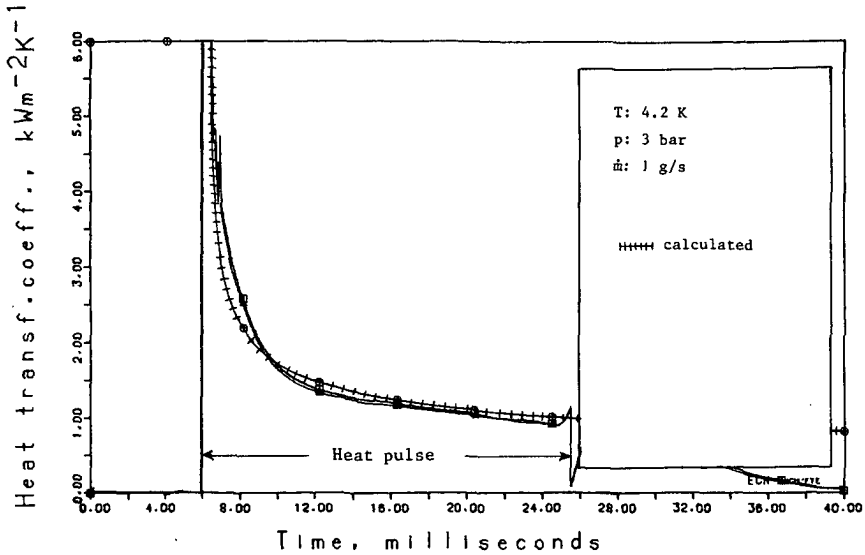
Figure 7.6   Comparison of experimental and empirically computed
heat transfer coefficients as a function of time.
Mass flow 1 g/s, pressure 3 bar, bulk inlet temperature
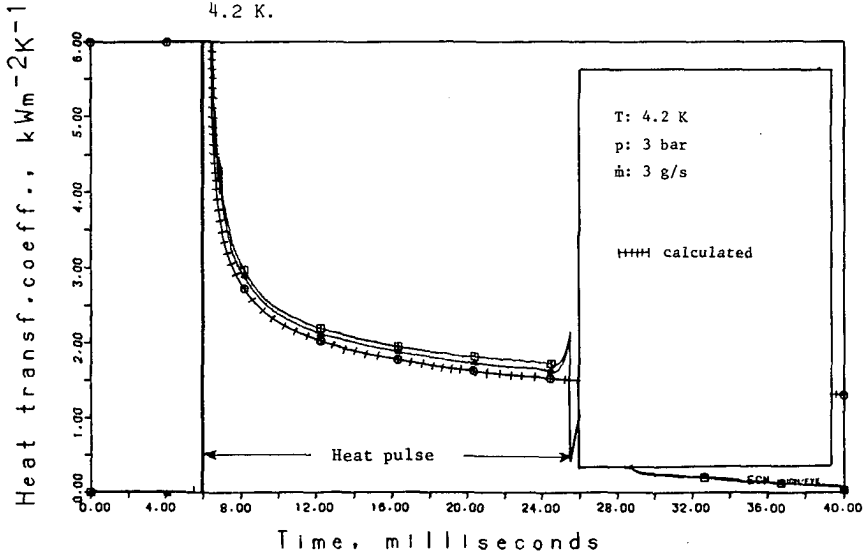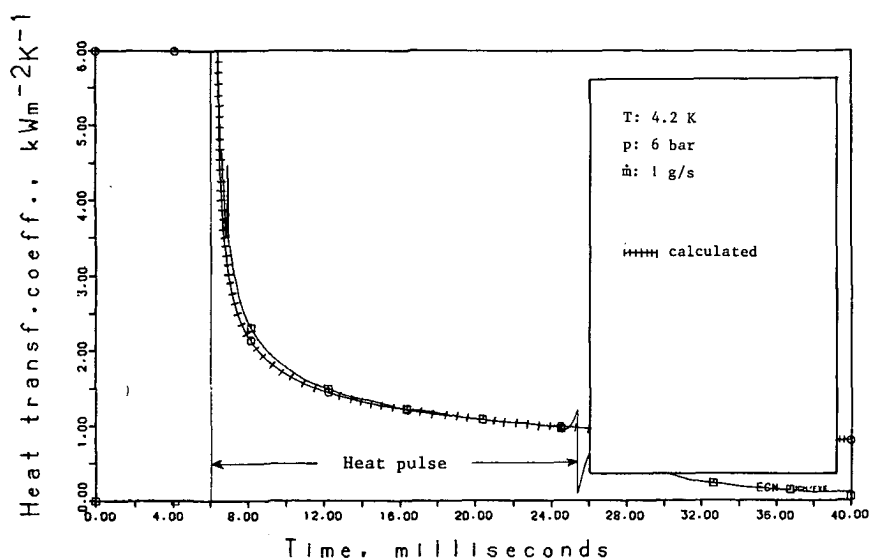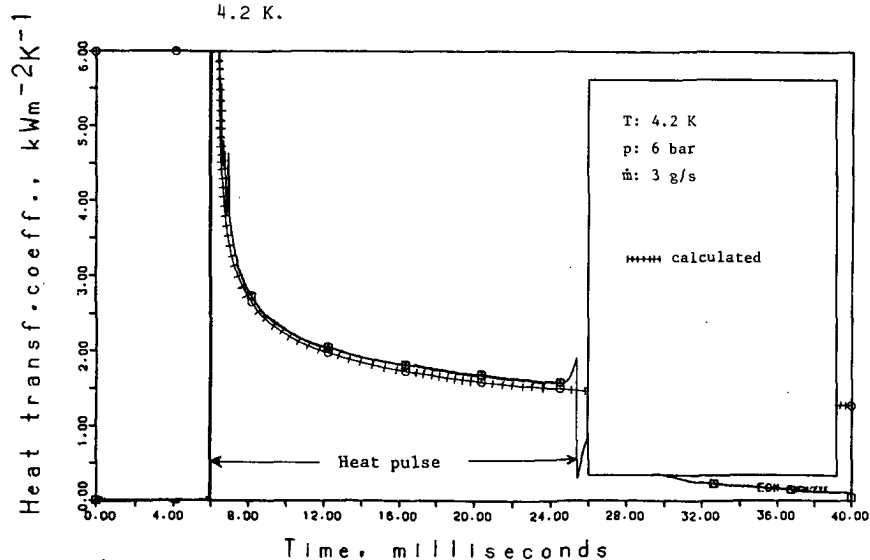4.2 K.

Figure 7.7   Comparison of experimental (2 measurements) and
empirically computed heat transfer coefficients as a
function of time.
Mass flow 3 g/s, pressure 3 bar, bulk inlet temperature
4.2 K.

Figure 7.8 Comparison of experimental and empirically computed
heat transfer coefficients as a function of time.
Mass flow 1 g/s, pressure 6 bar, bulk inlet temperature
4.2 K.

Figure 7.9 Comparison of experimental and empirically computed
heat transfer coefficients as a function of time.
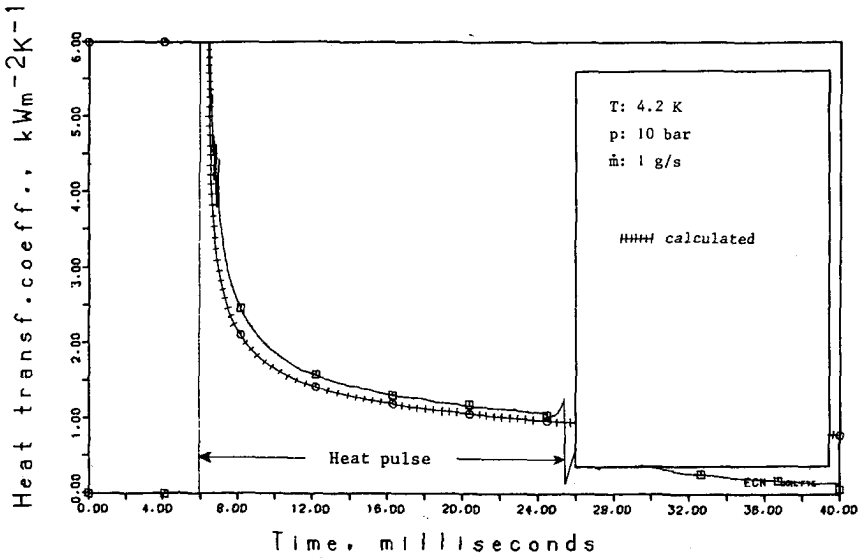Mass flow 3 g/s; p = 6 bar; bulk inlet temperature 4.2 K.

Figure 7.10   Comparison of experimental and empirically computed heat transfer coefficients as a function of time. Mass flow 1 g/s; p = 10 bar; bulk inlet temperature 4.2 K.
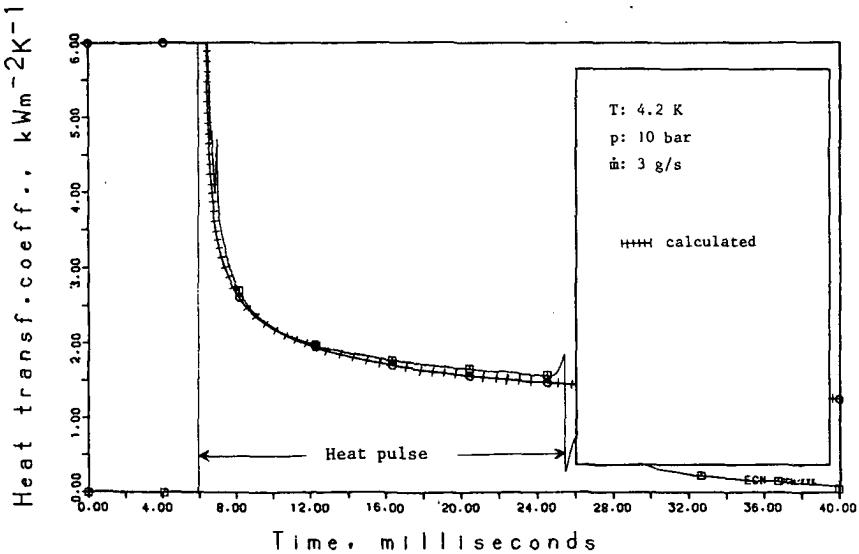

Figure 7.11   Comparison of experimental and empirically computed heat transfer coefficients as a function of time. Mass flow 3 g/s; p = 10 bar; bulk inlet temperature 4.2 K.

p (bar)	T_b (K)	T_w (K)	$\dot{m}$ (g/s)	h (W/(m^2K))	Nu	Re	Pr	$Nu/(Re^{0.8}Pr^{0.4})$
10	4.2	7.25	1	550	120.6	$5.2 \cdot 10^4$		0.0245
	4.2	8.65	1	575	126	$5.2 \cdot 10^4$		0.0256
	4.2	6.6	2	875	192	$10.4 \cdot 10^4$		0.0224
	4.2	5.65	3	1150	252	$15.6 \cdot 10^4$	0.63	0.0213
	4.2	5.9	3	1200	263	$15.6 \cdot 10^4$		0.0222
	4.2	6.6	3	1250	274	$15.6 \cdot 10^4$		0.0231
6	4.2	5.55	3	1250	295	$1.8 \cdot 10^5$		0.0218
	4.2	6.45	3	1325	312	$1.8 \cdot 10^5$	0.66	0.0230
	4.2	7.1	1	575	136	$6 \cdot 10^4$		0.0241
3	4.2	6.7	1	675	172	$6.9 \cdot 10^4$	0.73	0.0262
	4.2	7.4	1	650	166	$6.9 \cdot 10^4$		0.0253

Table 7.4. Determination of $Nu/(Re^{0.8}Pr^{0.4})$, mean value is 0.0236 with a standard deviation of 0.00165.

tient $Nu/(Re^{0.8}Pr^{0.4})$. The results are shown in Table 7.4 and from these it can be concluded that all the present data of heat transfer to supercritical helium can be correlated by the Dittus-Boelter correlation

$$Nu = 0.0236 \; Re^{0.8}Pr^{0.4} \qquad\qquad (7.21)$$

with a standard deviation in the coefficient of 0.0017 (7%). The constant 0.0236 is in perfect agreement with the Dittus-Boelter correlation (3.21), but is 9% smaller than the Giarratano correlation (3.22) and 8% larger than the Brassington-Cairns correlation (3.21). The experimental results of Ogata and Sako [34] are in the same range as eq. (7.21).

Using eq. (7.21) allows us a second method to compute the take-over-time t_t. As was mentioned in paragraph 7.1, turbulence starts governing the heat transfer mechanism when heat penetrated into the turbulent core. The steady state heat transfer coefficient from eq. (7.21) is ruled by turbulence and eq. (7.2) describes the heat penetration.

p (bar)	$\dot{m}$ (g/s)	$Re^{0.8}Pr^{0.4}$	t_t (ms)
10	1	4927	28.3
	3	11864	4.9
6	1	5620	24.9
	3	13553	4.3
3	1	6553	22
	3	15780	3.8

Table 7.5. Take-over-time (eq.(7.22)) as a
function of pressure and mass flow
(at 4.2 K).

The influence of turbulence becomes noticeable when the transient
heat transfer, eq. (7.2), equals the steady state heat transfer,
eq. (7.21). This moment is given by the take-over-time. Equating the
expressions (7.2) and (7.21) and using h = Nu λ/D give us an ex-
pression of the take-over-time:

$$t_t = \frac{\pi}{a} \left(\frac{D}{0.0472 \, Re^{0.8} \, Pr^{0.4}} \right)^2 . \qquad (7.22)$$

The helium properties in this correlation are related to the bulk
values.
Some values of t_t according to eq. (7.22) are gathered in Table 7.5.
The take-over-time of eq. (7.22) and eq. (7.13) are of the same
order, as can be seen in the Tables 7.2 and 7.5. From these tables it
can be concluded that the transient heat transfer is of importance
during the first 10 milliseconds for the large helium flows. The ex-
periments showed that steady state heat transfer dominates the heat
transfer processes within 0.1 s (Figs 6.21 - 6.23).

7.4. Radial heat transfer in the fluid

From the temperature measurements of the down flow thermometers of
test section 2 the heat absorption by the helium flow can be esti-
mated. It is assumed that the temperature T_3 of the second thermo-
meter section (Fig. 5.17) measured the overall helium bulk tempera-
ture. When the total heat release is absorbed by the helium flow, the
energy balance is

$$\phi_{abs} = \dot{m}\left(H(T_3) - H(T_0)\right) \tag{7.23}$$

where $H(T_3)$ is the enthalpy of the heated helium and $H(T_0)$ is the
enthalpy of the helium before entering the heated section. In
Table 7.6 ϕ_{abs} has been calculated. The released heat flow was 1.58 W
for the cases gathered in Table 7.6. If the model of eq. (7.23)
stands and the mass flow $\dot{m}$ is known, then the enthalpy $H(T_3)$ and the
belonging temperature T_3 can be calculated;

p	$\dot{m}$	T_0	T_e	T_3	H_0	H_{T_3}	$\dot{m}\Delta H$	ΔH
(bar)	(g/s)	(K)	(K)	(K)	(J/kg)	(J/kg)	(W)	(J/kg)
	1	4.22	7.2	4.75	13775	15479	1.704	1704
10	2	4.22	6.12	4.6	13775	14963	2.376	1188
	3	4.22	5.65	4.5	13775	14650	2.625	875
	1	4.25	7.1	4.75	11829	13584	1.755	1755
6	2	4.25	6.05	4.57	11829	12890	2.123	1061
	3	4.22	5.6	4.47	11729	12559	2.488	830
	1	4.25	6.7	4.7	10484	12524	2.04	2040
3	2	4.25	5.7	4.52	10484	11642	2.316	1158
	3	4.25	5.45	4.45	10484	11299	2.444	815

Table 7.6. The absorbed heat flow $\phi_{abs} = \dot{m}\Delta H$ in case of a totally heated
helium flow at various pressures and mass flows.

p (bar)	3			6			10		
ṁ (g/s)	1	2	3	1	2	3	1	2	3
$\frac{\phi_{rel}}{\dot{m}} = \Delta H_r$ (J/kg)	1580	790	527	1580	790	527	1580	790	527
H_0 (J/kg)	10484	10484	10484	11829	11829	11829	13775	13775	13775
$H_{T_3} = H_0 + \Delta H_r$ (J/kg)	12064	11274	11011	13409	12619	12356	15355	14565	14302
T_{3_c} (K)	4.61	4.44	4.39	4.71	4.49	4.38	4.71	4.47	4.39
T_{3_m} (K)	4.7	4.52	4.45	4.75	4.57	4.47	4.75	4.6	4.5
$T_{3_m} - T_{3_c}$ (K)	0.09	0.08	0.06	0.04	0.08	0.11	0.04	0.13	0.11

Table 7.7. Comparison of the measured (T_{3_m}) and calculated (T_{3_c}) temperatures of the second down stream thermometer of test section 2 ($\phi_{rel} = \phi_{released} = 1.58$ W).

$$H(T_3) = H(T_0) + \frac{\phi_{released}}{\dot{m}} \quad . \tag{7.24}$$

The results are shown in Table 7.7. The discrepancy between T_3-measured and T_3-calculated is small, of the order of 0.1 K or less. Thus the heat penetration in radial direction into the helium is large. This might be expected because the thermal conductivity related to the turbulence of the flow can be 100 to 300 times larger than the molecular conductivity (Knudsen and Katz [75]).

7.5. Comparison with other experimental results

Giarratano and Steward [46] published experimental data to helium during a step in heat flux. Subcritical and supercritical helium in a rectangular tube was heated on one side. The test section surface, a carbon film, served as heater as well as thermometer (see paragraph 4.1). The carbon film had the dimensions 5 × 10 mm; this film was situated inside the rectangular channel with the longer dimension parallel to the helium flow. The depth of the flow channel normal to
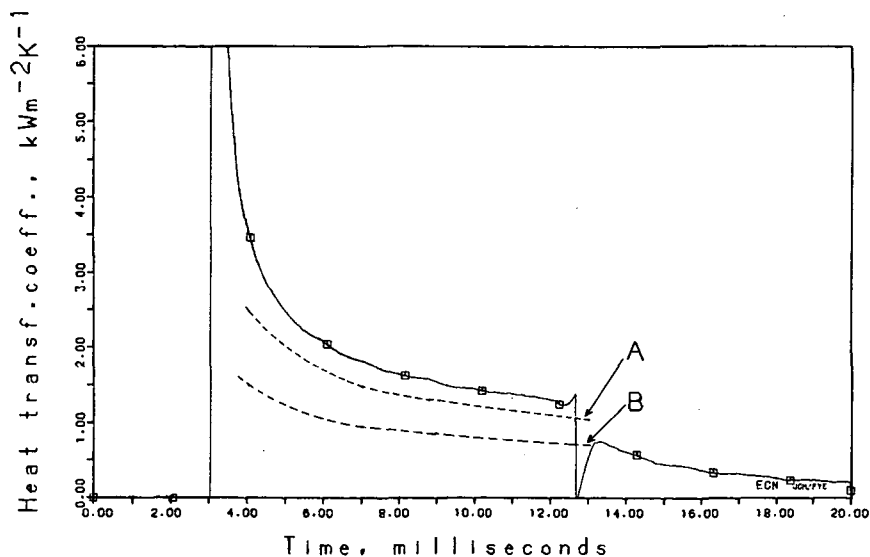
Figure 7.12 Comparison with the experimental results of Giarratano
and Steward. Pressure 10 bar.
　　　　Bloem: mass flow 1 g/s, released heat flux 4800 W/m².
　　　　Giarratano and Steward: stagnant helium, released
　　　　heat flux A: 1000 W/m² and B: = 10000 W/m².
　　　　Compare with Figures 6.5 and 6.7 (less difference
　　　　between 6 and 10 bar), especially the low flow of
　　　　0.1 g/s (nearly stagnant) at 6 bar (remark: note the
　　　　time scales).

the heater was 1.5 mm. A preheater preceded the test heater and was
maintained at the heat flux level of the test heater (length prehea-
ter 3.4 mm). The operation conditions covered the following ranges:
pressure 1 - 10 bar; inlet temperature 4 - 10 K; heat flux
10 - 100 kW/m²; Reynolds number 0 - 8 10^5.

The carbon film was deposited on a quartz substrate. The film was
located at the flow channel side and the other side of the substrate
was in contact with the helium which surrounded the test section.
The results of Giarratano and Steward according to the heat transfer
data are in poor agreement with the experiments of this report,
Figs 7.12 and 7.13. However, their results showed the same pressure-
temperature dependencies as mentioned in paragraph 7.1:

- no pressure dependence on the heat transfer coefficients at 4.2 K;
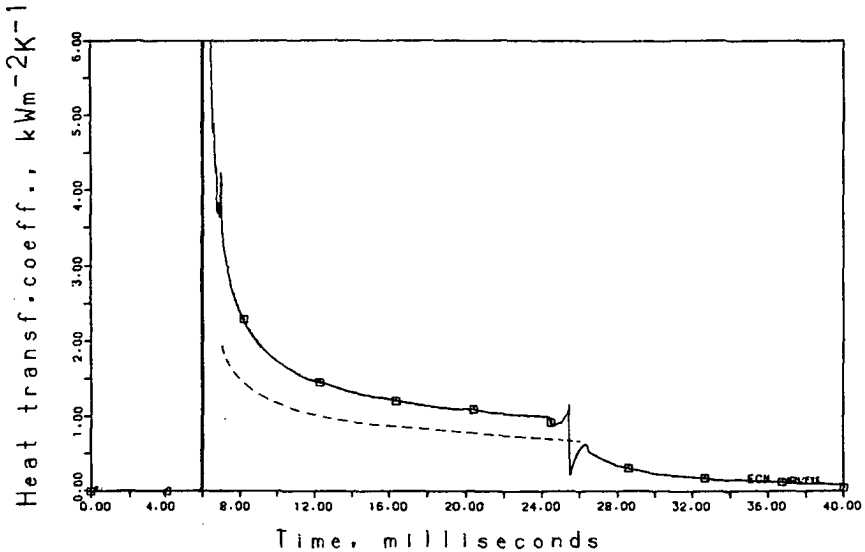- at high inlet temperatures and low pressures deterioration of the
  heat transfer;

Figure 7.13 Comparison with the experimental results of Giarratano
and Steward. Pressure 6 bar.
Bloem: mass flow 0.3 g/s, released heat flux 3150 W/m².
Giarratano and Steward: stagnant helium, released
heat flux 3000 W/m².

- their results can be described qualitatively with the function of
  ε as presented in paragraph 7.1.

The differences of the quantitative results may be caused by:

1) the preheater had a length of 1.5 D_h. this entrance length is too
   short to realize fully developed thermal hydraulic flow conditions
   in the measuring section;

2) there were uncertainties in their heat flux to the helium flow
   (10%) and in their mass flow measurements (20%).

7.6. Comparison with a numerical simulation model

Cornelissen [65] studied with the aid of a computer model numerically
the thermal stability of superconductors cooled by a turbulent flow
of supercritical helium. The advantages of Cornelissen's numerical
method is the use of extensive and detailed helium properties tables
and a well proven turbulence model. His numerically computed results
for stagnant supercritical helium showed that a turbulent flow can be

induced by releasing small heat pulses. Experiments by Shanfield et al. [77] on pulse heated copper capillaries containing stagnant supercritical helium confirm the results of Cornelissen.

We have used Cornelissen's computer model for simulating the heat transfer phenomena of the experiments of this report. The input data were fitted to the experimental setup. The heated section contained five numerical notes and cells. Corresponding to the experiments a heated length of 0.174 m was taken. This length includes the ends of the copper tube which were soldered for a length of 9.7 mm into the stainless steel bends (Fig. 5.14). The five numerical cells over 0.174 m result in an increment in axial direction of 0.0348 m. The total length of the tube considered in the calculations was 40 * 0.0348 m = 1.392 m (40 notes in axial direction). The heated section of 0.174 m was situated in the middle of the copper tube of 1.392 m. The helium flow was simulated with a numerical grid of 40 notes in axial direction and 13 notes in radial direction.
For the helium flow the computer code is two-dimensional, based on cylindrical symmetry. The rectangular tube of the experiments was re-placed in the calculations by a conduit with circular cross section with the same wetted perimeter, keeping the heat exchanging surface equal. The mean flow velocity of the experiments have been used in the simulations. As a consequence of the difference of the geometries in the experiments and the simulations, a discrepancy occurs in the value of mass flow and Reynolds number (Table 7.8).
In the computer program, the specific heat of the copper test section wall was calculated from eq. (6.6).
Some measurements were simulated with the computer model. The results are plotted in Figs 7.14 - 7.17 and compared with the mea-surements. In Appendix B results at higher inlet temperatures are given. The time step in the numerical calculations was 1 ms. The com-puted results were shifted in time with $(596*\text{sample rate} + 0.4*10^{-3})$ seconds. The first term is the delay of the transient recorder (para-graph 6.1) and the $0.4 * 10^{-3}$ s represents the response time of the thermometers.
The experimental results agree rather well, although there is a small discrepancy. This might be caused by the differences in geometry; the
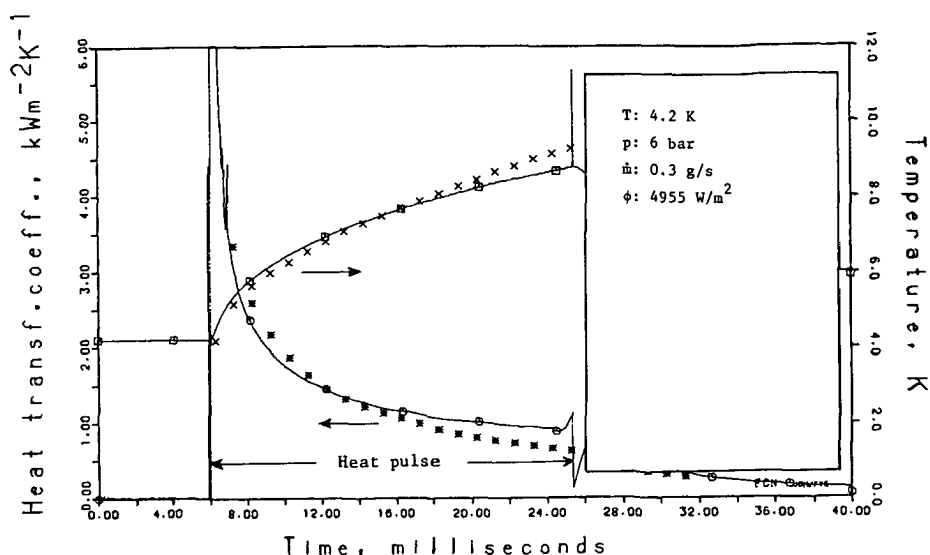
Figure 7.14   Comparison of experimental and numerical (= dots)
temperatures and belonging heat transfer coefficients.
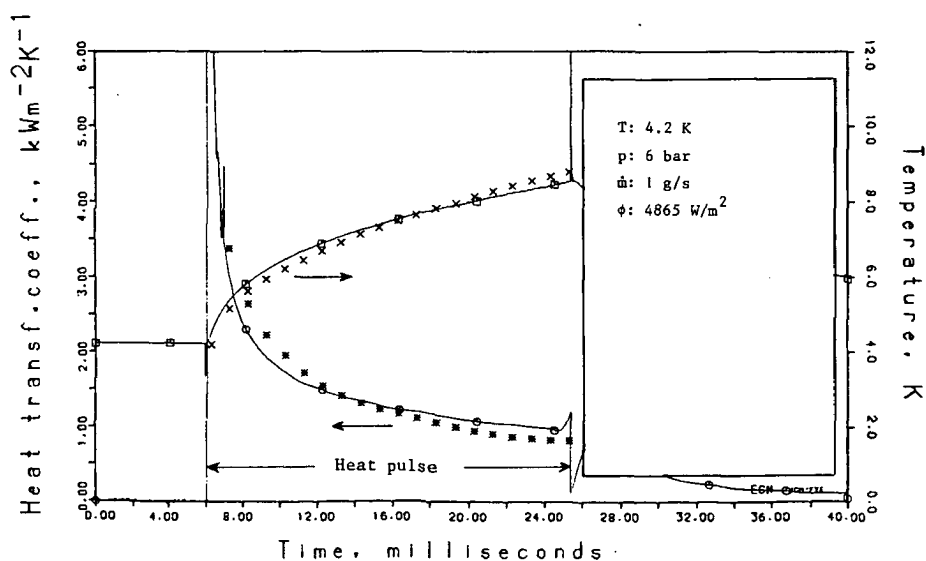

Figure 7.15   Comparison of experimental and numerical (= dots)
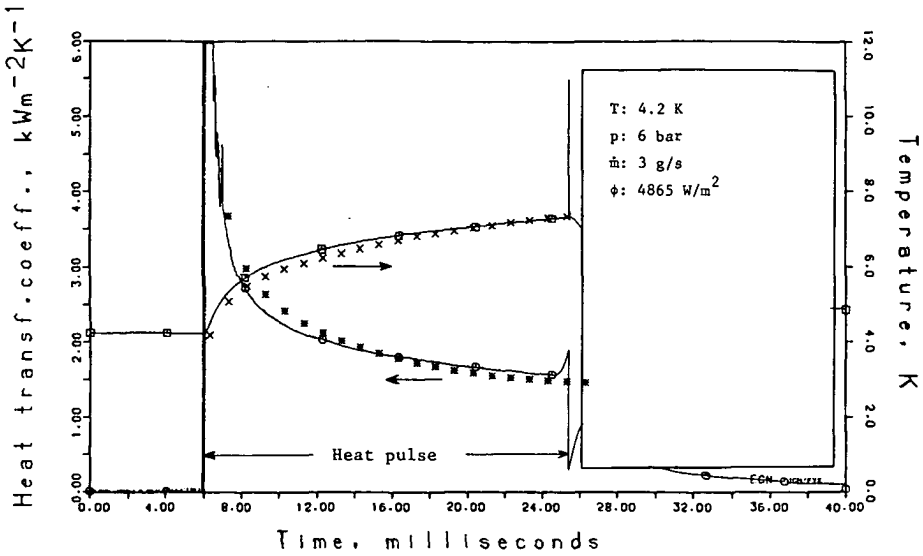temperatures and belonging heat transfer coefficients.

Figure 7.16   Comparison of experimental and numerical (= dots)
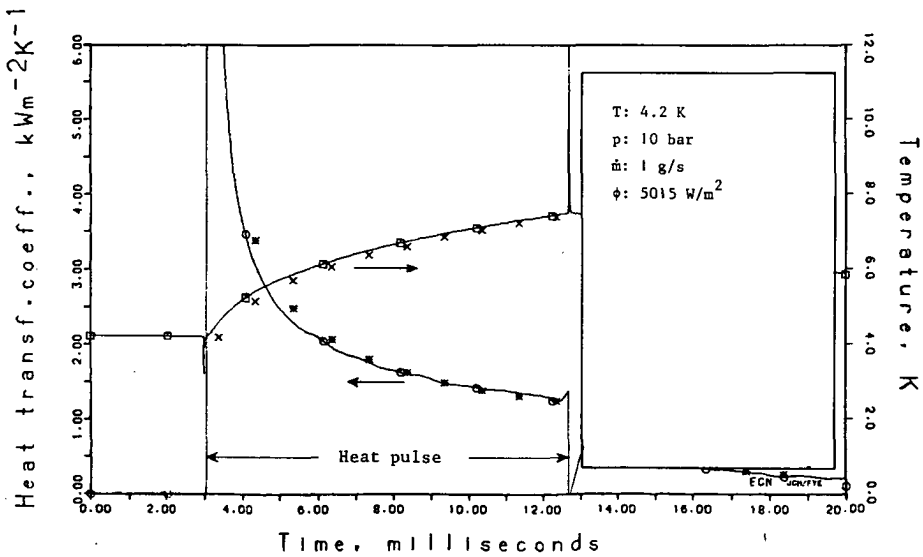temperatures and belonging heat transfer coefficients.

Figure 7.17   Comparison of experimental and numerical (= dots)
temperatures and belonging heat transfer coefficients.

	Rectangular cross section	Circular cross section
	a ⬚ b	⊕ — $2r$
wetted perimeter	$2(a + b)$	$2\pi r = 2(a + b)$
cross section	$a \times b$	$\frac{1}{\pi}(a + b)^2$
mean flow velocity	$\bar{v}$	$\bar{v}$
mass flow	$\rho\bar{v}(a \times b)$	$\rho\bar{v}\,\frac{1}{\pi}(a + b)^2$
Reynolds number	$\dfrac{\rho\,\bar{v}}{\eta}\,\dfrac{2(a \times b)}{(a + b)}$	$\dfrac{\rho\,\bar{v}}{\eta}\,\dfrac{2}{\pi}(a + b)$

Table 7.8. Geometry influence on the Reynolds number and
the mass flow, when wetted perimeter and mean
flow velocity have the same value.

experimental results were obtained from a rectangular tube. The tur-
bulence might have another character than in case of a tube with a
circular cross section. When the mass flow in the simulation was
given the value as used in the experiments, the same Reynolds number
occurs in the calculations as in the experiments, but then the nume-
rical mean velocity is lower than in reality. In the presented re-
sults, with the same mean velocity, the numerically computed Reynolds
number is larger than in reality (Table 7.8).

Cornelissen [65] discussed the poor agreement between his computed
results and the measurements of Giarratano and Steward [46]. Apart of
the uncertainty of the heat flux in the experiments of the latter,
Cornelissen suggested that the discrepancy might be caused by the
Kapitza resistances. A possible influence of these thermal resis-
tances was also discussed by Giarratano and Steward.
From the results presented here, it can be concluded that the Kapitza
boundary resistance is of less importance because i) the Kapitza
resistance mainly plays a role when helium is in the superfluid phase
and does not manifest in the He I phase (paragraph 3.4.2.2),
ii) although in the numerical simulation the Kapitza resistance was
not taken into account, the model predicts the experiments rather
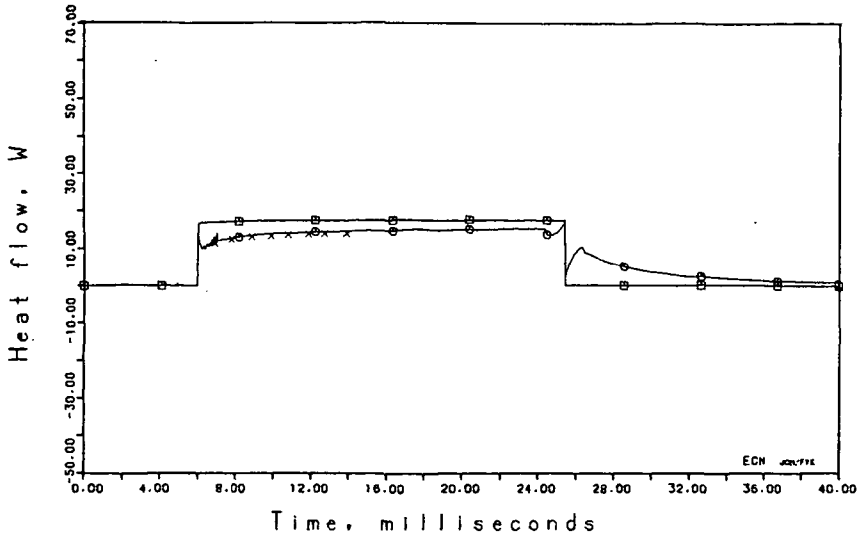well.

Figure 7.18 Released heat flow (block pulse) and the heat flow to
supercritical helium (mass flow 1 g/s, pressure 10 bar,
bulk inlet temperature 4.2 K).

In Fig. 7.18 the heat flow of one of the measurements and the corres-
ponding numerical simulation have been plotted. The block pulse is
the released heat flow of the heater and the delayed curve is the
heat flow to the helium (φ_{He}).
Also here the agreement is surprising. After one or two milliseconds
the heat flow becomes nearly constant. That means that the used model
of constant heat flux (proposed and used in paragraph 7.1) is plau-
sible.

CHAPTER 8

DISCUSSION AND CONCLUSIONS

The experiments showed that transient heat transfer to a forced flow
of supercritical helium takes place in a small layer of the coolant
along the wall of the conduit. The heat penetration is of the order
of tens of micrometers. Further radial heat transport in the fluid
from the outer layer to the core of the flow is governed by the tur-
bulence of the fluid. When a constant heat flux is forced to the
coolant the heat transfer becomes stationary after 0.1 second.

The transient heat transfer from a metal surface to supercritical
helium can be predicted qualitatively by considering the heat absorp-
tion coefficient ε, which is the product of the helium properties
thermal conductivity λ, density ρ and specific heat c_p. Especially
during the first milliseconds the heat transfer is completely
governed by the quantity ε. for the time range from 2 ms up to 100 ms
an empirical correlation was derived

$$Nu_{tr} = 0.06 \ Re^{0.75} \ (t_t/t)^{1/n} \tag{7.19}$$

with $n = 500 \ \dot{m} + 2.5$ (7.20)

where $\dot{m}$ in kg/s. It is possible to predict the transient heat trans-
fer within ten per cent with this correlation. The power of the time
function is a function of the mass flow. It is preferred to express
this dependence by a dimensionless parameter, the Reynolds number.
It was not possible to derive such an expression in the range of the
presented measurements. Some supplementary measurements have then to
be carried out with other tube diameters. Maintaining the mass flow
and reducing the diameter gives larger Reynolds numbers. In the set
of reported experiments some mass flows were the same, while the
Reynolds numbers varied by influence of different bulk temperatures,

but not more than 27% at a mass flow of 1 g/s. These experiments were
rather well described with the factor n according to eq. (7.20).

The developed thin film thermometers showed during all the experi-
ments a good reproducibility, also after the many cycles between room
and liquid helium temperatures. During the heat transfer experiments
the test section was heated many times and the thermometers never
failed.
Influences of moisture and gases on the resistivity have not been
noticed.

Pressure waves induced by small heat pulses were detected. In case of
a loaded superconducting magnet instabilities may produce locally
heat pulses. The accompanying pressure waves may have influence of
the cooling characteristic of further parts of the magnet. Further
study on the pressure waves and their effects are of interest.

At 4.2 K there is no large pressure dependence on the transient heat
transfer. That means that there is no advantage to cool at low pres-
sures; the large peak in the heat absorption $(\rho c_p$ as well as $\varepsilon)$ does
not manifest by getting lower temperature rises. At higher inlet tem-
peratures of the coolant the pressure influence became noticeable. At
low pressures and high inlet temperature the transient heat transfer
coefficient deteriorated, because ε was small. Because most super-
conducting devices are working at a temperature close to 4.2 K, it is
recommended to work at high pressures.
The advantages are 1) ε is relatively large at increasing tempera-
ture, 2) pressure oscillations are less probable, 3) at increasing
cooling temperature ε will still increase.
The experiments have shown that the transient heat transfer coeffi-
cient improves at Reynolds numbers larger than 100000.

The steady state heat transfer coefficient can be described by the
Dittus-Boelter correlation, $Nu = 0.0236 \ Re^{0.8} Pr^{0.4}$.
When the largest possible flow of supercritical helium through the

cooling tubes has been realized, the only possibility that remains to enlarge the heat transfer coefficient is enlargement of the heat exchanging surface.

Some of the experimental results were compared with numerical data obtained from using a computer simulation model (Cornelissen [65]). The results agree very well, but further improvement of the code is required to realize a closer agreement. Extension of the program to three dimensions has the advantage that the rectangular flow channel can be well simulated.

The applied function for the heat capacity of the test tube (eq. (6.6)) is of minor influence. The function is well defined and is used to correct the heat fluxes to the helium flow. The uncertainty of the experimental data of heat capacity mc_p of the tube is smaller than 10%. An uncertainty of 10% gives an error of about 2% in the experimental heat transfer coefficients. Because of the fact that the heat capacity mc_p is described well by eq. (6.6) it may be concluded that the (small) differences between the experimentally derived h and the numerically h have to be tried to find in the computer program. However, at this moment the numerical code is a good instrument for computing the thermal hydraulic behaviour of hollow superconductors to get any impression on stability and cooling performances.

APPENDIX A

Comparison of experimental and empirically computed heat transfer coefficients. The heat transfer coefficients were computed with the equation

$$Nu_{tr} = 0.06\ Re^{0.75}\ (t_t/t)^{1/n} \tag{7.19}$$

with

$$n = 500\ \dot{m} + 2.5 \tag{7.20}$$
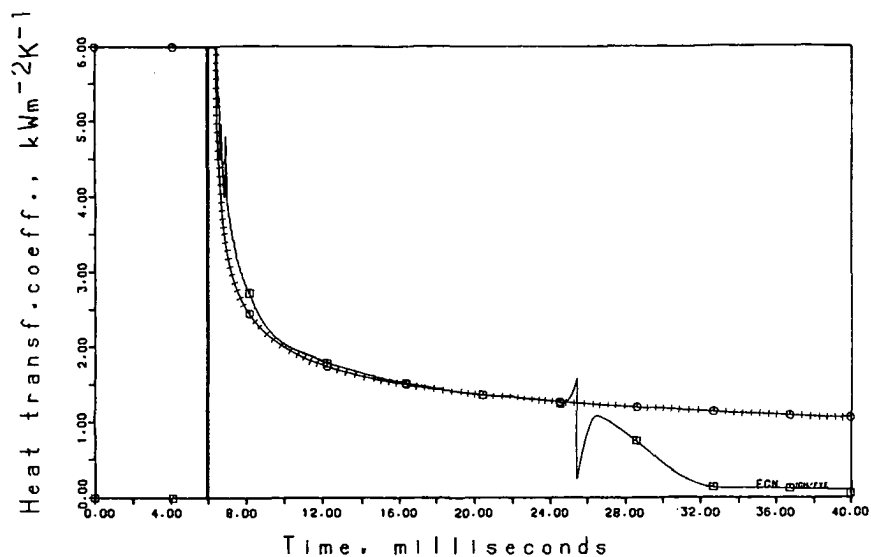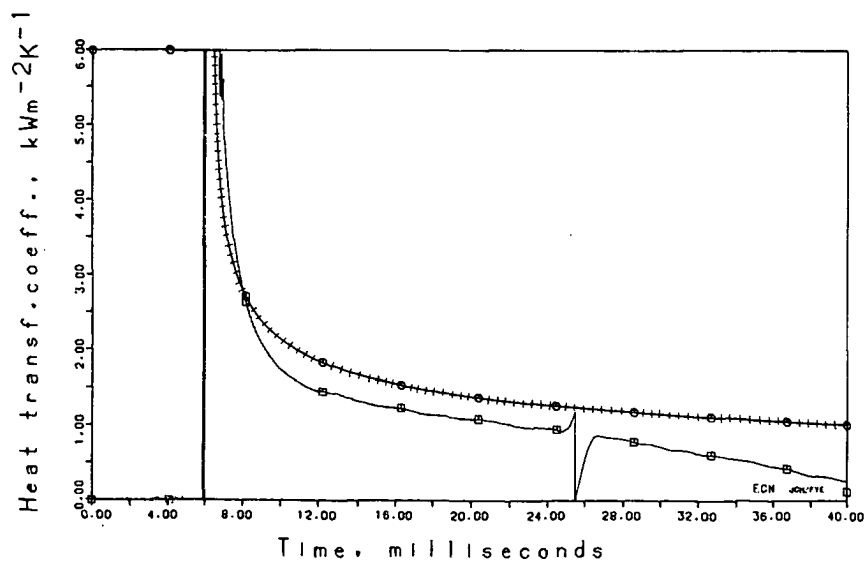
and $\dot{m}$ in kg/s.

Figure A1   Pressure   3 bar, bulk inlet temperature 4.2 K, mass flow 2 g/s.

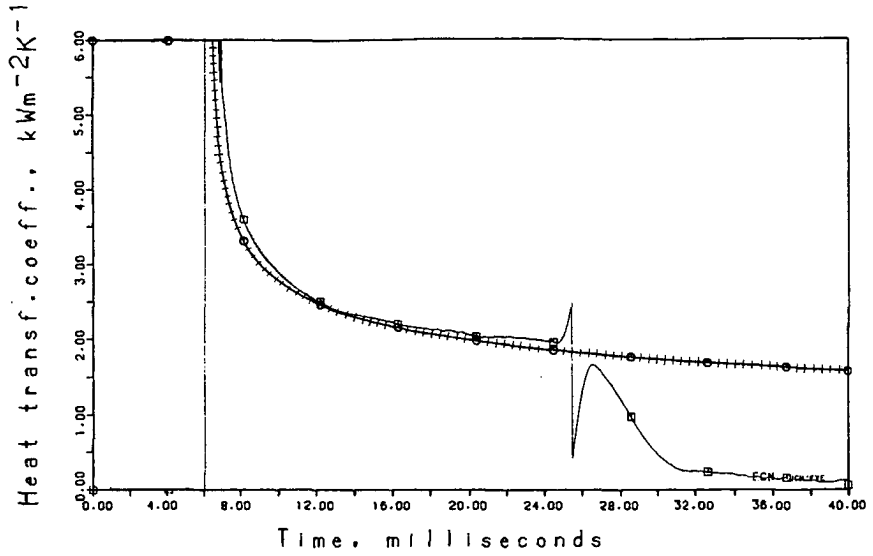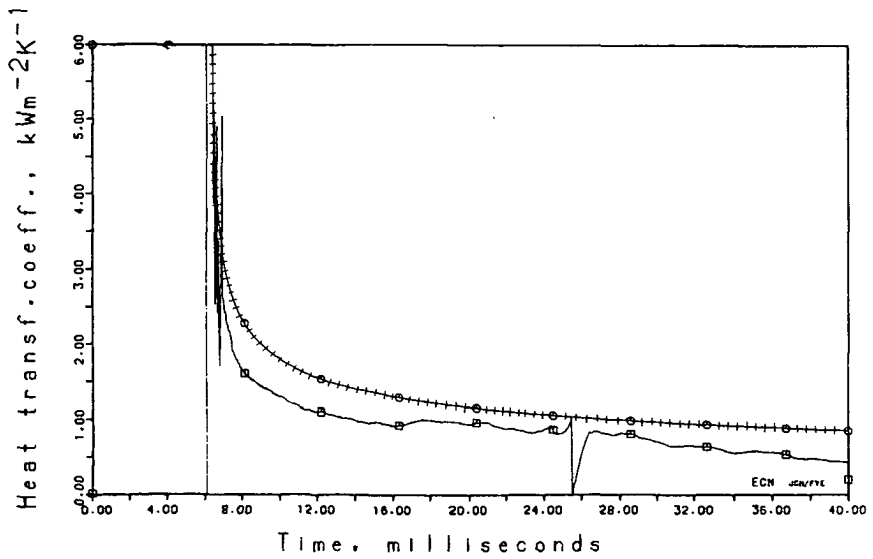Figure A2   Pressure   3 bar, bulk inlet temperature 5 K, mass flow 1 g/s.

Figure A3   Pressure   3 bar, bulk inlet temperature 5 K, mass flow 3 g/s.

Figure A4   Pressure   3 bar, bulk inlet temperature 6 K, mass flow 1 g/s.
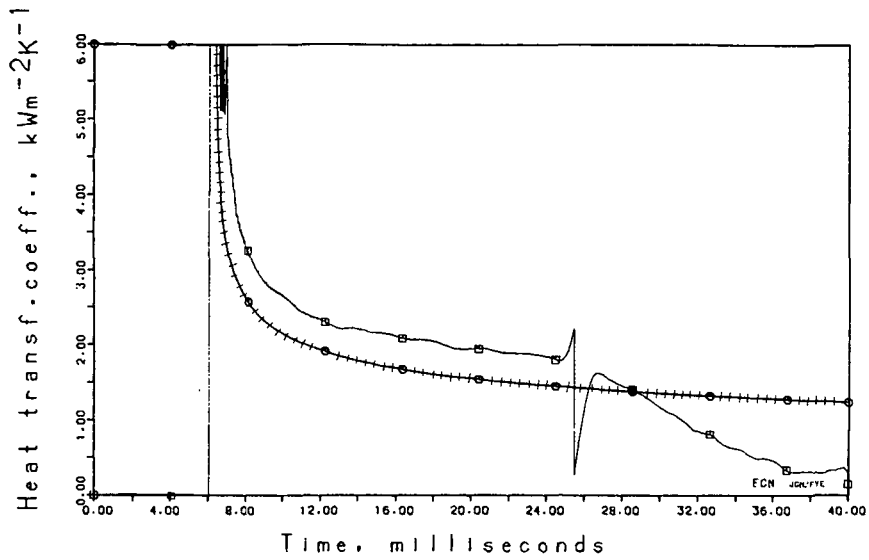
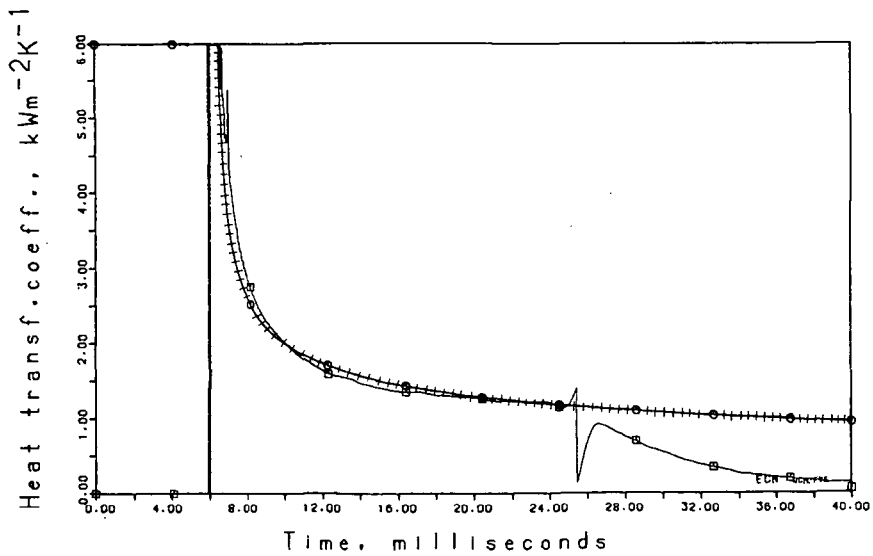Figure A5   Pressure 3 bar, bulk inlet temperature 5.6 K, mass flow 3 g/s.

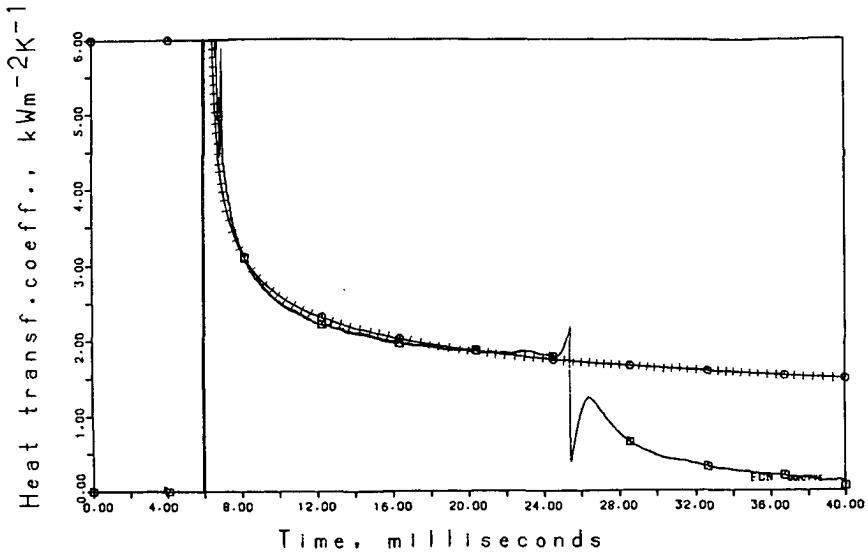Figure A6   Pressure 6 bar, bulk inlet temperature 5 K, mass flow 1 g/s.

Figure A7   Pressure 6 bar, bulk inlet temperature 5 K, mass flow 3 g/s.
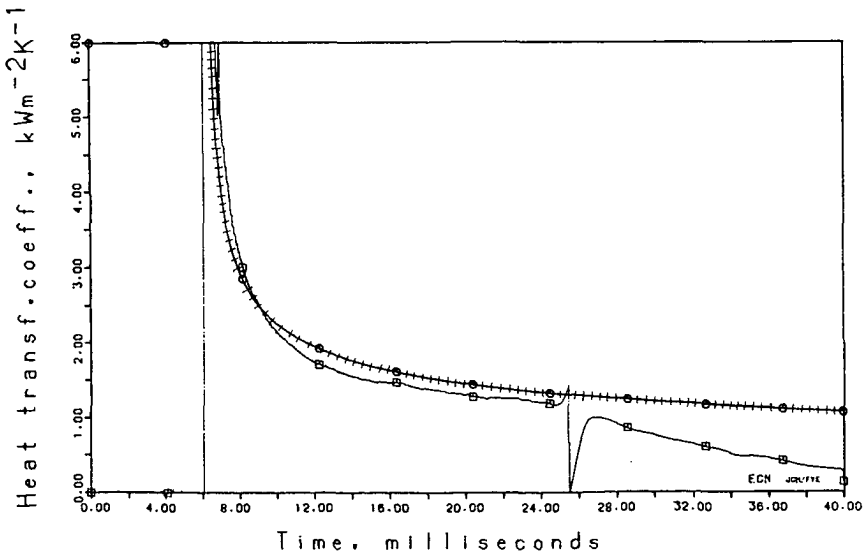

Figure A8   Pressure 6 bar, bulk inlet temperature 6 K, mass flow 1 g/s.
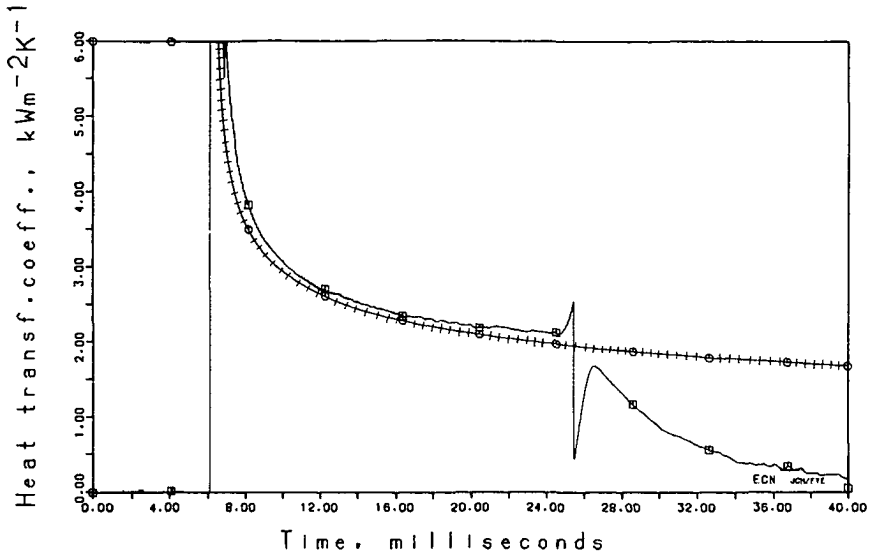
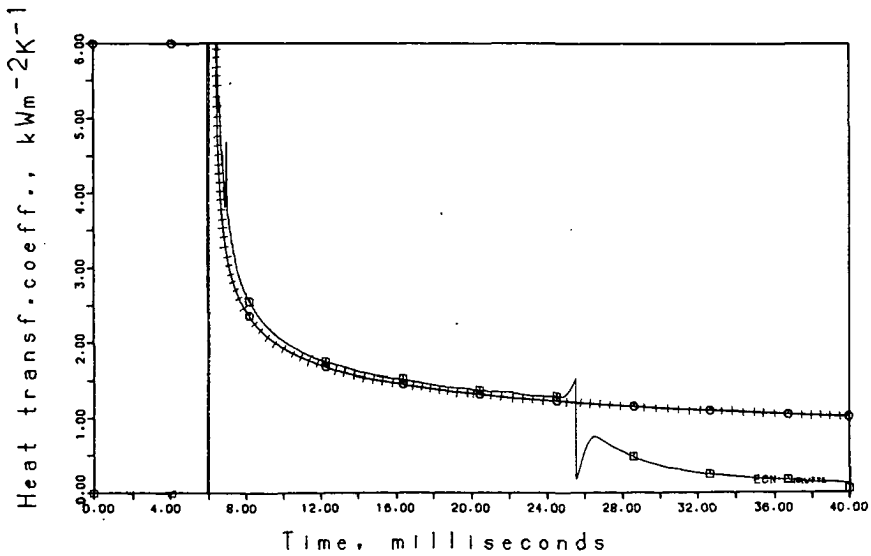Figure A9   Pressure 6 bar, bulk inlet temperature 6 K, mass flow 3 g/s.

Figure A10   Pressure 10 bar, bulk inlet temperature 4.2 K, mass flow 2 g/s.
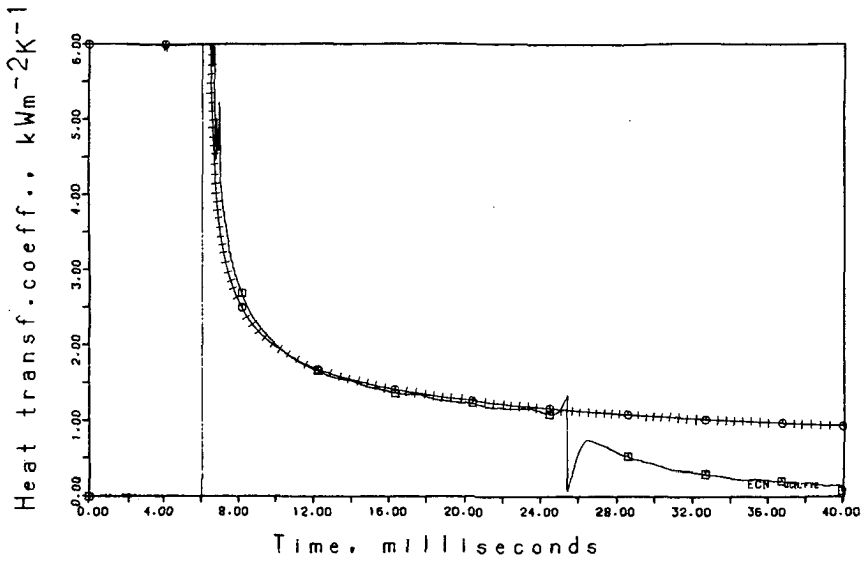
Figure A11   Pressure 10 bar, bulk inlet temperature 5 K, mass flow 1 g/s.
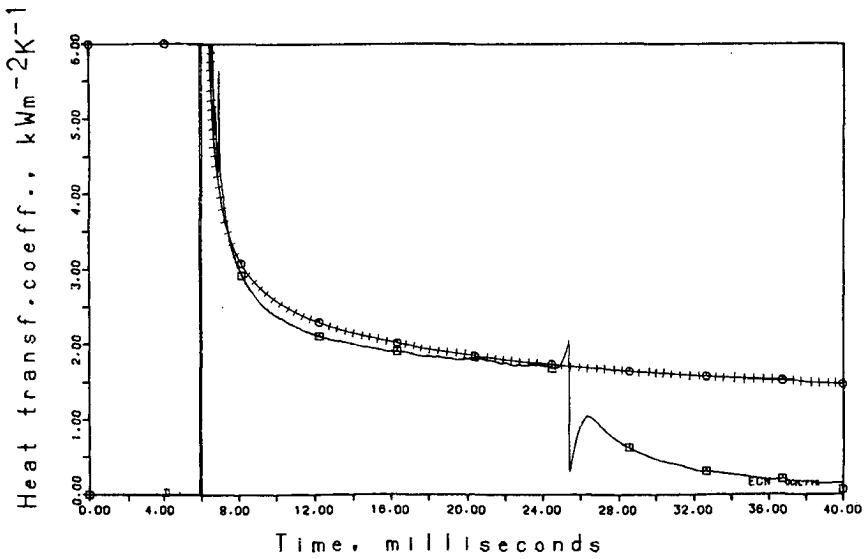
Figure A12   Pressure 10 bar, bulk inlet temperature 5 K, mass flow 3 g/s.
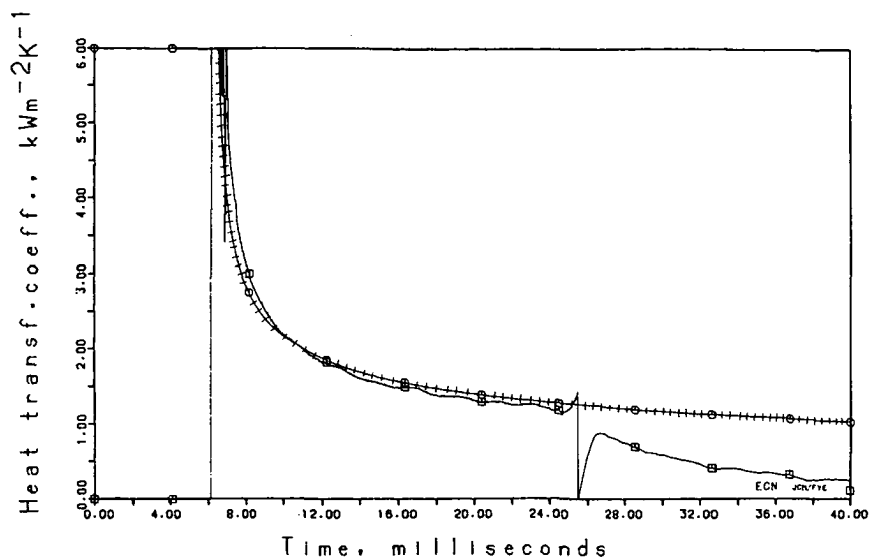
Figure A13   Pressure 10 bar, bulk inlet temperature 6 K, mass flow 1 g/s.
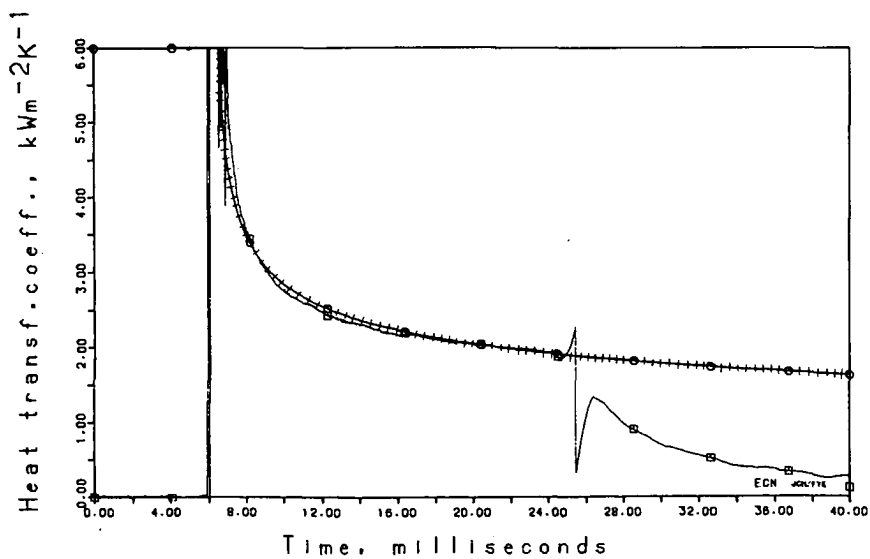
Figure A14   Pressure 10 bar, bulk inlet temperature 6 K, mass flow 3 g/s.

APPENDIX B

Numerical simulation of some experiments and comparison of the
results.
The numerical results were computed with a time step of 1 ms and
these results are marked with dots in the figures below. Heat pulse
started at 5.96 ms and lasted 19.4 ms (numerically 20 ms).

Figure B1   Pressure 6 bar, mass flow 1 g/s, inlet temperature 5 K,
heat flux 5105 W/m².

Figure B2   Pressure 6 bar, mass flow 1 g/s, inlet temperature 6 K,
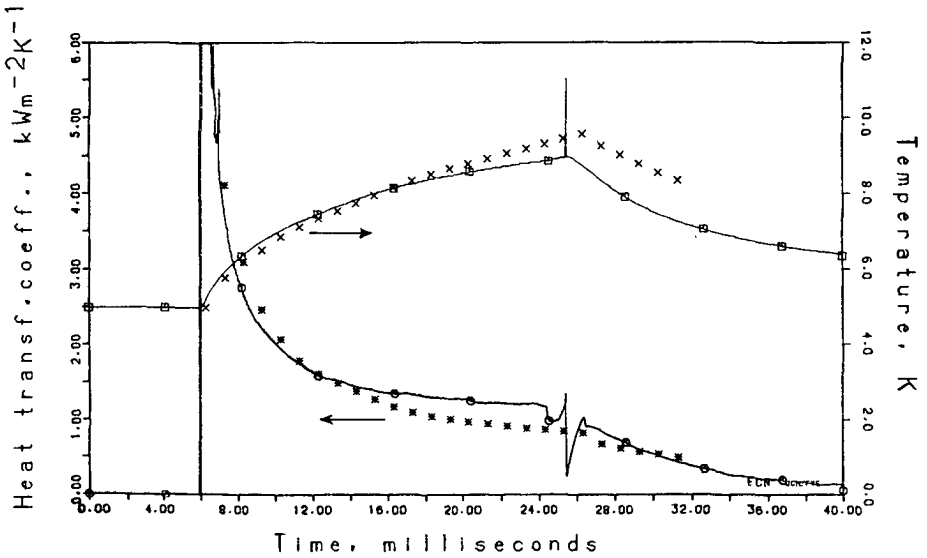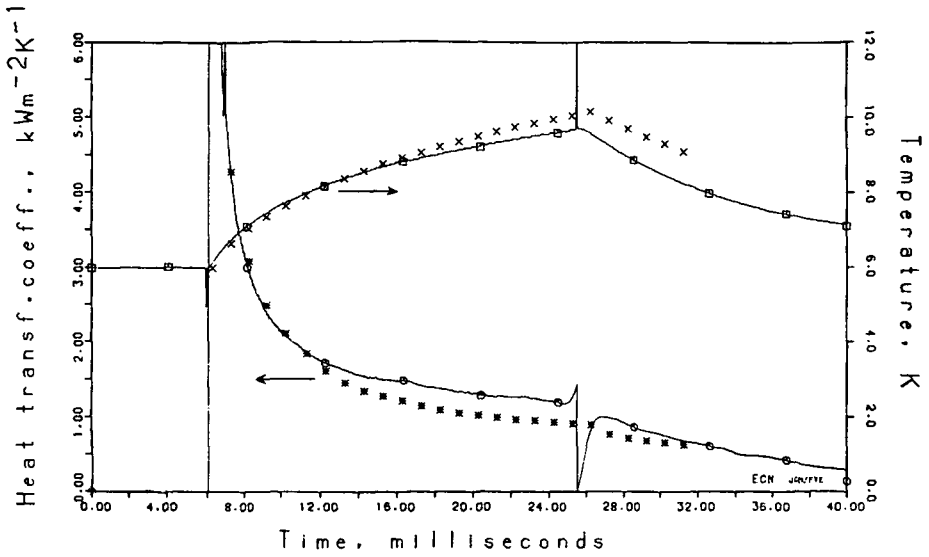   heat flux 5105 W/m².
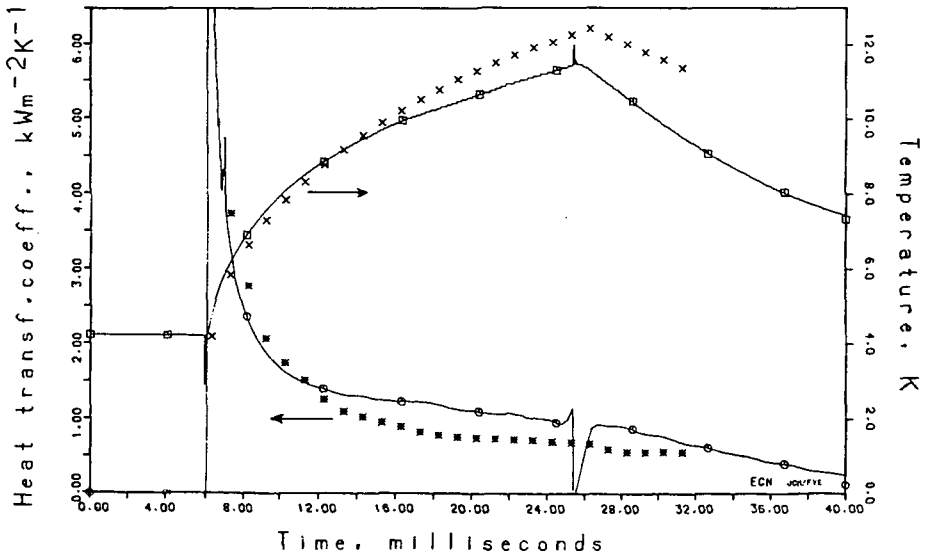
Figure B3   Pressure 6 bar, mass flow 1 g/s, inlet temperature 4.2 K,
            heat flux 9610 W/m².

APPENDIX C

List of addresses of manufacturers.

Acheson Colloïden, B.V., Haven N.Z. 6, 9679 TC Scheemda,
                        The Netherlands.

Emerson and Cuming Inc., Canton, Massachusetts 02021,
                        U.S.A.

Emerson and Cuming Europe N.V. Nijverheidsstraat 24, B-2431 Oevel,
                        Belgium.

Eriks N.V., Voormeer 33, 1813 SB Alkmaar,
                        The Netherlands.

Hollandse Metallurgische Industrie Billiton B.V., P.O. Box 38,
                        6800 LH Arnhem,
                        The Netherlands.

Isabellenhütte, Heusler GmbH, P.O. Box 360, 6340 Dillenburg,
                        Federal Republic of Germany.
                        (Swildens B.V., P.O. Box 121,
                        3640 Mijdrecht, The Netherlands)

Lake Shore Cryotronics Inc., 64E Walnut Street,
                        Westerville, Ohio 43081,
                        U.S.A.

Micro Measurements, Measurements Group, P.O. Box 27777, Raleigh,
                        North Carolina 27611,
                        U.S.A.
                        (J.J. Bos B.V., Fokkerstraat 12,
                        2722 NJ Zoetermeer, The Netherlands)

M.R.C. Material Research Corporation, Orangeburg, N.Y. 10962,
                        U.S.A.

M.R.C. Benelux, P.O. Box 3063, 3502 GA Utrecht,
                        The Netherlands.

Oxford Instruments Ltd., Osney Mead, Oxford, OX2 0DX,
                        United Kingdom.

Oxford Instruments B.V., Van Gijnstraat 13, 2288 GB Rijswijk,
                        The Netherlands.

Positronika Vacuum Technology, Watermolenstraat, 9440 Erembodegem,
                        Belgium.

Positronika Vacuum Technology, Dikkenbergstraat 1, 5628 EA Eindhoven,
                        The Netherlands.

APPENDIX D

List of instruments

Transient recorder :   Data Lab.
                        Memory Module DL 2004 (8×)
                        Mastertime base and Control Module DL 2003.

AC amplifier   :   Brookdeal precision a.c. amplifier, model 452.

AC/DC amplifier   :   ECN 911 AC-DC instrumentation amplifier.

Pulse generator   :   ECN 1068A single shot pulse generator
                        Delta power supply SM 6020.

DC amplifier   :   ECN 1119A DC instrumentation amplifiers
                        (30 kHz bandwidth).

Digital multimeters: Hewlett Packard 3455A digital multimeter.

Power supply   :   Delta E 030-1.

REFERENCES

[1] Onnes, H.K., Commun. Phys. Lab. Univ. Leiden, No. 120B (1911).
Onnes, H.K., Commun. Phys. Lab. Univ. Leiden, No. 122B (1911).
Onnes, H.K., Commun. Phys. Lab. Univ. Leiden, No. 124C (1911).

[2] Quin, D.J., Ittner, W.B. III, Journ. App. Phys., $\underline{33}$ (1962) 748.

[3] File, J., Mills, R.G., Phys. Rev. Lett., $\underline{10}$ (1963) 93.

[4] Onnes, H.K., Commun. Phys. Lab. Univ. Leiden, Supp. No. 34B
(1913).
Onnes, H.K., Commun. Phys. Lab. Univ. Leiden, No. 133D (1913).

[5] Onnes, H.K., Commun. Phys. Lab. Univ. Leiden, No. 139F (1914).

[6] Schwartz, B.B., Foner, S., Phys. Today, July 1977, 34.

[7] Veringa, H.J., Report ECN-96, Intrinsic stability of
technical superconductors, Netherlands Energy Research
Foundation ECN, Petten (1981).

[8] Iwasa, Y., Proc. Stability of Superconductors, International
Institute of Refrigeration, Paris (1981) 125.

[9] Bardeen, J., Cooper, L.N., Schrieffer, J.R., Phys. Rev. $\underline{106}$
(1957) 162, Phys. Rev. $\underline{108}$ (1957) 1175.

[10] Bobrov, E.S., Williams, J.E.C., Iwasa, Y., Cryogenics $\underline{25}$ (1985)
307.

[11] Smith, P.F., Coyler, B., Cryogenics $\underline{15}$ (1975) 201.

[12] Iwasa, Y., Bobrov, E.S., Tsukamoto, O., Takaghi, T.,
Fujita, H., Cryogenics $\underline{25}$ (1985) 317.

[13] Tsukamoto, O., Iwasa, Y., Proc. Stability of Superconductors, International Institute of Refrigeration, Paris (1981) 259.

[14] Kantrowitz, A.R., Stekly, Z.J.J., App. Phys. Lett. 6 (1965) 56.

[15] Stekly, Z.J.J., Zar, J.L., IEEE Trans. Nucl. Sci. 12 (1965) 367.

[16] Maddock, B.J., James, G.B., Norris, W.T., Cryogenics 9 (1969) 261.

[17] Wilson, M.N., Walters, C.R., Lewin, J.D., Smith, P.F., Journ. Phys. D 3 (1970) 1517.

[18] Brechna, H., Superconducting Magnet Systems, Springer, Berlin (1973).

[19] Carlslaw, H.S., Jaeger, J.C., Conduction of heat in solids, 2 ed. Clarendon Press, Oxford (1959).

[20] Fickett, F.R., Advances in Cryogenic Engineering 30, Plenum Press, New York (1984) 453.

[21] Schmidt, C., Proc. Stability of Superconductors, International Institute of Refrigeration, Paris (1981) 17.

[22] Lyon, D.N., Advances in Cryogenic Engineering 10, Plenum Press, New York (1965) 371.

[23] Boissin, J.C., Thibault, J.J., Roussel, J., Faddi, E., Advances in Cryogenic Engineering 13, Plenum Press, New York (1968) 607.

[24] Cumming, R.D., Smith, J.L., Liquid helium technology, Pergamon Press, Oxford (1966) 85.

[25] Ogata, H., Nakayama, W., Advances in Cryogenic Engineering 27, Plenum Press, New York (1982) 309.

[26] Lehongre, S., Boissin, J.C., Johannes, C., Harpe, A. dela,
     Proc. 2nd Int. Cryog. Eng. Conf., Brighton (1968) 274.

[27] Bailey, R.L., Proc. 5th Int. Conf. Magn. Techn. (MT-5), Lab.
     Nazionali del CNEN, Frascati (1975) 582.

[28] Tsuruga, H., Endoh, K., Proc. 9th Int. Cryog. Eng. Conf.,
     Grenoble (1982) 65.

[29] Johannes, C., Mollard, J., Advances in Cryogenic Engineering
     17, Plenum Press, New York (1972) 332.

[30] Johannes, C., Advances in Cryogenic Engineering 17, Plenum
     Press, New York (1972) 352.

[31] Shah, M.M., Cryogenics 25 (1984) 231.

[32] Subbotin, V.I., Deev, V.I., Pridantsev, A.I., Andreev, V.K.,
     Arkhipov, V.V., Novikov, V.N., Savin, A.N., Solodovnikov, V.V.,
     Cryogenics 25 (1985) 261.

[33] Giarratano, P.J., Arp, V.D., Smith, R.V., Cryogenics 11 (1971)
     385.

[34] Ogata, H., Sato, S., Proc. 4th Int. Cryog. Eng. Conf.,
     Eindhoven (1972) 291.

[35] Giarratano, P.J., Jones, M.C., Int. J. Heat Mass Transfer 18
     (1975) 649.

[36] Yaskin, L.A., Jones, M.C., Yeroshenko, V.M. Giarratano, P.J.,
     Arp, V.D., Cryogenics 27 (1977) 549.

[37] Brassington, D.J., Cairns, D.N.H., Int. J. Heat Mass Transfer
     20 (1977) 207.

[38] Bogachev, V.A., Yeroshenko, V.M., Snytina, O.F., Yaskin, L.A., Cryogenics 25 (1985) 198.

[39] Srinivasan, R., Hofmann, A., Cryogenics 25 (1985) 641 (part 1), 652 (part 2).

[40] Wilks, J., The properties of liquid and solid helium, Clarendon Press, Oxford (1967).

[41] Zemansky, M.W., Heat and Thermodynamics, 5 ed., Mc Graw Hill Kogakusha, Tokyo (1968).

[42] Bloem, W.B., Cryogenics 24 (1984) 159.

[43] Jackson, J., Cryogenics 9 (1969) 103.

[44] Schmidt, C., Appl. Phys. Lett. 32 (1978) 827.

[45] Steward, W.G., Int. J. Heat Mass Transfer 21 (1978) 863.

[46] Giarratano, P.J., Steward W.G., J. Heat Transfer 105 (1983) 350.

[47] Seki, M., Sanokawa, K., Cryogenics 22 (1982) 121.

[48] Franken, W.M.P. Spoorenberg, C.J.G., The design of the Sultan inner coil, Report ECN-109, Netherlands Energy Research Foundation ECN, Petten (1981).

[49] Sample, H.H., Rubin, L.G., Cryogenics 17 (1977) 597.

[50] Shen, L., Heberlein, D.C., Temperature 4, Instrument Society of America, Pittsburgh (1972) 791.

[51] Adkins, C.J., Freake, S.M., Hamilton, E.M., Phil. Mag. 22 (1970) 183.

[52] Mrozowski, S., Phys. Rev. 85 (1952) 609.

[53] Kupperman, D.S., Chan, C.K, Weinstock, H., Carbon 11 (1973)
      171.

[54] Hauser, J.J., Patel, J.R., Solid State Commun., 18 (1976) 789.

[55] Hauser, J.J., J. Non Crystal Sol. 23 (1977) 21.

[56] Sample, H.H., Brandt, B.L., Rubin, L.G., Rev. Sci. Instrum. 53
      (1982) 1129.

[57] Mathu, F., Meyer, H.C., Cryogenics 22 (1982) 428.

[58] Verein Deutsche Ingenieure, Deutsche Industrie Norm 1952,
      VDI-Durchflussmessregeln, Beuth-Vertrieb GmbH, Berlin (1963).

[59] Franken, W.M.P., Brieko, M.W., Gijze, A.C., Heil, J.A.,
      Roeterdink, J.A., Rij, H.M. van, IEEE Trans. Mag. 17 (1981)
      2011.

[60] Brechna, H., Proc. Stability of Superconductors, International
      Institute of Refrigeration, Paris (1981) 89.

[61] Mills, A.F., J. Mech. Eng. Science, 4 (1962) 63.

[62] Verein Deutsche Ingenieure, VDI Wärmeatlas, VDI Verlag GmbH,
      Düsseldorf (1963).

[63] Touloukian, Y.S., Powell, R.W., Ho, C.Y., Klemens, P.G.,
      Thermal properties of matter, Thermal Conductivity,
      vol. 1, 2, 3, IFI/Plenum Press, New York (1970).

[64] Radebaugh, R., Rev. Sci. Instrum., 48 (1977) 93.

[65] Cornelissen, M.C.M., Thermal stability of superconductors,
      magnets, Thesis, Delft University of Technology,
      The Netherlands (1984).

[66] Cornelissen, M.C.M., Hoogendoorn, C.J., Cryogenics 25 (1985)
185.

[67] Mc Carthy, R.D., Thermodynamic properties of helium 4 from 2 to
1500 K at pressures to 10^8 Pa, J. Phys. Chem. Ref. Data,
vol. 2, no. 4 (1973) 923-1042.

[68] Breimesser, F., Intichar, L., Poppinger, M., Schnapper, C.,
Proc. 8th Int. Conf. Magn. Tech., Grenoble (1983) C1-671.

[69] Nemoto, T., Sasaki, S., Hakuraku, Y., Cryogenics 25 (1985) 531.

[70] Touloukian, Y.S., Buyco, E.H., Thermal properties of matter,
Specific Heat, vol. 4, 5, 6, IFI/Plenum Press, New York (1970).

[71] Acton, A., Kellner, K., Physica 90B (1977) 192.

[72] Carr, R.H. (ed.), Application of Cryogenic Technology, vol. 5,
Scholium International, Whitestone N.Y. (1973) 69.

[73] Daney, D.E. Ludtke, P.R., Cryogenics 18 (1978) 345.

[74] Junghans, Cryogenics 20 (1980) 633.

[75] Knudsen, J.G., Katz, D.L., Fluid dynamics and heat transfer,
Mc Graw Hill, New York (1958).

[76] Deissler, R.G., NACA RM E52 F05 (1952).

[77] Shanfield, S.R., Agatsuma, K., Montgomery, A.G., Hoenig, M.O.,
IEEE Trans. on Magn., vol. MAG-17, no. 5 (1981) 2019.

[78] Horvath, I., Vecsey, G., Weymuth, P., Zellweger, J.,
Balsamo, E.P., Pasotti, G., Ricci, M.V., Sacchetti, N.,
Spadoni, M., Elen, J.D., Franken, W.M.P., IEEE Trans. Mag.,
vol. MAG-19 (1983) 668.

[79] Dittus, F.W., Boelter, L.M.K., University of California,
Pubs. Engineering, vol. 2 (1930) 443.

[80] Franken, W.M.P., Elen, J.D., Plaum, J.M., Roeterdink, J.A.,
Proc. 9th Int. Conf. Magn. Techn. (MT 9), Zürich (1985) 611.

[81] Bloem, W.B., Cryogenics 26 (1986) 300.

[82] Bloem, W.B., Proceedings of Heat and Mass Transfer in
Cryoengineering and Refrigeration, International Centre Heat
Mass Transfer ICHMT, Dubrovnik, Yugoslavia (1986).

[83] Handbook on materials for superconducting machinery, Metals
and Ceramics Information Center Battelle, Columbus
Laboratories, Columbus, Ohio (1977).

[84] Borst, P., Essen, F.P.J. van, Hoebe, J.C., Priv. Comm.,
ECN report, memo no. 4.364-036, Petten (1979).

[85] Trentelman, P.J.Th., Priv. Comm., ECN report,
memo no. 4.372-021, Petten (1982).

CURRICULUM VITAE

26 oktober 1955   Geboren te Beverwijk.

1962 - 1968   Lager onderwijs genoten op de Julianaschool te Beverwijk.

1968 - 1974   V.W.O. opleiding aan het Berlingh College te Beverwijk. Eindexamen Atheneum B.

1974 - 1981   Studie voor natuurkundig ingenieur aan de Technische Hogeschool Delft.

1978 - 1981 4^e en 5^e jaarswerk in de vakgroep Lage Temperaturen op het gebied van koeling van kernfysische trefplaten gevuld met vloeibaar ^3He o.l.v. Prof. Dr. H. Postma. Studentassistentschap.

16 juni 1981   Doctoraal examen natuurkundig ingenieur.

1981 - 1986   Promovendus bij het Energieonderzoek Centrum Nederland in de afdeling Energie Technologie, sectie Experimenten.

NAWOORD

Bij het verschijnen van dit proefschrift wil ik graag van de gelegen-
heid gebruik maken een ieder te bedanken voor hun bijdragen die mede
hebben geleid tot het tot stand komen van deze dissertatie.
Allereerst wil ik mijn promotor, prof. dr. H. Postma, bedanken voor
zijn begeleiding, adviezen en de discussies tijdens het onderzoek.
Dank zij zijn bemiddeling was het mogelijk om de opdampwerkzaamheden
voor de thermometers bij de Technische Universiteit Delft uit te
voeren.
Het onderzoek is uitgevoerd bij de Stichting Energieonderzoek Centrum
Nederland te Petten in de afdeling Energie Technologie. Ik ben de
ECN-directie zeer dankbaar voor het beschikbaar stellen van een
promotieplaats. Drs. J.D. Elen en ir. W.G. Bonsel wil ik bedanken
voor de inpassing van het onderzoek binnen het ECN-programma en het
scheppen van de middelen en faciliteiten om het onderzoek tot een
goed einde te brengen.
Een bijzonder woord van dank wil ik richten aan Wout Franken, die als
ECN-begeleider de afgelopen vijf jaar het onderzoek een warm hart toe
droeg.
Marc Cornelissen, Rob van der Linden en prof. ir. C.J. Hoogendoorn
van de Technische Universiteit Delft ben ik zeer erkentelijk voor de
waardevolle contacten en gedachtewisselingen over het werk. Tevens
wil ik Leo Lander van de opdampkamer van de Technische Universiteit
Delft noemen voor zijn hulp en advies bij het opdampen van de dunne
laag koolthermometers.
Binnen het ECN bij de afdeling Energie Technologie, groep Experimen-
ten, wil ik al mijn collega's bedanken voor hun hulp en prettige
samenwerking. Een speciaal woord van dank aan Piet Deijmann voor zijn
assistentie tijdens al de experimenten. Wiebe Reiding en Lou Hoorn
construeerden de grootste gedeelten van de meetopstellingen en test-
secties. Roel Hoogland verwerkte een groot deel van de metingen. We
hebben samen 11 ordners vol gekregen met "plots".
En ten slotte ben ik veel dank verschuldigd aan Jenny Faber voor het
bewerken van een in een (te) klein handschrift geschreven manuscript
opdat er een leesbaar geheel ontstond.